Investigation into a GPS Time Pulse Radiator for Testing Time-stamp Accuracy of a Radio Telescope

Zwivhuya Romeo Ramudzuli

Thesis presented for the degree of Master of Science in Engineering
In the Department of Electrical Engineering

University of Cape Town
January 31, 2019

Declaration

I know the meaning of plagiarism and declare that all the work in the document, save for that which is properly acknowledged, is my own. This thesis/dissertation has been submitted to the Turnitin module (or equivalent similarity and originality checking software) and I confirm that my supervisor has seen my report and any concerns revealed by such have been resolved with my supervisor.

Signature of Author Signed by candidate .....

Cape Town
January 31, 2019

Abstract

The MeerKAT radio telescope in South Africa is required to tag the arrival time of a signal to within 10 ns of Coordinated Universal Time (UTC). The telescope has a local atomic clock ensemble and uses satellite based remote clock comparison techniques to compare the telescope time to UTC. The master clock timing edge is distributed to each telescope antenna via an optical fibre precise time transfer. Although the timing accuracy of the telescope time was measured internally by the telescope, there is a need for an independent method to verify how well each antenna and its associated processing stages are aligned to UTC. A portable GNSS time-pulse radiator (GTR) device for testing the time-stamp accuracy was developed. The GTR was calibrated at the National Metrology Institute of South Africa and laboratory characterisation tests measured its RF timing pulse to be 1.32 ± 0.100 μs ahead of the UTC second. The telescope's time and frequency reference clock ensemble consists of two hydrogen masers, an ultrastable crystal and GPS disciplined Rubidium clocks. During operation, the GTR radiates a broadband GPS time synchronised RF timing signal at a known distance from the telescope antennas and the corresponding timestamps were compared to the expected value. Recent GTR timing tests performed on one of the MeerKAT antennas showed that the telescope's generated timestamps associated with the GTR's RF timing signal coincided with the expected delay of approximately 16 ± 0.1 μs measured from an antenna 4.8 km away from the telescope's master clock transmitter. Ultimately we used the GTR to verify that the telescope time and UTC were aligned to within 100 ns. Future work is planned to improve the profile of the transmitted signal and timing critical hardware in order to reduce the GTR's error budget.

Acknowledgements

I would first like to thank my research supervisor, Dr. WPF Schonken. He consistently allowed this thesis to be my own work, but steered me in the right direction whenever he thought I needed it. It is with immense gratitude that I acknowledge Thomas Abbott whose encouragement, guidance and support from the initial to the final stage enabled me to develop an understanding of the subject. His office was always open whenever I had questions about my research and was available in person for numerous field tests on MeerKAT site.

I would also like to thank the South African Radio Astronomy Observatory's (SARAO) Time and Frequency reference experts who were involved in the MeerKAT telescope time test for providing precise time test data for this research project: Dr. Johan Burger, Grant Adams, Renier Siebrits, and Dr. Romeo Gamatham. I would also like to thank my line managers, Dr. Marc Welz and Francois Kapp for their support during the execution of my thesis. I would also like to thank Vereese Van Tonder for generously offering her time to review my thesis. I would also like to thank Chris Matthee from the National Meteorology Institute of South Africa (NMISA) for making his lab available for the calibration exercise. This thesis would not have been possible without the funding and facilities provided by SARAO.

Lastly, I must express my very profound gratitude to my parents and siblings for providing me with unfailing support and continuous encouragement throughout my years of study and through the process of researching and writing this thesis.

List of Publications

The following paper has been peer reviewed and accepted for publication as a result of this thesis research:

Z.R. Ramudzuli and T. Abbott, "Investigation into a GPS Time Pulse Radiator for Testing Time-Stamp Accuracy of a Radio Telescope", in *Proceedings of the IEEE International Frequency Control Symposium (IFCS)*, 2018, pp. 233-236, isbn. 978-1-5386-3214-7.

Contents

Acronyms

1PPS	1 Pules-per-second
ADC	Analogue-to-Digital converter
ATNF	Pulsar group of the Australia telescope national facility
BDT	Barycenter dynamic time
BIPM	International Bureau of Weights and Measures
C/A	Coarse-acquisition code
C/N_0	Carrier-to-noise power density ratio
CSOC	Consolidated Space Operations Center
DSP	Digital signal processing
EMC	Electromagnetic compatibility
EMI	Electromagnetic interference
GDOP	Geometric dilution of precision
GNSS	Global navigation satellite system
GPS	Global Positioning System
GTR	GPS time pulse radiator
HDOP	Horizontal dilution of precision
JD	Julian date
KTT	Karoo Telescope Time
IERS	International Earth Rotation and Reference Systems Service
IF	Intermediate frequency
LED	Light-emitting diode
LNA	Low noise amplifier
MJD	Modified Julian date
MTIE	Maximum time interval error
NANOGrav	North American Nanohertz Observatory for Gravitational Waves
NMISA	National Metrology Institute of South Africa
OCXO	Oven compensated crystal oscillators
PCB	Printed circuit board
PDF	Probability distribution function
PDOP	Position dilution of precision

PPS	Precise positioning service
PRN	Pseudorandom noise
RF	Radio frequency
RFI	Radio frequency interference
SARAO	South African Radio Astronomy Observatory
SKA	Square Kilometre Array
SKAO	Square Kilometre Array Organisation
SPS	Standard positioning service
SNR	Signal-to-noise ratio
TAI	Temps Atomique International (International Atomic Time)
TCXO	Temperature compensated crystal oscillators
TDOP	Time dilution of precision
TDT	Terrestrial dynamical time
TOA	Time of arrival
USNO	US Naval Observatory
UERE	User equivalent range error
UT	Universal time
UTCOE	UTC offset error
UTC	Coordinated Universal Time
VDOP	Vertical dilution of precision

List of Figures

List of Tables

Chapter 1

Introduction

Some of the most interesting activity in the universe happens at radio frequencies. In order to study these activities, astronomers, engineers and scientists have been designing and building radio telescopes to probe deep into celestial bodies emitting radio frequency (RF) signals. These instruments enable astronomers to study the evolution of galaxies so as to understand the mysteries of the Big Bang, black holes, cosmic magnetism, gravitational waves, the cradle of terrestrial and possibilities of extraterrestrial life. In 2012, the Square Kilometre Array Organisation (SKAO) responsible for coordinating engineering, science and operation activities of the Square Kilometre Array (SKA) project took a momentous decision to co-site the SKA in South Africa and Australia. The SKA project is a collaborative scientific effort to build the world's largest radio telescope called the Square Kilometre Array. The project hopes to achieve this by combining thousands of individual receivers from across the world.

Since then, South Africa embarked on a mission to construct a precursor instrument consisting of an array of 64 receivers called the MeerKAT radio telescope, situated at the Losberg site in the Karoo, as a contributing receiver of the larger SKA radio telescope. The South African Radio Astronomy Observatory (SARAO), then known as SKA South Africa, is responsible for coordinating engineering, science and operation activities for the MeerKAT telescope. Since 2016, SARAO collaborated with the National Metrology Institute of South Africa (NMISA) to directly link the MeerKAT radio telescope's time to international atomic time (TIA) and universal coordinated time (UTC). NMISA is responsible for maintaining the national measurements including providing UTC South Africa UTC(ZA) time traceable to the UTC standard. The institute also contributes to the coordinated dissemination of UTC, an average time consisting of many state-of-the-art atomic clocks around the world. Given that Losberg is a remote and radio quiet area on which the MeerKAT radio telescope is located, SARAO will use satellite based remote clock comparison techniques (common-view) in order to compare the telescope's clocks with NMISA's UTC(ZA) clocks. The collaboration will enable the MeerKAT radio

telescope to accurately map the skies and detect undiscovered galactic radio sources. On 13 July 2018, the MeerKAT radio telescope was inaugurated and has already produced the clearest image of the region rounding the black hole located at the center of of the Milky Way Galaxy.

In order to produce such images, the MeerKAT radio telescope uses ultra stable atomic clocks to synchronously integrate all radio signals from the 64 receivers that are kilometers apart. In order to keep the time error to a minimum, optical fibre links are used to transport the time pulses from the primary atomic clocks to the digitiser of each receiver. The digitiser is responsible for recording samples of the signals emanating from the galaxies. Each of the digitisers inserts a time-stamp on each sample taken at a rate of 1.712 million samples per second. These time-stamps directly link the telescopes time to world-wide UTC through NMISA's UTC(ZA) time standard. To ensure that systematic delays (cable delays, optical fibre delays or processing delays) introduced by the telescope's subsystems are accounted for, there is a need for an independent method to test how well the receivers, intermediate subsystems and final data products are aligned to true UTC. Providing an independent method to verify MeerKAT telescope's time traceability to UTC(ZA) is the motivation for this thesis.

1.1 Motivation and contribution

Since NMISA is mandated to maintain national measurement standards, they have to regularly improve UTC(ZA)'s link to UTC with regards to their timing standards. The institution achieves this by using satellite systems such as the global positioning system (GPS), as a common view timing source to regularly monitor and steer their atomic clocks to within a few nanoseconds of UTC. SARAO's ability to synchronise its clocks with UTC will depend on advanced calibration with NMISA. Since calibrating SARAO's atomic clocks, switching them off and transporting them significantly changes their value of oscillation, the satellite based remote clock comparison technique was used to transfer NMISA's calibration time standard to the Losberg site. Once SARAO determined how far its clocks were from UTC, they distribute MeerKAT telescope time to individual receivers via optical fibre precise time transfer systems. Although the timing accuracy of MeerKAT telescope time to each of its receivers is known, there is a need for an independent method to test how well the receivers, intermediate subsystems and final data products are aligned to UTC. It is useful to discover any delays unaccounted for in the receiver that has a distributed time network. This thesis proposes a portable GPS time pulse radiator (GTR) device for testing the time-stamp accuracy of radio telescope data products.

The GTR was attractive in that it was independent to the timing infrastructure of the radio telescopes. In addition to being an independent system to the radio telescope,

the GTR device was desirable in that being a portable time fault finding instrument, it enabled users to isolate and individually test radio telescope receivers that form part of the larger system. The GTR's timing signal presents an opportunity for pulsar timing as it leveraged properties of pulsar signals with which pulsar timing systems can be used to evaluate the radio telescope time. The GTR has already been used by SARAO's time and frequency reference department, and pulsar timing astronomers for testing time-stamp accuracy of the MeerKAT radio telescope. The GTR was therefore an invaluable tool for verifying measurements of radio telescope precise transfer timing systems. It is important to note that the key to qualifying the GTR as a precise verification tool relied predominately on its accuracy. Calibration and rigorous error analysis was therefore one of the most important aspects demonstrated in this thesis. As MeerKAT's infrastructure

Figure 1.1: MeerKAT radio telescope.

evolves, it is imperative that the influence of the receivers, beamformer, correlator and optical fibre time transfer systems on the telescope's time relative to the time-stamps on final data products is known. The GTR device can be used on any similar radio telescope as a tool to comprehensively verify the timing accuracy of final data products time-stamps to UTC. The GTR's timing accuracy with respect to UTC was determined through calibration at NMISA. The analyses of the MeerKAT telescope's data products time-stamps with the aid of the GTR allowed for a holistic determination of the telescope's timing accuracy with respect to UTC(ZA) and UTC.

1.2 Research scope

In July 2015, Array Release 1 (AR1) of the MeerKAT radio telescope was announced. The AR1 milestone stated that MeerKAT would be ready to perform science by June 2016

with an array of 16 receivers. As MeerKAT's commissioning milestone was reached, the GTR concept shortly followed. As construction towards the full 64 receivers continued, an iterative design process was used to design, build, test and perform GTR field tests. This iterative design process was chosen so that MeerKAT's time accuracy could be evaluated as its telescope time ensemble evolved and number of receivers increased from 2016 to date. This would enable time and frequency reference (TFR) engineers to monitor the systematic impact of upgrading the telescopes timing infrastructure on the final data products produced by the MeerKAT telescope.

The final deliverable of this thesis is a portable GPS time pulse radiating device referred to as the GTR. The work documented in this thesis relates to the GTR's design, calibration and results collected during the field test. The objective of this research is to establish traceability of the device's time to UTC(ZA) through calibration with NMISA. The timing accuracy to be investigated is of the GTR device and not of the receiver under test such as the MeerKAT radio telescope. The GTR acts as a verification instrument and the timing uncertainties discovered from the radio telescope's data products are assumed to be of the respective radio telescope. The GTR's timing performance shall depend on the GPS receiver and associated hardware chosen. The radiated signal's frequency shall be within the intended receiver's frequency band (L-band for the MeerKAT telescope) and shall comply with the radio frequency interference (RFI) restrictions imposed on the observatory.

Chapter 2

Background theory and literature review

Section 2.1 initially discusses the literature review that establishes the background and context of the research. Subsequent sections provide the theoretical framework necessary to understand the underlying principles and technologies that the GPS time-pulse radiator (GTR) system is based on is further discussed. Section 2.2 outlines the two reference standards from which time is decimated from, namely, terrestrial timing standards and celestial timing standards. Section 2.3 introduces the global navigation satellite system (GNSS) concepts and elaborates on the determination of propagation delay of the signal transmitted by the satellites. The delay measurements are based on pseudorange measurements which are in addition used to determine position and clock bias. Dilution of precision quantifies the biases introduced by satellite spatial geometry relative to the observer. Sources of multipath, and mitigation techniques to minimise errors in the time solution are identified. Section 2.4 provides a brief technical overview of the GPS systems architecture, signals, measurements and performance.

2.1 Literature review

Telescopes are instruments that allow faint and distant objects to be seen as if they were brighter and closer to the observer. The earliest telescopes used an arrangement of lenses and mirrors to collect and magnify visible light that is emitted or reflected by stars or planets, some have evolved to detect radiation from sources emitting signals with wavelength's shorter and longer on the electromagnetic spectrum than visible light such as optical, radio, X-ray, Gamma-ray, and gravitational wave telescopes. Since the atmosphere is impenetrable for most of the electromagnetic spectrum, Earth bound telescopes located in radio observatories can only observe a few bands near infrared and radio waves. Gamma rays, X-rays, ultraviolet rays, and most of infrared rays are best observable from

space by satellite based telescopes. Radio telescopes are electronic instruments used in astronomy to locate celestial objects that emit signals not detectable by usual optical methods. They use directional antennas which receive signals from a specific direction allowing increased sensitivity and reduced interference from unwanted sources. The purpose of the antenna is to transform the astronomical signals arriving from a specific direction to electrical signals by a receiver. The receiver is configured to be sensitive to specific frequencies of interest and which amplifies and filters them before producing the output signal. When the radio telescope points in the direction of a celestial source, a signal appears at the receivers output and provides radio astronomers with measurements of the celestial body. The measurements consists of information such as the signal's strength and polarisation. Similar to optical telescopes, the resolution of the radio telescopes is deduced by the formulae λ/D, where λ is the wavelength used and D is the antenna diameter [16]. Having a large antenna array increases the telescope's sensitivity as a result of high angular resolution. Time and frequency reference signals are key to the operation of the radio telescope's time dependent equipment responsible for precise measurements of any type of precision radio astronomy measurement. Furthermore, telescope systems have very low phase noise requirements to enable high signal-to-noise (SNR) for astronomical observations [17].

The telescope receiver requires synchronisation among its digital instruments and the master clock that generates the reference signals. In order to form actual timestamps, various radio telescope architectures use global navigation satellite system (GNSS), atomic clocks, high precision phase synchronisation, and network access systems [18]. The time accuracy and stability of the telescope receiver is primarily attributed to the frequency standard of its local reference master clock. The local master clock implements the telescope's reference timescale. In order to establish traceability between the telescope's timescale and the International Systems of Units (SI), the current state of the art in time and frequency transfer involves the use of a GNSS common-view methodology which uses sophisticated GNSS receivers as a precise time and frequency transfer standard. The common-view methodology allows time and frequency laboratories to prove traceability of their local timescale to international timescales such as the Universal Coordinated Time (UTC) without the need to transport their standards for calibration [19].

Television transmission signals and other radar based time and frequency transfer system besides GPS cannot be used to synchronise the receivers as that would deem astronomical signals as unobservable. Radio astronomy observatories impose strict radio quiet zone policies to restrict transmitters within the vicinity of the telescope receivers. Currently, radio telescopes use high precision optical fibre based frequency synchronisation systems derived from their local atomic clock ensembles. Traceability is often easily proven between the telescope's master clock timescale and other international timescales using global navigation satellite systems such as GPS, however there is a need for time

traceability systems that can easily and independently prove traceability of telescope generated timestamps to international timescales. This area has been surprisingly neglected until recently, as the majority of the literature has been focused on the development of ultrastable atomic and optical clocks, timescale design, free space and fibre-optic based frequency synchronisation networks to time dependent equipment[17, 20, 21, 22].

The current state of the art in phase array time and frequency transfer involves high precision long-distance fibre based time and frequency synchronisation systems of ultra-stable atomic clock based reference signals transfer [23, 24, 25]. The radio telescope receiver designs require phase-coherent frequency reference signals at each antenna in the array to synchronise the received astronomical data [26]. Frequency coherence at each antenna is crucial in detecting astronomical signals with the best possible sensitivity attributed to the stability of the atomic clocks from which the reference frequency signals are derived. The astronomy data product timestamps are uniquely traceable to the radio telescope's timescale and is primarily intended to distinguish the generated data products from each other. The timestamping of astronomical signals is typically performed directly on the analog-to-digital converter (ADC) of the receiver. Verifying traceability through timestamps is advantageous as it presents a unique and holistic methodology of measuring systematic delays introduced by frequency synchronisation spanning science data processing, correlator and digitiser systems relative to the telescope's time and UTC. Timestamp accuracy verification checks performed with the use of the GPS time pulse radiator (GTR) instrument would be helpful in verifying the alignment of telescope time to UTC.

2.2 Time reference standards

All clocks use a physical phenomenon whose laws and progression is known [27]. In practice, time measurement is a frequency determination process. Traditionally, the measurements of time and position is based on terrestrial frequency standards with stability approaching 10^{-17} with significantly shorter averaging times. Due to the developments in astronomical geodetic applications, celestial reference systems were also realised. For practical time and frequency reference system applications, timescales were introduced to standardise the relationship of terrestrial clocks located in various spatial regions[6].

2.2.1 Terrestrial timing standards

Various time systems based on periodic processes such as atomic time and Earth rotation exits. The accuracy of satellite navigation fundamentally depends on the synchronisation of navigation satellite signals depicted in Figure 2.7 to onboard atomic clocks. Atomic clocks based on electron transition frequencies such as caesium, hydrogen, rubidium and

quartz as reference frequency standards. The caesium and hydrogen frequency standards have better long term stability whereas the quartz and rubidium have a better short term stability [6]. The electron transition frequencies *f(t)* can be modelled by the equation

$$f(t) = f_n + \Delta f + (t - t_0)\dot{f} + \tilde{f}(t) \tag{2.1}$$

where t denotes the time, t_0 denotes the reference epoch, f_n denotes the nominal frequency, Δf is the frequency offset, $\dot{f}$ is the frequency drift and $\tilde{f}(t)$ denotes the random frequency component. The frequency offset Δf can be calibrated and frequency drift $\dot{f}$ estimated using statistical methods such as Allan variance. The random frequency error $\tilde{f}$(t) is the main uncertainty[6].

Stability measures of frequency standards

The performance of frequency standards is characterised in terms of accuracy and stability. Frequency accuracy refers to the measure of ability of the frequency standard to resonate at the desired specification frequency. The measure of frequency deviation F is typically given as a specification frequency normalised defined as

$$F = \frac{f - f_0}{f_0} = \frac{\Delta f}{f_0} \tag{2.2}$$

where f and f_0 is the actual frequency, and specification frequency respectively. The frequency deviation error results in a time error over time Δ. The time error over a period T is defined as

$$\frac{\Delta f}{f} = \frac{t - t_0}{T} = \frac{\Delta t}{T} \text{ [19]} \tag{2.3}$$

Stability measure refers to the frequency standard's ability to resonate at the desired specification frequency over a period of time as expressed. The stability is typically quantified as short term referring to a one second period, or long term stability referring to a day's period. In practice, clocks have systematic and random frequency deviations due to the resonator frequency standard, environmental factors such as humidity, pressure, temperature, and vibration. Most GPS receivers are based on the quartz crystal oscillator oscillators such as oven compensated crystal oscillators (OCXO) and temperature compensated crystal oscillators (TCXO) as their source time. The quartz crystal oscillators have a short term stability of 10^{-9} to 10^{-11} and a long term stability two to three orders of degree worse[7]. Caesium and Rubidium oscillators have a good short term stability within the same order as quartz and an even better stability of 10^{-12} to 10^{-13}. The stability of quartz crystal oscillators is adequate enough to allow a GPS receiver to acquire and track GPS signals. The stability of clocks has exponentially improved over recent decades as illustrated in Figure 2.1. Figure 2.2 compares the rms error in the clock

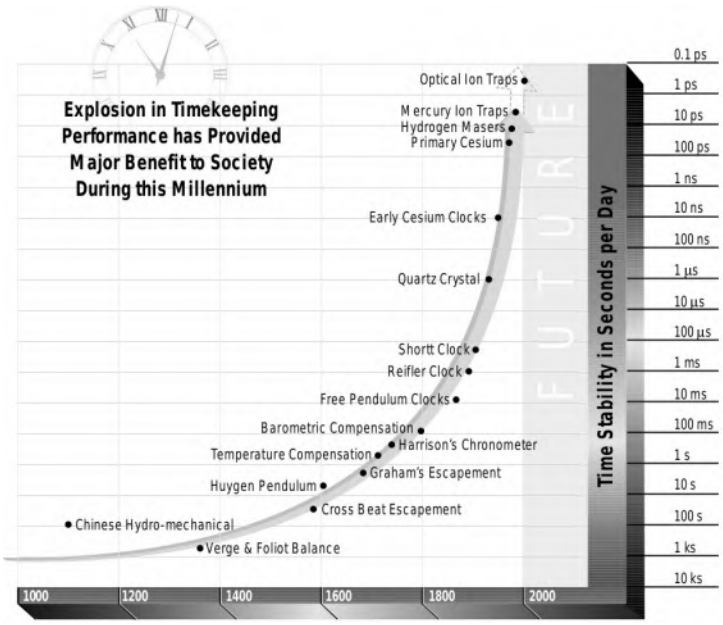

Figure 2.1: Evolution in timekeeping performance over the decades [1].

bias computed using 4-D estimates from differential GPS data of an OCXO, TXCO, Rubidium and Caesium oscillator over a 12 hour period. The purpose of the figure is to highlight predictable qualitative features of the different clocks. The Caesium oscillator has exceptional frequency stability without any apparent frequency drift. The Rubidium oscillator shows a constant frequency drift over an hour and a slight linear frequency drift over a 6 hour period. The OCXO oscillator resembles a significant quadratic trend with an average position and clock bias of 2 m/s and a drift rate of one part in a million. The TXCO oscillator did not resemble a predictable frequency stability and had an average position and clock bias of 200 m/s with a drift rate of hundred parts in a million. The

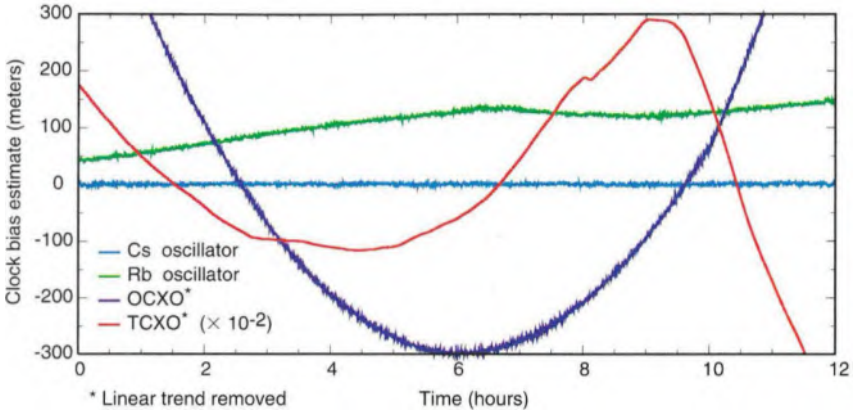

Figure 2.2: Clock stability comparison [2].

atomic clocks provide a method for timekeeping, however in order to create time standards expressing the time of day across different Earth time zones, properties of the solar system are taken into account. Earth's rotation is measured as the hour angle that lies between the reference Greenwich meridian and the meridian of fixed stars such as the sun.

Universal time (UT) is a time standard defined by the hour angle of an astronomical body or point on the Greenwich meridian with reference to the earth's equatorial plane. The hour angle of the vernal equinox defines the sidereal time. The earth's rotation angular velocity is not constant due to polar motions and Earth's rotational axis, as a result, the sidereal and solar time are nonuniform. The time standard UT1 is a polar motion corrected form of universal time and is given by the equation

$$UT1 = UTC + DUT1 \text{ [28]} \tag{2.4}$$

where DUT1 is the difference UT1-UTC as monitored and provided by the International Earth Rotation and Reference Systems Service (IERS) Bulletin A. When the absolute value of the term DUT1 is larger than 0.9, a second is added to UTC.

Dynamic time standards

Dynamic time standards are derived from planetary motions in the solar system[28]. The barycentric dynamical time (BDT) is a relativistic time standard that corrects for Earth's motion due to gravitational force of the solar system. The terrestrial dynamic time (TDT) standard, introduced before BDT, is one of earlier approximation to a uniform time for planetary motion calculations tied to atomic time by a constant offset of 32.184 seconds and is defined by the equation

$$TDT = TAI + 32.184 = UTC + (number\ of\ leap\ seconds) + 32.184 \text{ [28]} \tag{2.5}$$

The dynamic time standards are synthesized using atomic time standards[28]. International atomic time (TAI) is the current primary time standard that defines the SI (System International) second. TAI is realised by combining many clocks around the world. Each of the contributing clocks is corrected for known environmental and relativistic effects, as such TAI is an Earth based timescale. Universal coordinated time (UTC) is a time standard based on TAI, designed to coincide with UT1, as a result leap seconds are inserted. As a result, UTC is a discontinuous timescale. UTC time is given by the equation

$$UTC = TAI - (number\ of\ leap\ seconds) \text{ [28]} \tag{2.6}$$

2.2.2 Celestial timing standards (Pulsars)

The objective of this section is to provide a brief introduction and technical overview of pulsars as a potential time reference system. Pulsars are extremely dense, magnetised and rapidly spinning neutron stars characterised by periodic RF pulses. Pulsars can provide an independent precise time standard through which systems can be calibrated and potentially improve the atomic time timescale. Given the stability and lifetime of

millisecond pulsars, timekeepers have raised questions about whether pulsars can be used for timekeeping.

2.2.2.1 Lighthouse model

As neutron stars rotate, each pulse is observed when the electromagnetic beam crosses the observer's line of sight as described by the lighthouse model. The pulsar's repetition interval is determined by the rotation period of the neutron star. Pulsars are weak radio sources that require highly sensitive low-noise receivers performing long coherent integration with large samples to produce a detectable profile. Although each pulse is dispersive and has a unique profile at a given observation frequency, the resulting integrated profile is stable [4]. The key to accurate pulsar timing lies with the integration profile stability. Pulsars are given names after their position in the sky. Figure 2.3 shows a variety of pulsar profiles.

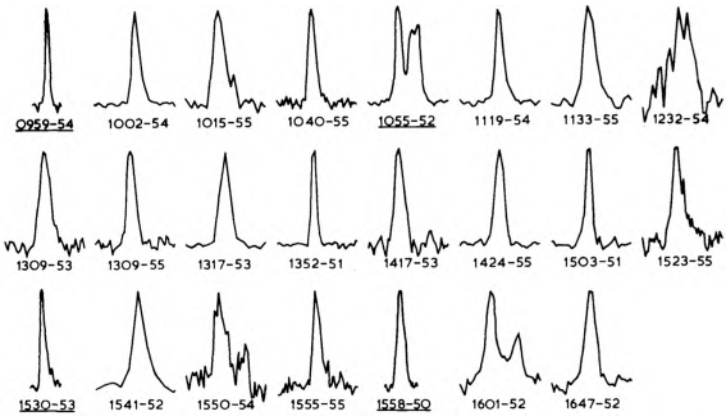

Figure 2.3: A variety of pulsar profiles [3].

2.2.2.2 Pulsar searches

As radio telescope sensitivity improves, the radio sky continues to be searched for new pulsars. Pulsar astronomers use a variety of search strategies which include all sky searches, galactic planes searches, intermediate and high galactic latitude searches, targeted globular cluster searches, targeted searches of other regions, and extragalactic searches. High galactic latitude all sky searches for millisecond pulsars have been effective in discovering the oldest radio pulsar population. Galactic plane searches have been effective in detecting newly formed pulsars. The pulsar surveys performed by Parkes, Arecibo and Effelberg radio telescopes have discovered large populations of young pulsars [29, 30]. The Parkes multi-beam pulsar intermediate and high galactic latitude searches have also been used to search deeply into the pulsar clusters. The deep probes helps pulsar astronomers better understand pulsar formations. Pulsars at high altitudes are important for millisecond pulsar timing arrays and gravitational wave search correlations. Rapid millisecond and

binary pulsar formations have been know to occur ten times more abundantly in the globular clusters than in the galactic disk [31]. As a result, targeted globular cluster searches have been effective in making those discoveries. Although globular cluster targets are known to contain large populations of millisecond pulsars, unidentified sources in other regions of the galaxy become regions of interest. The Allen, China's Aperture Spherical, Square Kilometre Array Pathfinder, and MeerKAT radio telescope will provide significant advancements for pulsar research [5].

2.2.2.3 Pulsar timing

The first pulsar to be discovered was found to be stable to one part in 10^7 over a few months and soon after, the millisecond pulsar B1937+21 was found stable to one part in 10^{13} [32, 33]. Soon after these discoveries, it was apparent that pulsars were remarkable celestial clocks. Regular pulsar timing measurements are performed monthly over the course of a year in order to study their characteristics. Figure 2.4 shows the main stages in pulsar timing measurements. The main objective of pulsar timing is to determine the time of arrival (TOA) of a radio beam (pulse) from neutron stars of interest using a radio telescope. Given that pulsars are weak signals and arrive at each receiver at different times, the telescope's processing resources perform de-dispersion and on-line folding to align the signals in time in order to expose the pulses by increasing the signal-to-noise ratio (SNR). During the measurements, the telescope's analog to digital converter (ADC)

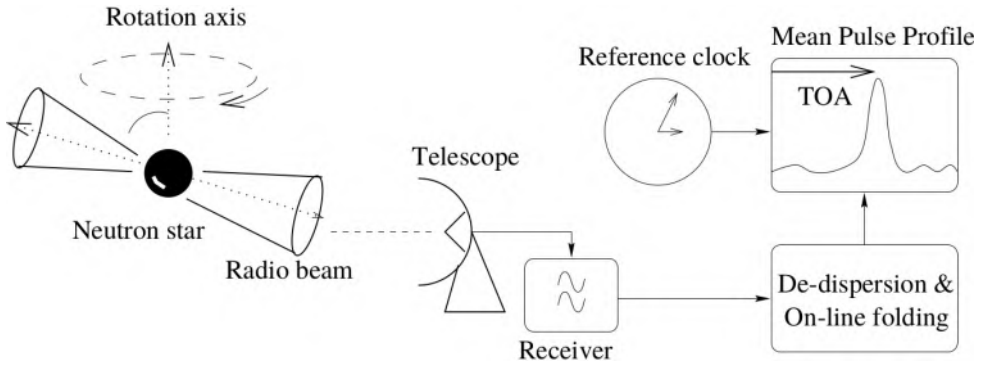

Figure 2.4: Main stages in pulsar timing measurements [4].

transforms the radio signals into digital signals and adds unique timestamps to each sample. In radio astronomy, the timestamps are usually coherent to an atomic timescale based on caesium or hydrogen maser frequency standards. Given that radio astronomy observatories are usually located in remote and radio quiet locations, their timestamps are traceable to their local metrology laboratory through GPS common-view technology [19]. The TOA is defined at a fiducial point on the integrated pulsar profile relative to some reference time since the measurement began. Since a pulsar profile is stable at any measurement frequency, the TOA can be accurately determined by cross-correlating the integrated pulsar profile with some noise free, high SNR, pulsar template. The TOA

uncertainty ϵ_{TOA} is defined as the ratio of the integrated pulse width and the SNR. The TOA uncertainty maybe written as [4]

$$\frac{\epsilon_{TOA}}{P} = \left(\frac{S}{mJy}\right)^{-1} \left(\frac{T_{rec} + T_{sky}}{K}\right) \left(\frac{G}{KJy^{-1}}\right)^{-1} \left(\frac{\Delta\nu}{MHz}\right)^{-\frac{1}{2}} \left(\frac{t_{int}}{s}\right)^{-\frac{1}{2}} \left(\frac{W}{P}\right)^{\frac{3}{2}} \quad (2.7)$$

where G represents the antenna gain, S represents the pulsar's flux density, T_{rec} and T_{sky} represent the receiver and sky noise temperature, $\Delta\nu$ represents the receiver's bandwidth, P represents the integrated pulse period and W represents the pulse width. In order to minimise the TOA uncertainty, the measurements should be performed on pulsar sources with large flux densities, short pulse width and short duty cycle using a large radio telescope with low noise and wide bandwidth receivers. An optimal measurement bandwidth should be chosen as wide band receivers increase pulse dispersion which increases the pulse width W and the TOA uncertainty ϵ_{TOA}. The receivers are usually configured in arrays because the combined sensitivity increases linearly with an increase in collecting area. Dispersion can be minimised by incoherent de-dispersion processing. Pulsars with short periods such as millisecond pulsars allow for excellent timing precision. The current state-of-the-art show that the advancements leading to the increase in low noise, wide-band receiver arrays, has decreased pulsar timing residuals while increasing their timing precision by 2–3 orders of magnitude over the past decade [5] as depicted in Figure 2.5.

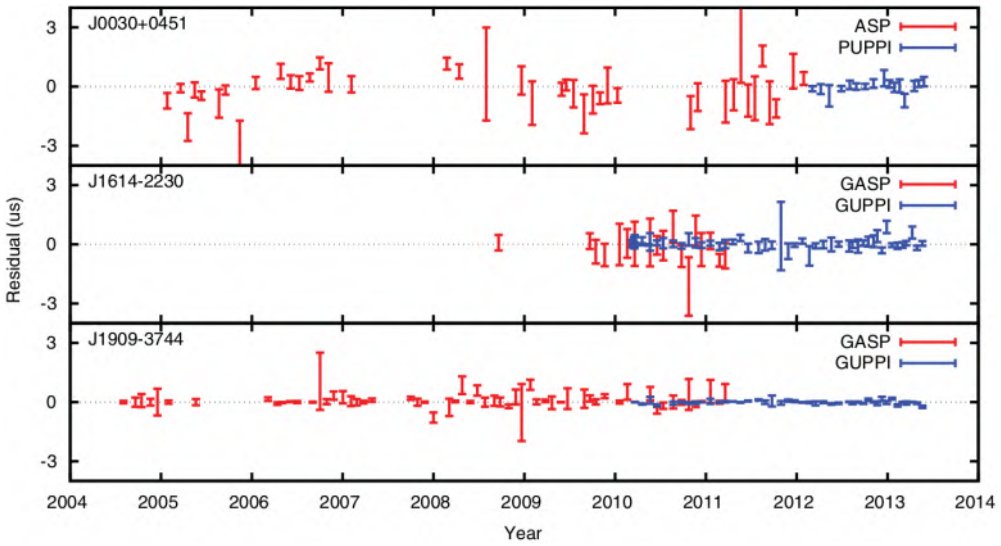

Figure 2.5: Improved timing residuals of three millisecond pulsars timed by NANOGrav [5].

2.2.2.4 Timing model

Ideally, the neutron star rotational properties require TOA measurements from an inertial observer. A radio astronomy observatory on Earth experiences gravitational accelerations relative to the neutron star due to Earth's rotation and solar orbit. The observatory is

therefore not in the inertial reference frame. The inertial reference frame is defined as the solar center of mass which is also refereed to as a barycenter. The TOAs determined on Earth are transformed to an inertial frame using planetary ephemeris [34]. The inertial frame transformation is given by

$$\tau - t = \frac{r \cdot \hat{s}}{c} + \frac{(r \cdot \hat{s})^2 - ^2}{2 \cdot c \cdot d} + \Delta t_{rel} - \Delta t_{DM} \tag{2.8}$$

where τ is the barycentric TOA, t is the observed TOA, c is the speed of light, r is the position of the observer relative to the barycenter and $\hat{s}$ is a unit vector in the direction of the pulsar at a distance d. The difference between the barycentric and observed TOA on the left of equation 2.8 is equal to the propagation time of light travelling from the barycenter to the observatory. The second term represents the spherical wave-front delay. The term Δt_{rel} is the general relativistic time delay correction. The term Δt_{DM} represents the observed TOA's equivalent observed at infinite frequency. The timing model given by equation 2.8 would have to be extended to account for additional barycentric motion if binary pulsars are considered.

2.2.2.5 Timing stability

The timing model given by equation 2.8 is ideally expected to return uncorrelated timing residuals with a zero mean and a Gaussian distributed scatter with a standard deviation that coincides with the TOA uncertainty. Practically, this is not always true as the most pulsar timing residuals resemble a pseudo-periodic response in time. The youngest of normal pulsars resemble this pseudo-periodic response the most when compared to much older millisecond pulsars [35]. It was soon discovered that the stability of pulsars is related to their lifetime [36]. The characteristics of the timing residuals can be better understood by improving measurement precision of the observing system [4]. Pulsar measurements spanning over a decade performed by groups in Berkeley, Jodrell Bank, Princeton, Swinburne and Pulsar Group of the Australia Telescope National Facility (ATNF) have demonstrated that millisecond pulsars provide timing stability comparable to terrestrial atomic clocks [4, 37, 38]. Figure 2.6 shows the outstanding stability expressed as Allan variance of a terrestrial atomic clock and three millisecond pulsars. Both B1855+09 and B1937+21 pulsars are comparable overall and slightly worse than the atomic clock after year 2 to 5 due to timing noise [36, 39]. In 2008, the precision timing results of the J0437–4715 millisecond pulsar located out of the Galactic plane, show that it is a phenomenally stable clock of about two orders of magnitude better than the other pulsars and atomic clock.

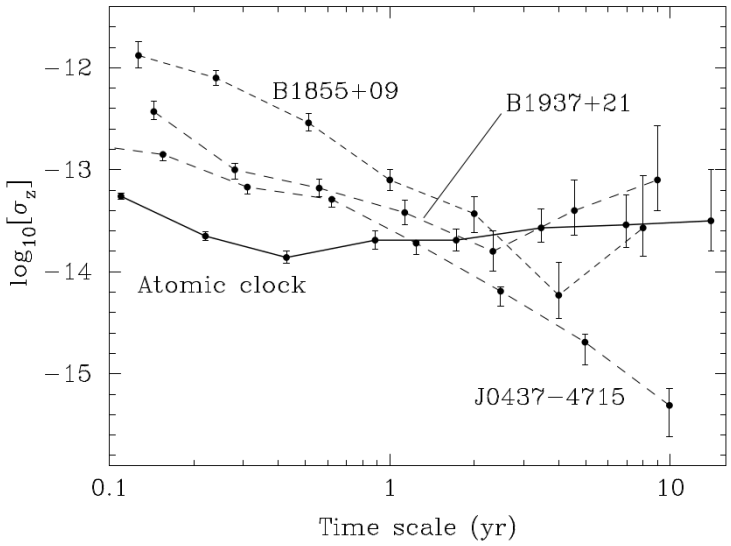

Figure 2.6: Stability comparison of a terrestrial atomic clock and three millisecond pulsars [4].

2.2.2.6 Pulsar time limitations

The limitations imposed on using millisecond pulsars as calibrators and space-time reference frames include inherent pulsar instabilities, uncertainties in terrestrial atomic timescales, pulsar position uncertainties introduced by the solar system planetary ephemeris, interstellar medium propagation errors and gravitation wave background noise, additional errors in terrestrial observer's receiver noise, time transfer system errors and uncertainties in binary orbit effects [36, 40]. The primary limitation in millisecond stability comes from the uncertainties in the neutron star rotation physics which is influence by the star's interior. Studies performed on large pulsar populations suggest that there is a correlation between the pulsar timing noise and the its rotation rate. This could be correlated to the magnetic breakdown slowing down the pulsar over its lifetime [41].

2.2.2.7 Future of pulsar timing

In order to define an inertial space-time reference, early pulsar timing specifications required a pulsar timing array of 10 millisecond pulsars with an approximately 100 ns rms timing residual over a 10 years measurement period [36]. Meeting such requirements would imply a timing accuracy of 10–20 ns and a stability of 10 ns over a year resulting in timing performance that rivals that of terrestrial atomic clocks. Given an ensemble of such pulsars, pulsars themselves would be used as the primary reference timescale. These naturally occurring clocks would also offer an independent method for Earth-based atomic clock verification, aid in gravitational wave detection and modelling of solar system planetary ephemeris. Terrestrial timescales such as UTC would only be required as carrier timescales to transfers pulsar TOA measurements during observations. A pulsar-based time reference frame would enable independent spacecraft navigation eliminating

the current two way space vehicle to Earth-time frame navigation system. The Parkes researchers have been processing pulsar observation datasets from a large number of pulsars to identify signals common to all pulsars in order to recover known pulsar offsets to the TAI and Terrestrial time as maintained by the International Bureau of Weights and Measures (BIPM) [40]. However, the observation datasets have different noise forms such as intrinsic pulsar timing noise that increase the timing residuals. They are currently improving routines to account for unmodelled noise sources to improve their pulsar-based time standard.

2.3 Global Navigation Satellite System (GNSS) observables

Satellite navigation systems can be classified into one way or two way active or passive ranging system. The three major GNSS constellations GPS, Galileo and GLONASS are passive one way ranging systems because users are required to only receive signals in order to determine their position, velocity and time (PVT). In contrast, two way ranging systems are classified as active systems because they require the user to transmit and receiver signals in order to determine their PVT.

2.3.1 Satellites signals

GNSS signals are designed to enable usage by an unlimited number of users for real-time ranging measurements. The signals are designed such that they do not interfere with signals of other systems as per International Telecommunication Union (ITU) restrictions. As depicted in Figure 2.7 the satellite's navigation signal consists of three layers, namely data-link, ranging code and physical layer [6]. The method of determining the propagation delay relies on transmitting a periodic continuous modulated signal that is synchronised to the system's time-pulse. The modulated continuous signal is exploited by the receivers correlation computations to determine the signal propagation delay. The physical layer defines the electrical properties of the signal in space. The data-link layer is responsible for generating the satellite ephemeris and time of transmission amongst other encoded information. Each satellite generated signal that is modulated by the ranging code and generated data message which is synchronously controlled by the onboard atomic clock as depicted in Figure 2.7[6]. The modulated signal is transmitted over a carrier frequency. GPS satellites carries frequencies are denoted by L1 (1575.42 MHz), L2 (1227.60 MHz) and L3 (1176.45 MHz). The transmitted signal propagates towards the receiver where position information is determined. A generic GNSS receiver consists of three functional block which includes a radio frequency (RF) front end, digital signal processing (DSP) and a navigation processor depicted in Figure 2.8[6]. The incident signal is received by

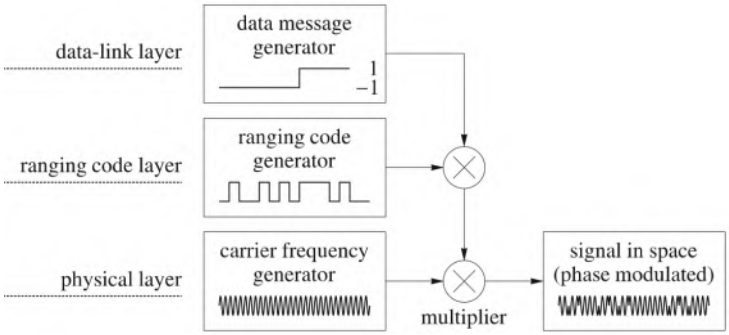

Figure 2.7: The figure shows the composition of the navigation satellite signal [6].

the antenna from which it is transformed from an electromagnetic signal into an electrical signal. The electrical signal is transferred to the front end where it is conditioned, down converted to an intermediate frequency (IF), and sampled by the ADC. For synchronisation, the front end implements the frequency standard that provide reference frequencies required for the determination of position, time and velocity information. Common inexpensive receivers use quartz crystal oscillators as their frequency standard. High-end receivers use rubidium standards as their frequency standard. The quartz crystal and rubidium standards do not provide the same stability as atomic clocks onboard the satellites. The DSP performs correlation computations between the receiver generated signal and the received signal to determine the phase, Doppler frequency and code ranges. The navigation message is decoded by the navigation processor to extract the ephemerides, almanac and time to determine the receiver position, time and velocity information.

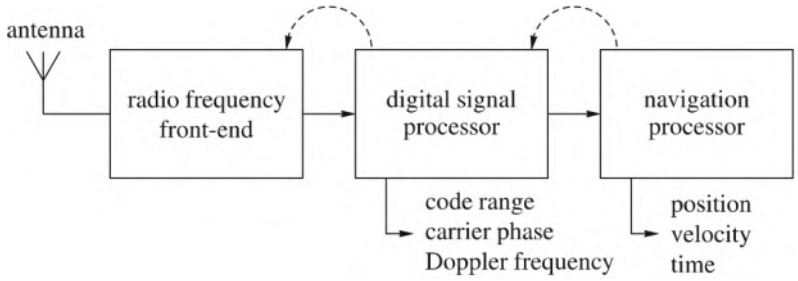

Figure 2.8: The figure shows the functional flow diagram of a GNSS receiver [6].

Electromagnetic waves are affected by various physical phenomenon differently depending on the frequency [6, 7]. Some of these phenomenon include reflections, refraction and energy change. An incident electromagnetic wave propagating between two different medium experiences partial reflection. There exists a symmetry between the reflected and incident wave. The electromagnetic waves not only propagating within the line of site of a transmitter and receiver but also reflected or scattered by object is referred to as multipath waves. An incident electromagnetic wave changes direction when it propagates from one medium into another through a process called refraction. Snell's law states that the secondary wave will be refracted by an amount equal to the ratio of the refractive indices

of both mediums. The electromagnetic wave energy changes are is propagates through the atmosphere. The change in energy is caused by absorption, attenuation, fading and interference.

The atmosphere is made up of five principal layers of gas surrounding the Earth. The neutral atmosphere that is extended from the earth surface to about 50 km height comprises of the troposphere and the stratosphere, introduces a delay to the electromagnetic wave called a tropospheric delay. The magnitude of the delay is determined by the temperature, pressure and water vapour. The GPS constellation for example, use signal in the L-band frequencies because they penetrate clouds, rain, fog and vegetation, as a result, GPS is operational in all weather conditions [7]. The ionosphere is the ionised upper most layer of the Earth's atmosphere. The electrical potential defined by the electron density of the ionosphere depends on the time of day. The ionospheric gasses alter the electromagnetic wave by advancing its phase. The receiver can determine the degree to which wave's phase change depending on its operational frequency.

2.3.2 Pseudorange measurements

Positioning and navigation with satellites conceptually involves time and phase determination through which the receiver to satellite range is calculated. Satellite navigation is based on a one-way passive ranging system consisting of a common system time on two clocks, namely the receiver clock and the satellite clock. The determined range is referred to as pseudorange because it is biased by the receiver and satellite clock errors. A GPS receiver estimates its 3-D position and clock bias with the aid of four or more pseudorange measurements. The overall accuracy of the receivers position depends on the pseudorange measurements and models used. The pseudorange given by equation 2.24 can be expressed as a matrix form by [42]

$$\Delta P_c = A\Delta x + e_c \tag{2.9}$$

where ΔP_c, Δx, A and e_c denote the k-length difference vector between modelled and corrected pseudorange values, four elements vector of the unknown receiver coordinates and clock bias, a $k\times4$ matrix of pseudorange partial derivatives with respect to the unknown receiver coordinates parameters, and k-length matrix of unknown biases respectively. Solving for the receiver coordinate and clock bias using the least squares method such as the Kalman filter gives the solution [42]

$$\Delta x = -\left(A^T W A\right)^{-1} A^T W \Delta P_c \tag{2.10}$$

The accuracy of the receiver coordinates given by equation 2.10 can be quantified by obtaining its covariance matrix $C_{\Delta x}$. The covariance matrix matrix of the unknown

receiver coordinates and clock bias is given by [42]

$$C_{\Delta x} = \left(A^T C_{\Delta P_c}^{-1}\right)^{-1} = \left(A^T A\right)^{-1} \sigma^2 = D\sigma^2 \tag{2.11}$$

where $C_{\Delta P_c}$ denotes the covariance matrix of the pseudorange measurements and σ^2 denotes the variance of the pseudorange measurements. The diagonal elements of the pseudorange covariance matrix $C_{\Delta x}$ are the required receiver coordinate estimate and receiver clock bias variance, and the other remaining elements quantify the correlation of these estimates.

2.3.3 Code pseudorange

The propagation delay of the signal transmitted by the satellite to the user receiver measured enables the determination of the pseudorange R. The satellite clock parameter t_{sat}, is transmitted in the satellites almanac as part of the navigation message. It contains the signal transmission time stamp with reference to the satellite's clock with a clock error δ_{sat} to the system time. The signal reception time t_rec with reference to the receiver's clock with a clock error δ_{rec} to the system time. The phase delay of the transmitted signal is equivalent to the time difference Δt between the reception and transmission time as determined by the correlation calculation. The time difference between the transmitted and received signal is given by [6]

$$t_{rec} - t_{sat} = (t_{rec} - \delta_{rec}) - (t_{sat} - \delta_{sat}) = \Delta t + \Delta\delta \tag{2.12}$$

where Δt denotes the clock error difference between the satellite and receiver clock. The satellites clock error correction for δ_{sat} is included in the navigation message, as a result, Δt is equivalent to the receivers clock error. The pseudorange R, obtained by multiplying equation 2.12 with the speed of light c, is given by [6]

$$R = c(\Delta t + \Delta\delta) = \varrho + c\Delta\delta \tag{2.13}$$

where ϱ is the true signal propagation distance between the satellite and receiver antenna.

2.3.4 Phase pseudorange

The phase equations describing the phase of the received $\varphi_{rec}(t)$ and receiver generated reference phase $\varphi_{ref}(t)$ signal, are given by [6]

$$\varphi_{rec} = f^{rec}(t - \frac{\varrho}{c}) - \varphi_{0rec} \tag{2.14}$$

$$\varphi_{ref} = f^{ref} t - \varphi_{0ref} \tag{2.15}$$

where f_{rec} denotes the frequency of the received signal, f_{ref} denotes the receivers carrier frequency reference and φ_0 denotes the initial signal phase. The phase difference between the received and reference signal at epoc t is given by

$$\Delta\varphi(t) = \varphi_{rec} - \varphi_{ref} = -f(\frac{\varrho}{c} + \Delta\delta) \tag{2.16}$$

According to [6], the phase of the satellite signal can be measured by the receiver with precision better than a millimetre for gigahertz range frequencies.

2.3.5 Dilution of precision

User equivalent range error (UERE) is a distance bias measure in meters, obtained inclusive of atmospheric error, ephemeris error, receiver noise error, satellite and receiver clock bias, and multipath. The UERE is typically expressed as the standard deviation of the estimated user position with the symbol σ_{UERE}. A smaller UERE value implies an improved estimation accuracy of the receiver coordinate and clock bias. The elements of matrix D in equation 2.11 are a function of the satellite to receiver spatial geometry, and their scaling factor referred to as the geometric dilution of precision (GDOP) implies a measure of pseudorange error. The corresponding position dilution of precision (PDOP), vertical dilution of precision (VDOP), horizontal dilution of precision (HDOP) and time dilution of precision (TDOP) are given by [42]

$$PDOP = \sqrt{D_{11} + D_{22} + D_{33}} \tag{2.17a}$$

$$VDOP = \sqrt{D_{11} + D_{22}} \tag{2.17b}$$

$$HDOP = \sqrt{D_{33}} \tag{2.17c}$$

$$TDOP = \sqrt{D_{44}} \tag{2.17d}$$

where D_{11}, D_{22}, D_{33} and D_{44} denotes the diagonal elements of matrix D of the pseudorandom covariance matrix given in equation 2.11. This research is an application of GPS time and frequency transfer for stationary receivers, which implies that the observation activities seek to obtain the smallest possible TDOP. The tips of the virtual tetrahedron shape formed by the spatial geometry of the GPS satellites and the receiver is related to the DOP. The larger the tetrahedrons volume, the smaller the DOP.

2.3.6 Satellite ranging errors

The code pseudorange, doppler measurements and phase pseudorange described by Equation 2.12 and 2.16 suffer systematic errors. The systematic errors can be divided into three categories, namely propagation errors, receiver errors and satellite errors. The propagation errors are introduced by atmospheric refractions as a result of the electromagnetic

waves propagating through the various layers of the atmosphere. Propagation errors can be corrected for by performing deviation measurements with the aid of tropospheric models on dual frequency data. The receiver errors are introduced by clock errors, antenna phase center variations and multipath. Receiver errors can be corrected for by using stable frequency standards, using antennas designed to mitigate multipath, using receivers in an environment least prone to reflections and performing deviation measurements between two satellites and one receiver [6]. The satellite errors are transmitted as part of the navigation message and are corrected for by the receiver. Additional satellite biases can also be eliminated by deviation measurements on data collected from two receivers tracking a single satellite [6].

2.3.7 Multipath

Satellite transmitted signals arrive at the receiver's antenna through direct and indirect paths. Reflective surfaces near the receiver's antenna, reflect signals arriving from an indirect path towards the receiver's antenna causing multipath. Multipath signals have a phase shift which equals the path length difference between the reflective path and the direct path. Performing a deviation measurement between ionosphere free carrier phases and code ranges exposes the systematic noise and multipath errors [6]. According to [43], multipath affects code pseudoranges by typically 10 to 20 m and more than 100 m in extreme cases such as when a receiver in close vicinity to a building [6]. For long baseline stationary GNSS surveys, multipath contamination least affects the pseudoranges compared to shorter baselines. The satellite transmitted signals r_{direct} propagating directly towards the receiver is given by [6]

$$r_{direct} = a\cos\varphi \tag{2.18}$$

where a denotes the signals amplitude and φ denotes the signals phase. The satellite transmitted signals $r_{indirect}$ propagating indirectly towards the receiver can be described by [6]

$$r_{indirect} = \beta\dot{a}\cos(\varphi + \Delta\varphi) \tag{2.19}$$

where β and Δ denotes the signals reflection damping factor and the delayed signal's phase shift. The damping factor β ranges between 0 and 1 depending on the properties of the reflective surface. The sum of both signals is given by [6]

$$r = a\cos\varphi + \beta\dot{a}\cos(\varphi + \Delta\varphi) = \beta_{indirect}a\cos(\varphi + \Delta\varphi_{indirect}) \tag{2.20a}$$

$$\beta_{indirect} = \sqrt{1 + \beta^2 + 2\beta\cos\Delta\varphi} \tag{2.20b}$$

$$\Delta_{indirect} = \frac{1}{2}\Delta\varphi \tag{2.20c}$$

where $\beta_{indirect}$ and $\varphi_{indirect}$ denote the damping factor and the delayed phase shift of the combined signal. Multipath is most destructive to the integrity of the direct signal when the damping factor β is equal to 1 and the phase shift $\varphi_{indirect}$ is equal to 90° which translates to a range of $\lambda/4$.

Multipath reduction

According to [44], various multipath mitigation techniques include receiver antenna based mitigation, receiver technology improvement and improved digital signal processing. Receiver antenna based mitigation techniques comprises of antenna design that takes takes advantage of signal polarisation, improves antenna gain pattern by choke ring designs and creating other specialised antenna designs and arrays. Choke ring antennas mitigate multipath by rejecting multipath signals. Receiver processing improvement comprises of digital filtering. Receiver technology improvement comprises of the use of multipath estimation delay locked loops, multipath correlation rejection and correlation spacing narrowing. According to [6], multipath can also be effectively mitigated by avoiding reflecting environment such as elevated structures, placing receiver antennas on the ground and using the receiver in a stationary mode.

2.4 Global Positioning System (GPS)

GPS positioning is based on determining the propagation time of the signal that is transmitted by the satellites and received by the users. All satellite positions in orbit are known to within an accuracy of a few meters due to the precise measurements of propagation time aided by ultrastable atomic clocks onboard the satellite. To measure the true propagation time, the GPS satellites and receiver need to be synchronised. The satellite places precise time markers and other clock parameters in its navigation message which the receiver uses for synchronisation [7]. The objective of satellite navigation is to determine the users three coordinate of position and time. The resulting equation ρ and clock bias b are given in Figure 2.9. In addition to GPS, other satellite navigation systems including the Russian Global Navigation Satellite System (GLONASS), European Galileo and the Chinese regional system Beidou were developed. The term Global navigation satellite system (GNSS) is a collective term used for all satellite based navigation systems. GPS is the pioneer, most matured and leading satellite navigation system which currently has the largest uniformly distributed constellation with 31 satellites in orbit. In order to calibrate the GTR instrument and maintain a known timing accuracy, a single GNSS system is used to avoid contaminating its accuracy with small time offsets between different GNSS systems. It is for this reason this research was based solely on the GPS system.

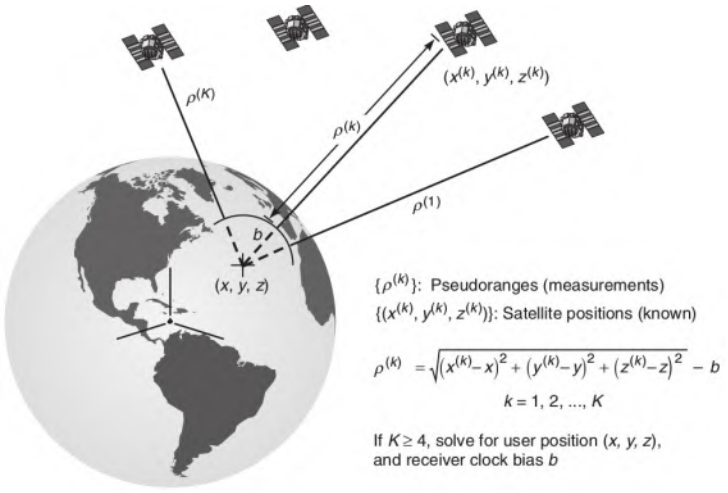

Figure 2.9: Principle of satellite navigation [7].

2.4.1 Time system

GPS system time is based on the GPS atomic timescale implemented by the GPS ground control segment. GPS time coincides with UTC atomic timescale as maintained by USNO by an integer offset of 18 seconds in August 2019. The offset increases when leap seconds are added onto the UTC timescale. GPS time coincides with the TAI timescale with an integer constant offset of 19 seconds. The relationship of GPS and TAI timescale is given by [6]

$$TAI = GPS + 19 \ seconds \tag{2.21}$$

GPS time has a standard epoc beginning midnight January 6, 1980. The system time of GPS is expressed in terms of GPS weeks and seconds of the current week. The GPS week can be determined using [6]

$$GPS_{week} = integer(\frac{JD - 2444244.5}{7}) \tag{2.22}$$

where JD denotes the Julian date. The timing accuracy of a relatively cheap GPS receivers is comparable to that of expensive clocks. GPS technology has since enabled global time distribution.

2.4.2 System architecture

GPS architecture consists of three segments, namely, the user, control and space segment. The control segment consists of equipment responsible for managing the GPS satellite consultation and the space segment refers to the satellite constellation in orbit. The user segment consists of civilian and military equipment that provide an interface to the GPS systems observations such as position, velocity and time.

2.4.2.1 Space segment

The GPS satellite constellation has a nearly circular orbit at an altitude around 20200 km and a 12 sidereal hour period. A nominal constellation providing 24 hour world wide coverage consists of at least 24 satellites of which a minimum 4 satellites are visible at each of the six orbital planes. There are between four to eight satellites providing worldwide visibility above 15° elevation at any time of the day [6]. GPS satellites are categorised into various Blocks, namely Block I, Block II, Block IIA (Block II advanced), Block IIR (Block II replacement), Block IIR-M (Block IIR modernised), Block IIF (Block II follow on) and Block III. Each GPS constellation Block revision is designed for a limited operation duration which allows for incrementally modernised satellites. The next generation Block III, also referred to as GPS III constellation, is expected to be launched no earlier than October 2018 [45]. It will further the modernisation standards of the GPS constellation by providing enhanced accuracy, availability, integrity and reliability.

2.4.2.2 Control segment

The control segment consists of a master control station, numerous monitoring stations and ground antennas [7]. The control segment is responsible for tracking and predicting the GPS constellation's orbit, atomic clock parameters and time synchronisation. Key satellite parameters can be modified in real time through the master controller's data upload capability. GPS time is defined through an ensemble of atomic clocks in the monitoring stations and satellites. The master control station maintains synchronisation with the satellites by monitoring and predicting the offsets and clock drifts of each satellite, and uploading the correction parameters of such errors in the satellites navigation message. The functions of the master control station are:

- To maintain and monitor satellites health.
- To maintain, monitor and predict satellites orbits.
- To maintain the GPS timescale.
- To monitor and predict satellite clock and navigation parameters.

The master control station collects satellite tracking data from various monitoring stations in order to predict clock and orbit parameters using the Kalman filter. With the help of ground antennas, the predicted corrections are uploaded to the GPS constellation. Each GPS monitoring station is responsible for measuring pseudoranges to each satellite of the GPS constellation every 1.5 seconds. The pseudoranges are further corrected for ionospheric and meteorological errors to produce data with a 15 minute interval which is transferred to the master control station. The ground antennas responsible for uploading and downloading data to and from the GPS constellation are situated at the monitoring station. The antennas are designed to receive ranging and telemetry data from the satellites and to transmit control instructions and data to the satellites. The ground antenna

to GPS satellite communication occurs over an S-band RF carrier three times a day [6]. The predicted ephemeris and clock data that is uploaded to the GPS satellite allows for a reduced degradation of GPS position accuracy in the event of a ground antenna failure.The control segment's modernisation project seeks to improve system performance and reduce operational costs. The main improvement brought by modernisation include [46, 47]

- Upgrading the infrastructure in the master control station, monitor stations and associated ground antennas.
- Incremental improvement of ranging accuracy by improving the navigation message and other signals.
- Implementing a master control station that is fully equipped with both the monitoring and ground antenna capabilities.
- Improving the Kalman filter responsible for pseudorange estimations.
- Improving orbit and clock information, and the ability to monitor GPS constellation performance overall.

2.4.2.3 User segment

Advancement of GPS over the decades has resulted in spectacular developments in integrated circuits, which has significantly contributed to miniaturised, light and inexpensive receivers. The development of GPS receivers has produced novel inventions in consumer products, land and marine transportation, aviation and space navigation, and high-precision metrology services.

2.4.3 Positioning services

GPS provides positioning and timing with two grades of accuracy, namely the standard positioning service (SPS) designated for civilian users and precise positioning service (PPS) designated for authorised users. The accuracy of the GPS system depends highly on the stability of the onboard atomic clocks which are typically based on the hydrogen maser and caesium frequency standards with a long term stability reaching 10^{-13} and 10^{-14} parts per day [6]. Two GPS signals carrier frequencies L1 (1575.42 MHz), L2 (1227.60 MHz) and L5 (1176 MHz) are derived from the atomic clock resonant frequency of 10.23 MHz which is multiplied by 154, 120 and 115 respectively. The two signals allow the dual frequency receivers to remove ionospheric errors as mentioned in Section 2.3.6. The L1 signal is modulated with a coarse-acquisition (C/A) code which implements the freely available SPS for civilian users. The SPS signal in space accuracy based on 95% probability and satellites in view with an elevation mask of 5° is summarised in Table 2.1. The signal in space accuracy does not account for atmospheric, multipath and receiver errors. The general accuracy is stable and consistent but the perceived performance depends on

conditions unique to the user [48]. The L2 signal is modulated with a precise (P) code

Table 2.1: Standard positioning service (SPS) accuracy [6].

SPS accuracy standard	Conditions and constraints
$\leq$ 22 m vertical $\leq$ 13 m horizontal	Global average based on 24 hours averaged data-set of all satellites in view with a 5∘ elevation mask.
$\leq$ 77 m vertical $\leq$ 36 m horizontal	Worst global average based on 24 hours averaged data-set of all satellites in view with a 5∘ elevation mask.
$\leq$ 40 ns time transfer	Global average based on 24 hours averaged data-set of all satellites in view with a 5∘ elevation mask.

to implement PPS for authorised users. The P code is also modulated into the L1 signal but remains encrypted to deny full system accuracy to unauthorized users with single frequency receivers. The PPS signal in space accuracy based on 95% probability as given by [14] is summarised in Table 2.2. PPS provides enhanced accuracy, availability and

Table 2.2: Precise positioning service (SPS) accuracy [14].

SIS accuracy standard	**Conditions and constraints**
Dual frequency P(Y) code for visible satellite marked healthy in the navigation message	
	Global average based on any age of data
$\leq$ 11.8 m	Global average UTC offset error (UTCOE) based on any age of data
$\leq$ 40 ns	
$\leq$ 0.006 m/s	Global average over any 3 s interval at any age of data
Single frequency P(Y) code for visible satellite marked healthy in the navigation message	
$\leq$ 12.6 m	Global average based on any age of data
$\leq$ 40 ns	Global average UTCOE based on any age of data
$\leq$ 0.006 m/s	Global average over any 3-second interval at any age of data

immunity to interference or jamming compared to SPS. The advantages of these enhancements are further apparent by providing immunity to a military scenario where enemy combatants may jam electronic communication.

2.4.4 Signal structure

Each of the GPS satellite signals consists of three components:

- *Carrier frequency*: GPS satellite RF signal with frequency L1, L2 and other additional frequencies.
- *Pseudo-random noise (PRN) code*: Each satellite is identified by a unique binary sequence called a PRN code. The unique sequences are designed to allow multiple satellite to transmit signals simultaneously on the same carrier frequencies without mutual interference and allow the receiver to determine the signals propagation time. The transmitted signals consists of two codes, namely, a course/acquisition code (C/A) and a precision (P(Y)) code. The unique C/A code is made up of 1023 bits and has a period of 1 μs with a 300 m wavelength. Unlike the C/A code, P(Y) code is a much longer 10^{14} bit sequence with a shorter 30 m wavelength. The shorter wavelength improves the precision of the range measurements than of the C/A code [7]. The P(Y) code is encrypted and usable only to authorised users with decryption keys.
- *Navigation data*: The navigation message contains satellite almanac, health status, orbit information and clock bias information. It is transmitted by the satellites at a 50 bits per seconds rate, and it takes 12.5 minutes to transmit the entire message. GPS receivers use the navigation message to estimate the signals propagation time for position estimation.

These components are combined synchronously from an atomic standard to produce GPS signals. The GPS signal transmitted by the nth satellite is given by [7]

$$\begin{aligned} s^{(n)} = &\sqrt{2P_c}x^n(t)D^n(t)\sin(2\pi f_{L1}t + \theta_{L1}) + \\ &\sqrt{2P_{Y1}}y^n(t)D^n(t)\cos(2\pi f_{L1}t + \theta_{L1}) + \\ &\sqrt{2P_{Y2}}y^n(t)D^n(t)\cos(2\pi f_{L2}t + \theta_{L2}) \end{aligned} \tag{2.23}$$

where P_c, P_{Y1} and P_{Y2} is the power of the signals that contain the C/A and P(Y) codes on the carrier frequency *L1* and *L2*. $D^{(n)}$, θ_{L1} and $\theta L2$ denotes the navigation data binary sequence, and phase offset respectively. The signals provided in the approved lexicon of GPS signals [49] are the main signal of interest in this research and does not include other signals such the S band RF carrier used by the ground antennas for two way communication with the GPS satellites. GPS satellites have been transmitting ranging signals over the L1 and L2 carrier frequency since the early GPS constellations. The recent introduction of the L1C and L5 carrier frequency and additional navigation messages complements the GPS modernisation objective by providing more signal power, improved interference resistance through the military M code, better signal correlation and improved precision [48]. The satellite's beam pattern is limited to an angle of 27.8° and satellite's footprint defined as the portion of the earth's surface visible from the satellite, covers approximately 38% of the earth's surface [14]. Various GPS receivers have an adjustable masking angle which should be chosen as a function of the environment within

which the receiver will be used and the minimum received signal power required. All GPS satellite signals are circularly polarised and deviate from perfect polarisation by no more than 3.2 dB [6]. The key to accurate satellite ranging depends on the inter carrier frequency code sequence synchronisation between multiple GPS satellites.

2.4.5 GPS receiver

A GPS receiver collects signals using an omnidirectional antenna. Assuming the receiver has received the complete navigation messages, it extracts the constellations health, coarse orbit and clock bias information to determine the receivers rough position from the satellites in view [7]. Given the satellites PRN codes, the receiver generates local replicas of the expected C/A codes, and uses them to acquire and track the signals from all visible satellites. The receiver performs auto-correlation of the received signal and the receiver generated replica to acquire the signal. When the two signals align, the correlation produces a peak with an error limited to the 1023 code bits. After acquiring the signal, the receiver uses the aid of the navigation message to indirectly acquire the P(Y) code. In order to continuously align and track the local replica code to that of the acquired signal, the receiver makes use of a delay locked loop and phase locked loop. The acquired signals propagation time is measured as the time shift required to align the replica code and the received signals code modulo one millisecond. The receivers position is determined by taking pseudorange measurements from four or more satellites. Given the satellite's velocity vector derived from the navigation message and the pseudorange rate, the receivers velocity can be determined. The GPS receiver is responsible for the following

- To receive satellite transmitted RF signals.
- To uniquely identify satellite signals.
- To determine signal propagation time and pseudoranges.
- To analyse the navigation message in order to resolve satellite position, velocity and clock biases.
- To determine GPS user position, velocity and time.

2.4.5.1 Position, velocity and time (PVT)

The accuracy of the user PVT estimates depends on two factors, namely, the number of visible navigation satellite and their observation geometry in orbit, and the accuracy of the pseudorange measurements. The observation geometry represents the satellite arrangements in the sky relative to the GPS receiver on earth. In order to maximise PVT accuracy, the tips of four visible receiver to satellite unit vectors should form a tetrahedron figure. The more the satellites are spread across the sky, larger the tetrahedron volume which results in better PVT estimates [42]. The measure of observation geometry quality if typically expressed as position dilution of precision (PDOP). Depending on the time of day

and location, the estimate error introduced by the observation geometric factor gives the error in position or time. The choice of the best four satellites to use in the measurements depends on the receivers satellite selection algorithm. The seconds factor influencing the accuracy of the user PVT estimate is the accuracy of the pseudorange measurements. The errors in the parameters of the satellites navigation message introduces additional errors in receiver estimated pseudorange measurements [7]. Signal distortions such as atmospheric propagation delays contribute the largest source of errors and can be mitigated by the use of dual frequency receivers. Depending on the observation environment, multipath errors may dominate the position measurements and can be mitigated by using choke ringed receiver antennas. Electronic equipment have an inherent system noise which can be characterised through calibration in order to mitigate measurement errors. The transmitted signal given by equation 2.23 propagates through the atmosphere and is received by the receivers antenna. The model of the pseudorange measurement from the nth satellite is given by [7]

$$\rho^{(n)} = \sqrt{(x^{(n)} - x)^2 + (y^{(n)} - y)^2 + (z^{(n)} - z)^2 + b + \rho^{(n)}} \tag{2.24}$$

where $(x^{(n)}, y^{(n)}, z^{(n)})$ denotes the nth satellites position as given in the navigation message, b and $\rho^{(n)}$ denotes the unknown receiver clock error and other unknown measurement errors respectively. In order to solve for the receivers position, four equations are required to solve for the four unknown pseudorange parameters. Consequently, a minimum of four GPS satellites are required to solve for the PVT observables.

2.4.5.2 Time transfer

The concepts of accurately determining and establishing time traceability to a calibrated laboratory are key to the GTR's timing accuracy. The timing community typically make use of GPS timing receivers which produces a 1-pulse-per-second (1PPS) clock signal indicating the exact time. Actually, the 1PPS clock signal generated by GPS receivers is synchronised to UTC (USNO) realised by the U.S. Naval Observatory. The GTR instrument presented in this thesis uses its receiver generated 1PPS signal as the reference clock signal against which the receiver under test's clock is compared. The specially designed timing signal transmitted by the GTR is synchronously modulated by this 1PPS signal. Given the MeerKAT telescope as an example, the offset of the GTR's 1PPS clock signal relative to the telescope time can be determined from the time-stamps assigned to the dataset of the captured GTR's timing signal. The telescope time can also be determined by sampling the GTR 1PPS clock signal using its pulsar timing system. These timing tests are elaborated further in Chapter 3.

Unlike navigation receivers, timing receivers typically average their stationary antenna position over some extended survey period and at the end of the period will save

the final average position as the reference position. The timing receiver then no longer solves its position, it instead switches into the timing mode during which it only solves for clock error and clock bias using the available GPS satellites. In order to generate the 1PPS clock signal, the GPS receiver has to deal with the following timescales [7].

- The satellite's clock time (t_{sat}).
- GPS time (t_{GPS}) as kept by the U.S. Naval Observatory.
- UTC(USNO) ($t_{UTC(USNO)}$) as kept by the U.S. Naval Observatory.
- The user's receiver clock (t_{user}).

The satellite clock bias to GPS time t_{GPS} is given by [7]

$$\delta t_{sat} = t_{sat} - t_{GPS} \tag{2.25}$$

The value of δt_{sat} is provided as one of the correction parameters in the navigation message. The offset of GPS time relative to UTC (USNO) is given by equation 2.26 [7]. The offset information is provided to GPS's control segment.

$$\delta t_{UTC(USNO)} = t_{GPS} - t_{UTC(USNO)} \tag{2.26}$$

The bias between GPS time and UTC (USNO) can be instantaneously determined from

$$\delta t_{UTC(USNO)} = A_0 + A_1(t_{GPS} - t_{0U}) + \Delta t_{LS} \text{ [7]} \tag{2.27}$$

where A_0 and $A_1(t_{GPS} - t_{0U})$ specify the bias modulo 1 second, and Δt_{LS} is the integer number of leap seconds added to UTC. The values of the parameters required by equation 2.27 transmitted as part of each satellite's navigation message. The receiver clock bias δt_{user} relative to GPS time is given by [7]

$$\delta t_{user} = t_{user} - t_{GPS} \tag{2.28}$$

The receiver clock bias term δt_{user} includes delays due to the antenna cable, preamplifier, and receiver hardware. The error in the estimated receiver clock bias can be determined by accounting for the UERE standard deviation σ_{UERE} and TDOP presented in section 2.3.5. The rms error in δt_{user} is given by [42]

$$\sigma(\delta t_{user}) = \sigma_{UERE} \cdot TDOP \tag{2.29}$$

Given a 24 satellite constellation, the term σ_{UERE} is typically 6 m and TDOP $\approx$ 1–1.5, therefore, a receiver clock bias with an rms error $\sigma \approx$ 25ns can be expected [7]. Finally,

the receiver generated 1PPS clock signal synchronised to UTC (USNO) is given by [7]

$$t_{UTC(USNO)} = t_{user} - \delta t_{user} - \delta t_{UTC(USNO)} \tag{2.30}$$

GPS provides two techniques of distributing time, namely, direct time distribution and common-view (comparison of remote clocks). Given the antenna position, a receiver can routinely determine the precise time by tracking a single GPS satellite with an accuracy of approximately 30–100 ns [19, 7]. The direct time distribution concept is based on this concept as illustrated in Figure 2.10. The GTR instrument uses the direct time distribution technique primarily because of mobility requirements as stated in section 1.2. In this scenario, GPS becomes a time transfer standard that provides GTR traceability to USNO. GTR's traceability to NMISA is established through calibration and is elaborated further in Chapter 3.

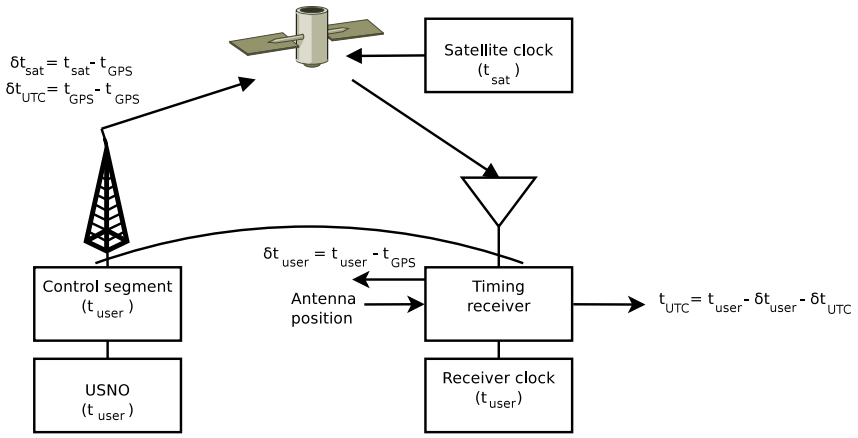

Figure 2.10: GPS direct time transfer [7].

Specialised users apply common-view time transfer techniques to achieve better timing performances. This technique is typically used in internationally recognised timing laboratories and radio astronomy observatories which require receiver clock errors in the orders of a few nanoseconds. The observing laboratories equipped with atomic clocks kept in a controlled environment track common satellites, using the same protocols over the same survey period and exchange timing information to compare their clocks. GPS common-view can provides time transfer with an accuracy of approximately 1–5 ns [19, 7]. The frequency difference between two laboratories observing a common GPS satellite k is given by

$$(LAB_A - GPS_k) - (LAB_B - GPS_k) = (LAB_A - LAB_B)\ [19] \tag{2.31}$$

where LAB_A and LAB_B are the two laboratories respectively. The right hand terms of equation 2.31 shows that the frequency difference can also be calculated by taking the reciprocal of the time difference between the two laboratories. Given the absolute

frequency of one of the laboratory clock, the absolute frequency of the second laboratory clock can be calculated. In this scenario, GPS becomes a time transfer standard that shares traceability between the laboratories. The concept is illustrated in Figure 2.11. The

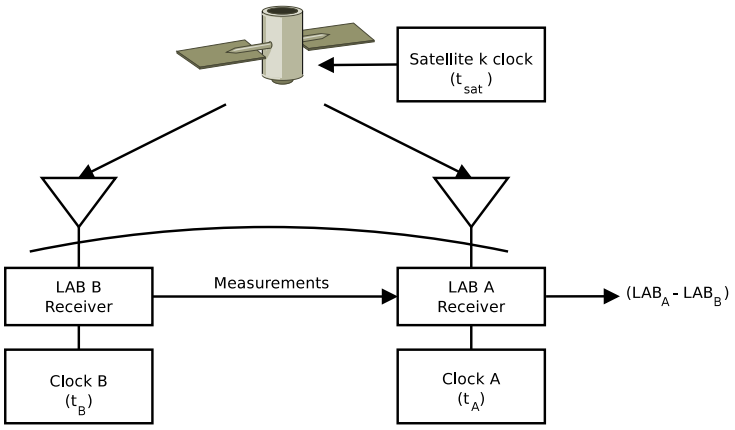

Figure 2.11: GPS common-view time transfer [7].

BIPM maintains the UTC timescale and is responsible for regularly collecting common-view timing data from participating international timing centers. The data is correlated in order to remove errors to the extent possible in order to disseminate UTC.

Chapter 3

Design and implementation

In order to test time-stamp accuracy of a radio telescope, this chapter discusses the detailed design and implementation of the proposed GPS time-pulse radiator (GTR) instrument. The GTR instrument used an onboard GPS timing receiver to acquire and track the GPS constellation in order to determine its position, and precise time. Once the precise time was determined, the GTR generated a 1-pulse-per-second (1PPS) clock signal synchronised to the universal coordinate time (UTC) standard which served as the reference time. The 1PPS clock signal was used as the instrument's reference clock responsible for modulating the radiated timing signal. The time-stamp testing device called the "GTR instrument" will be refereed to as "GTR" for the rest of this thesis. The concept and intended application is depicted in Figure 3.1.

In this chapter, the GTR's user and system requirements are stated in Section 3.1. Given the finite financial resources and imposed requirements, the resources, limitations and subsystem details used in the design are discussed in Section 3.2. The concepts on which each of the GTR's subsystems is based on are given in Section 3.2. The GTR's detailed design and implementation is given in Section 3.3. The detailed design on calibration and error analysis methodologies used to determine the GTR's timing accuracy are given in Section 3.4. The detailed designs of methods used to test radio telescopes are given in Section 3.5. The summary of the project tasks and how they were implemented is given in Section 3.6.

3.1 Requirements

The GTR instrument's had two main users, namely, MeerKAT system engineers and commissioning scientists. The user requirements were determined through requirements gathering involving a series of meetings with the users. The requirements gathering process involved solicit system requirements, prioritising project goals, and identifying risk to ensures that each requirement was achievable, verifiable, unambiguous, and complete. The associated system requirements were solicited and derived.

3.1.1 User requirements

1. The instrument shall radiate a timing signal that coincide with UTC to be used for testing time-stamp accuracy of a radio telescope.
2. The instrument shall use GPS for time and position.
3. The instrument shall be calibrated using a scientifically acceptable method.
4. The instrument shall comply with radio frequency interference (RFI) restrictions at MeerKAT site.
5. The user shall be able to carry the instrument and perform tests on various receivers with ease.
6. The instrument shall have a self contained power supply able to run the instrument for a full work day without recharging.

3.1.2 System requirements

1. The GTR shall radiate a periodic timing signal that coincide with UTC(USNO) standard.
   (a) The GPS timing receiver shall be calibrated at an official metrology institution.
   (b) Each pulse shall coincide with the UTC second with an offset not more than 500 μs.
   (c) The pulse shall be emitted only when GPS is locked.
   (d) The timing signal rise time shall shall be no more than 1 μs.
2. The timing signal shall comply with radio frequency interference (RFI) restriction imposed by the radio astronomy observatory.
3. The GTR instrument shall be portable.
   (a) The GTR shall be battery powered.
   (b) The GTR shall use low cost disposable batteries.
   (c) The battery shall have a lifetime not less than 8 hours.
   (d) The battery shall be easy to replace without the use of tools.
4. The GTR design shall use human factors and ergonomics principles.
   (a) The GTR shall not harm its operator.
   (b) The GTR shall have no vulnerable protruding breakable parts.
   (c) The GTR shall provide visual indicators for battery life and other major operations.
   (d) The instruments shall have clearly visible markers of name, purpose, frequency, output and other items visible on the enclosure.
5. The GTR shall operate successfully in both dry and wet weather conditions.

The requirements and associated constraints influence the exploration of possible solutions

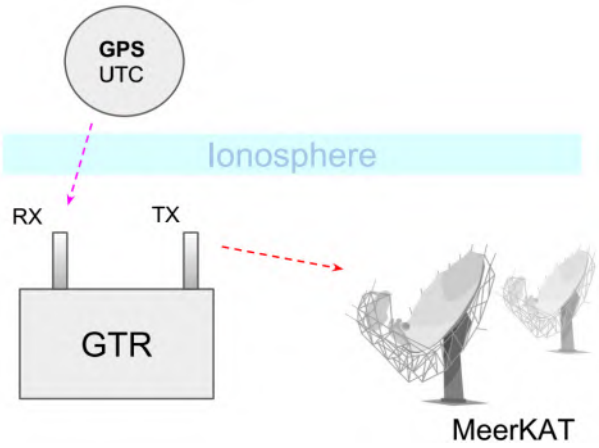

Figure 3.1: The figure depicts the concept and intended application of the GTR.

and final choice of solution. Given that the GTR is made up of various subsystems, the choice of subsystem level solutions are such that the final integrated system satisfies the requirements.

3.2 Approach

This section discuses the concept on which each of the GTR's subsystems is based. In each subsystem, numerous possible solutions are proposed and the criterion used to chose the appropriate solution is given. Mission critical subsystems such as the time and position, and RF signal conditioner subsystem require specialised solutions where as the power supply and operation controller subsystem require generic solutions often satisfied by an ensemble of readily available components.

3.2.1 GPS time-pulse radiator (GTR) context diagram

The GTR instrument consisted of four internal subsystems, namely, power supply, time and position, operation controller, and the RF conditioner. The GTR instrument's context diagram has been been identified as shows in Figure 3.2. The time and position subsystem is responsible for determining the GTR antenna's position and providing a reference 1-pulse-per-second (1PPS) signal. The operation controller is responsible for selecting the instruments mode of operations such as initialisation, frequency selection and on/off power. The RF conditioner generates, amplifies, filters and modulates the timing signal with the 1PPS signal up to the transmission stage of the instruments antenna. There are two external systems that the instrument interfaces with, namely, the GPS satellites and radio telescope. The GPS satellites provide navigation data which the GTR uses to determine determine position and time. The radio telescope is the device under test (DUT) or receiver to which the GTR instrument broadcasts the timing signal

for receiver timing delay determination.

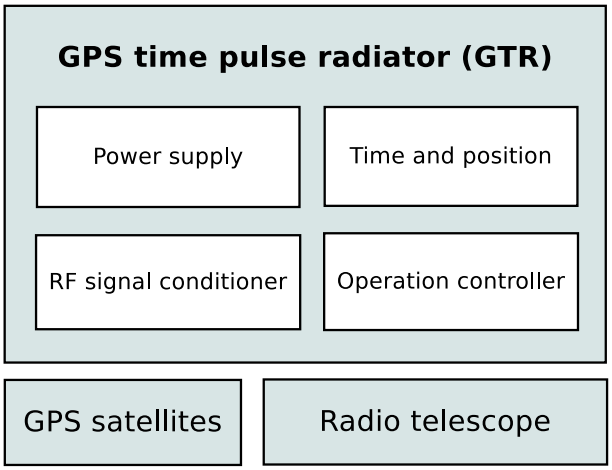

Figure 3.2: GTR context diagram.

3.2.2 Power supply

The power supply subsystem consisted of an ensemble responsible for proving electrical power to the various electric components of the GTR. The power supply ensemble consisted of a battery, fuse, power converter and voltage regulator. Given that the GTR must be a portable instrument, the battery is consequently the main source of electrical power. The fuse is an electrical circuit breaker that is used to protect the GTR from excessive current that could permanently damage its electronics. In order to extend the operational duration of a battery operated device, large capacity batteries are used and often with high voltage ratings. A power converter was required to lower the battery voltage such that the voltage was within the input voltage limit of the voltage regulator that supplied components with different intermediate voltages. Voltage regulators dissipate excessive heat when considerable current is drawn from a significantly large input voltage for a much lower output voltage, the power converter acts as an intermediary that efficiently lowers the regulator's input voltage systematically reducing heat dissipation. The chosen power converter was the muRata OKI-78SR-5 DC-DC converter which converted the battery 12 Vdc input to a 5 Vdc output. The flow diagram of the power supply subsystem is depicted by Figure 3.3. Suitable batteries are available in various chemistries including

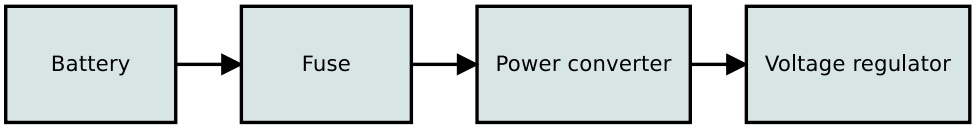

Figure 3.3: Flow diagram of the GTR's power supply subsystem.

lead-acid, lithium-ion, solid state and nickel metal hydride rechargeable batteries. When selecting the suitable battery, size, weight, power capacity, cost, life cycle and safety were

considered. Lead-acid batteries are typically bulkier, heavier, have shorter life cycle, are cheaper and least disposable. Solid state batteries are by far the smallest and lightest but are by far the most expensive, uncommon to the market and have insufficient power capacity than required. Lithium-ion and nickel metal hydride batteries have a large power capacity, lightweight and longer life cycle at a cost effective price. The lithium-ion and nickel metal hydride batteries are desirable in that they are approved for both land and air transportation. SARAO engineers will be able to drive or fly the GTR to the MeerKAT and other international radio telescopes sites without making special handling arrangements as would be required for lead-acid batteries. The RS Pro 12V, 4000mAh nickel metal hydride rechargeable battery pack was chosen as the primary voltage source.

3.2.3 Operation controller

The operational controller subsystem provides an interface through which a user interacts with the GTR. The power supply switch is responsible for making or breaking the conductive path of the electric circuit between the battery and the GTR's electronics representing the instruments on and off state. The signal generator selector switch is used to select between the two primary signal sources available to the GTR. The operation controller interface provides three visual indicators in the form of light-emitting diodes (LED). The power indicator LED indicates whether the GTR is turned on or off, the low battery indicator LED illuminates when the battery is low, and the 1PPS LED illuminates when the GTR has acquired valid time from the GPS satellites. The flow diagram of the operation controller subsystem is depicted by Figure 3.4.

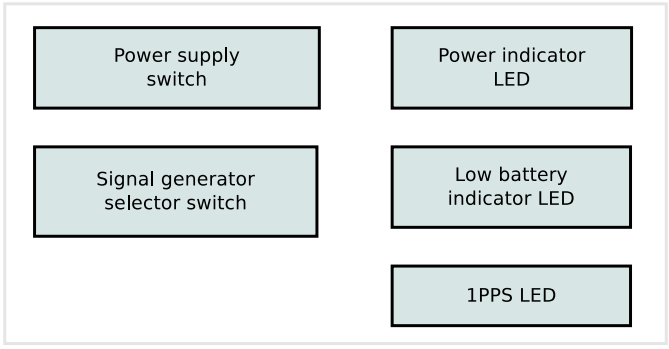

Figure 3.4: Flow diagram of the GTR's operation controller subsystem.

3.2.4 Time and position

The time and position subsystem is responsible for providing the GTR's time and frequency reference. GPS is the pioneering, most matured, and leading satellite navigation system and currently has the largest uniformly distributed constellation with 31 satellites in orbit. In order to calibrate the GTR instrument and maintain a known timing accuracy,

a single Global navigation satellite system (GNSS) system was used to avoid contaminating its accuracy with small time offsets between different GNSS systems. The time and position subsystem makes uses of GPS based navigation to determine the GTR antenna's position and precise time. The antenna is the interface between the GPS satellite signals and the radio telescope. The GPS receiver is the main mission critical component in timing and decodes the received signals to determine its position, velocity and time. Given that the GTR is kept stationary during operation, the receiver's navigation algorithm is configured with a bias towards determining position and time accurately. The receiver generates a 1PPS signal that represents the precise time. The 1PPS signal serves as the time reference from which the GTR's broadcast timing signal is derived. The time reference is expressed in the US Naval Observatories UTC(USNO) standard. The flow diagram of the time and position subsystem is depicted by Figure 3.5. Possible solutions

Figure 3.5: Flow diagram of the GTR's time and position subsystem.

to the choice of GPR receiver includes the Tremble ThunderBolt E single frequency GPS Disciplined Clock, Symmetricom's 58540A single frequency GPS time and frequency reference receiver, u-blox M8F timing receiver, Novatel FlexPak6D dual-frequency receiver and Septentrio PolaRx5 multi-frequency receiver. The ideal GPS receiver would be a dual frequency receiver with have the least 1PPS timing error, an operational voltage well within that provided by common batteries and reasonably priced. Given the GTR requirements stated in Section 3.1.2, the GPS receiver timing accuracy should be no larger than 500 μs, capable of operating from a battery and reasonably priced considering a conservative budget. It is important to emphasise the objective of error analysis in this research that states that given a receiver, its time offset to true UTC must be known such that it is predictable over a wide range of conditions. This approach makes the GTR unique in that an inexpensive single frequency receiver can be used as a precise reference provided that all possible timing offsets to true UTC are known through rigorous calibration. The chosen GPS receiver was the u-blox M8F timing receiver because of its low power consumption, operational voltage common to most portable disposable batteries, timing error well below the 500 μs constraint, and price. The receiver specifications given in Table 3.1 are those provided in the manufacturer datasheet and typical of receiver's with such specifications. The actual performance will significantly differ when used in an uncontrolled environment with varying user equipment. The Symmetricom 58540A timing receiver could have been chosen but had an uncommon high operational voltage to portable disposable batteries, and had a longer supplier lead time at the time the design decision had to be made.

Table 3.1: Possible GPS receiver solutions.

	Tremble ThunderBolt E	**Symmetricom 58540A**	**u-blox M8F**	**Novatel FlexPak6D**	**Septentrio PolaRx5**
Frequencies tracked	Single	Single	Single	Dual	Dual
Update rate	1 Hz	1 Hz	1 Hz	$\leq$ 20 Hz	$\leq$ 100 Hz
Frequency standard	OCXO	OCXO	VCTCXO	VCTCXO	OCXO
1PPS accuracy to UTC (USNO)	15 ns (one sigma)	$\leq$110 ns	$\leq$200 ns	$\leq$20 ns	$\leq$5 ns
Power supply	19–34 Vdc	18–32 Vdc	3–3.6 Vdc	6–36 Vdc	9–30 Vdc
Price	\$200–\$499	\$150	\$150–\$200	$\geq$\$500	$\geq$\$1000

Antennas are a critical component to any GPS receiver and play a critical role in determining the overall navigation performance of the GPS receiver. GPS signals are weak and impose significant design requirements on the antenna. The performance of the most sophisticated receivers will suffer due to a poor antenna. For optimal performance, an ideal antenna design implements the following parameters parameters:

- High gain.
- Filter for interference suppression.
- Low noise amplifier (LNA) with low noise figure.
- Low directivity for optimal coverage.
- Good cable impedance match between the antenna and receiver.

Antenna design can be categorised as active or passive. Passive antennas simply receive the weak GPS signals and pass them directly to the receiver whereas active antennas amplify the received signal. The performance comparison between active and passive antennas is summarised in Table 3.2. Given that the chosen GPS receiver allows for active antennas, an active antenna was chosen in order to leverage the benefits of such design. According to the RF design considerations for u-blox GPS Receivers [50], an active antenna should be used if RF cable between the receiver and antenna is longer than 10 cm, the antenna LNA gain should not overload the receiver, and the antenna LNA gain for u-blox receivers need not exceed 26 dB for optimal performance. The GPS receiver came with a high performance u-blox ANN-SM active GPS patch antenna as part

Figure 3.6: u-blox M8F timing receiver evaluation kit [8].

Table 3.2: Active and passive antenna performance comparison [15].

Active antenna	**Passive antenna**
External power required and contributes to overall receiver power consumption.	No external power required.
Tolerant to cable impedance mismatch due to cable length.	Antenna carefully designed with a micro strip of no longer than 10 cm length.
Cable length loss after the LNA does not affect the overall receiver noise figure.	Highly susceptible to RFI/jamming signals detrimental to performance.
Least affected by RFI/jamming when equipped with filters.	Specialised knowledge in RF design required to optimise antenna design.

of the evaluation kit and a similar Taoglas active GPS patch antenna with different gain parameters was used to evaluate the overall receiver timing performance. The antenna parameters of the two antenna were compared in Table 3.3. The chosen antenna was the Taoglas active GPS antenna because of higher antenna gain, and ability to received more GNSS signals from other constellations, however the u-blox ANN-SM active GPS antenna's sensitivity was attributed to the low noise figure.

3.2.5 RF signal conditioner

The RF signal conditioner subsystem consisted of an ensemble responsible for generating, amplifying, attenuating, filtering and broadcasting the GTR's timing signal that coincides with UTC(USNO). The signal generator produced the intermediate signal which was encoded with the timing information. The amplifier increased the intermediate signal power before the filtering process attenuated the signal further. The bandpass filter is responsible for filtering the intermediate signal such that the transmitted signal is within the radio telescope's bandwidth whilst suppressing signals in other frequencies. The

Table 3.3: u-blox ANN-SM and Taoglas active GPS antenna comparison [15, 9].

	u-blox ANN-SM active GPS antenna	**Taoglas active GPS antenna**
Antenna gain (dBic)	4 dBic min ($\geq 7\ cm^2$ ground plane)	26 ± 3dBic, zenith at 1575.42 MHz 27 ± 3dBic, zenith at 1602 MHz
Amplifier gain (dB)	29 dB typical	22 dB (1.8 Vdc), 28 dB (3 Vdc), 31 dB (5 Vdc)
Amplifier noise figure (dB)	0.9 dB maximum	2.6 dB (1.8– 5.5 Vdc)
Power consumption	8.5±4.5 mA typical	5 mA (1.8 Vdc), 10 mA (3 Vdc), 23 mA (5.5 Vdc)
Center frequency	1575 ± 3 MHz	1574–1610 MHz
Polarisation	Right hand circular	Right hand circular
Vertical standing wave ratio	2.0 max	2.0 max
Impedance	50 Ω	50 Ω
Dimensions and cable	48 x 40 x13 mm	65.7 x 49.7 x 21.4 mm
Cable and connector	5 m RG174, SMA (M)	3 m RG174, SMA (M)

attenuator was responsible for reducing the signal power such that the transmitted signal power was below the limits of the intended radio telescope. The RF switch synchronously modulates the noise signal with the GPS receiver's 1PPS reference signal to produce the timing signal. This type of modulation is referred to as amplitude modulation. The transmission antenna provides an interface between the GTR's timing signal and the radio telescope's receiver. The flow diagram of the time and position subsystem is depicted by Figure 3.8. A directive antenna was chosen to mitigate unintended self jamming that could occur since the GTR's GPS receiver antenna is located at close proximity to the enclosure and transmitting antenna. The MeerKAT radio telescope's L-band receiver bandwidth includes GPS signals, broadcasting in L-band would corrupt the weaker GPS signals and corrupt the GPS receivers pseudorange measurements. The chosen directive transmitter antenna was the Com-Power AH-118 double ridge horn antenna designed to radiate signals over wide range of frequencies. The amplifier, bandpass filter, attenuator and RF switch are common readily available components and were chosen such that they operate within the L-band frequencies of the MeerKAT radio telescope receivers.

Figure 3.7: Taoglas active GPS patch antenna [9].

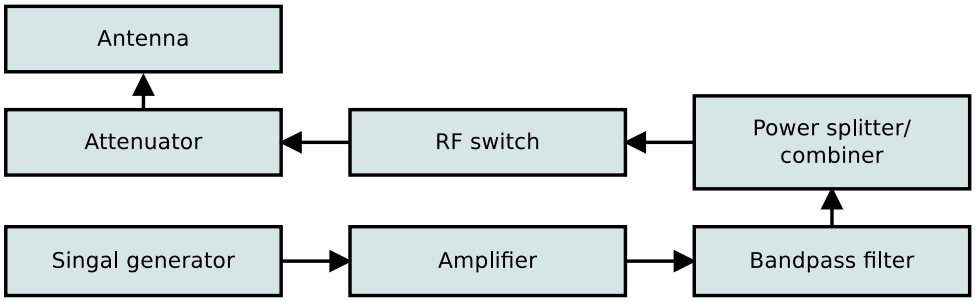

Figure 3.8: Flow diagram of the GTR's RF signal conditioner subsystem.

The chosen low noise amplifier amplifier, bandpass filter, attenuator and RF switch were the Mini-circuits ZX60-P162LN+, Mini-circuits VBFZ-1065+, Mini-circuits VAR-10+/-3+ and Mini-circuits ZX80-DR230+ respectively. The timing signals were derived from

Figure 3.9: Com-Power AH-118 double ridge horn antenna [10].

two signal generators, namely, a reference oscillator and a Zener diode wideband white noise signal generator. The reference oscillator provides a method for testing the radio telescope's frequency spectrum. By radiating a signal from a oscillator with a know frequency, frequency variations in the receiver under test can be used to support an investigation into the receiver's frequency response. The narrowband 1 GHz Crystek sine wave SAW(surface acoustic wave) oscillator was the chosen reference oscillator. The reference oscillator signal was useful as an indicator to confirm the receiver was operational through observing its frequency spectrum but was not appropriate for timing. It was also used to self test the GTR's RF chain to verify that the GTR transmitted signals in L-band

(1–2 GHz) whilst maintaining the integrity of the timing signal's carrier frequency. The noise signal was desirable for timing because the amplitude had a distinct shape when turned on unlike the 1 GHz sinusoidal signal, thereby made the noise signal invaluable for embedding time markers in the time domain when modulated with a precise time signal. A Zener diode based wideband white noise signal generator was chosen because of its distinct amplitude profile for timing and capabilities of generating signals over wideband frequencies within L-band receiver frequency range intended for MeerKAT. The noise source was designed from first principles because the wideband white noise can be generated using inexpensive components.

3.2.6 Packaging

Radio telescopes are sensitive instruments typically located in radio quiet areas in which signal power levels from radiocommunications equipment such as television transmitters, mobile telephones and citizen band radios are controlled to limit interference to radio telescopes. Interstellar radio sources astronomers are interested in are typically weak signals that required long integration times to detect. RFI signals are much stronger signals that saturate the radio telescope such that the signals of interest are buried within the saturated signal such that no interstellar signals are recoverable. The GTR as a transmitter is thereby required to transmit a well characterised signal that is only permissible for use in exceptional commissioning scenarios such as telescope timing test. Given that the GTR's timing signal complies with the observatories electromagnetic compatibility (EMC) and RFI standards, its enclosure was chosen such that no unintended EMC and RFI is generated from its electronics such as the GPS receiver and signal generator. An aluminium IP68, electromagnetic interference(EMI) and RFI shielded enclosure with protection against dust and water was thereby chosen.

Figure 3.10: EMI RFI shielded aluminium enclosure [11].

3.2.7 Electromagnetic reverberation chamber test

An electromagnetic reverberation chamber is an EMI RFI shielded structure within which a device under test (DUT) is tested for radiation susceptibility, total radiated power and

shielding effectiveness. The measurements produce an RF spectrum showing the DUT's total emission power over a wide range of frequencies, thereby providing a method to verify that the timing signal was the only GTR RF emission.

3.3 Detailed design and implementation

3.3.1 Hardware design and implementation

The design and implementation of the GTR instrument was broken down into four subsystems. The power supply subsystem consisted of an ensemble responsible for proving electrical power to the various electric components of the GTR. The operational controller subsystem provided an interface through which a user interacted with the GTR. The interface made use of switches to turn the instrument on or off, and activate or deactivate the transmission of the timing signal. LEDs indicating the instruments on/off sate, low battery detection and GPS time acquisition status. The time and position subsystem was responsible for providing the GTR's time and frequency reference. It made uses of GPS based navigation to determine the GTR antenna's position and precise time. The RF signal conditioner subsystem consisted of an ensemble responsible for generating, amplifying, attenuating, filtering and broadcasting the GTR's timing signal that coincides with UTC(USNO). All component values not given explicitly in this thesis are assumed to be specified in the respective components datasheet.

3.3.1.1 Power supply

The power supply transforms the battery power to low-voltage regulated DC power. The 5 Vdc regulated voltage provided power to the LEDs, GPS receiver and Zener noise diode's DC-DC converter. The 4 Vdc regulated voltage achieved through a 0.72 Vdc voltage drop across a 1N4448 diode with a 5 V rails provided power to the low noise amplifiers. The 3.3 Vdc regulated voltage provided power to the sine wave oscillator. The 1 μF capacitors were recommenced by the respective voltage regulator datasheet in order to slow down voltage changes, thereby improving the overall regulation stability. The power supply circuit is given in Figure 3.11. To obtain a figure for the total power consumption, the GTR was powered from a laboratory programmable power supply with the voltage set to 12 V and a current limit set to 170 mA. The programmable power supply showed readings of the voltage and current of the GTR as its runtime modes where changed in order to obtain data from which its power consumption could be determined. The recorded current and voltage readings are given in Table 3.4.

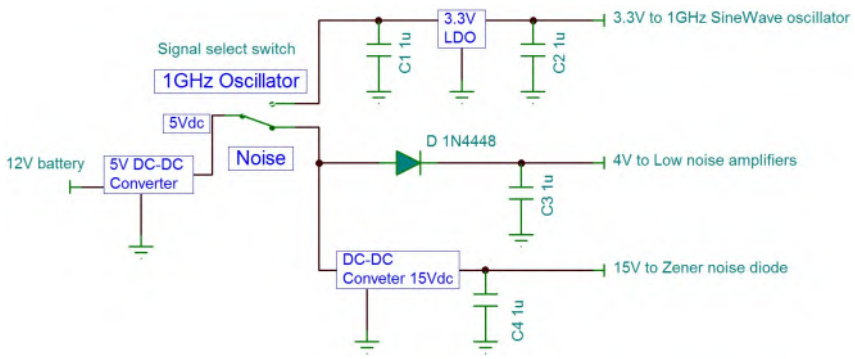

Figure 3.11: Power supply circuit.

Table 3.4: GTR runtime power consumption readings.

GTR runtime state/mode	**Current and voltage reading**
Standby	$V_{on} = 12$ V $I_{on} = 42$ mA
Noise diode turned on	$V_{on} = 12$ V $I_{on} = 150$ mA
SineWave oscillator turned on	$V_{on} = 12$ V $I_{on} = 57$ mA

$$\begin{aligned} Battery\ capacity &= average\ current\ consumption \times expected\ runtime \\ &= 150\ mA \times 8h \\ &= 1200\ mAh \end{aligned} \tag{3.1}$$

In order to satisfy the runtime time requirement given in Section 3.1.2, a battery capacity of at least 1200 mAh was required as calculated in Equation 3.1. The chosen RS Pro 12V, 4000mAh nickel metal hydride rechargeable battery pack was able to provide up to 26 hours of runtime. The noise diode consumed the most power due to the Morsun A0515D-1W 5V to 15V DC-DC converter used to provide excess voltage to the Zener diode operating in the breakdown region.

3.3.1.2 Operation controller

The operational controller subsystem provided an interface through which an operator interacted with the GTR instrument depicted in Figure 3.12. The control panel had an ON or OFF toggle switch controlling the instruments power and the *Osc/Noise* toggle switch used to select the type of signal generator. There were two BNC female connectors designed to allow external time pulse (1PPS) signal inputs and outputs useful for laboratory based timing tests. The *Aux 1PPS in* connector was used as a time pulse source in

cases where the GPS could not provide a reference time pulse signal. The *Aux 1PPS out* is time delayed version of the *Aux 1PPS in* signal used as a reference when analysing the transmitted signal from the GTR's antenna. The delay was measured to be equal to that of the *Aux 1PPS in* connector to the RF transmitter's connector. The three LEDs are used to indicate power state, 1PPS signal activity and low battery indication respectively. The instrument's power status was indicated by an illuminating green LED. Given a 5 V

Figure 3.12: Operation controller user interface.

supply, the datasheet recommended that a resistor be used to limit the current to at most 20 mA. Using Ohm's law, the current limiting resistor was calculated to be 250 Ω but a slightly larger resistance of 330 Ω was used to operate below the maximum current ratting. The low battery detection circuit used an operational amplifier and a resistor network. The resistor network values were chosen such that the operational amplifier's output voltage latched high when the difference between its inputs was not in the 0–1.2 V range. The common voltage difference is given by

$$V_{common} = 5 \times \left(\frac{P1}{P1 + R4}\right) - 12 \times \left(\frac{R7}{R7 + R1}\right) \tag{3.2}$$

The variable resistor *P1* was adjusted with the help of a variable power supply in order to

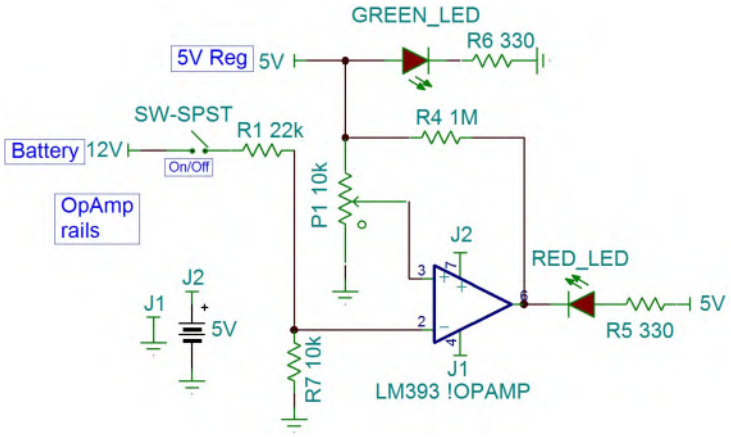

Figure 3.13: Power state indicator and low battery detection circuit.

achieve a low battery state when the battery voltage dropped to below 11 V. In the event that the battery is low, the GTR will continue to operate thereby giving the operator a warning suggesting a battery recharge or replacement for reliable continuous operation.

3.3.1.3 Time and position

GPS performance is significantly affected by the antenna choice, implementation and mounting position. The receiver's antenna needs to receive signals from as many visible GPS satellite as possible. The antenna must maintain full view of the sky ensuring direct line-of-sight with all visible satellites. When patch antennas are used, antenna's plane should be parallel to the geographic horizon. Objects that may obstruct the antenna's line-of-sight with the satellite, attenuate the weak GPS signals. Protruding may introduce multipath that degrades the pseudorange measurements. Poor satellite visibility degrades the GPS receivers navigation performance resulting in prolonged time to first fix, position drifts and time drifts which are undesirable in timing critical applications. The impact of satellite visibility on the accuracy of position and time determination were described in terms of dilution of precision (DOP) in Section 2.3.5. During normal operations, the

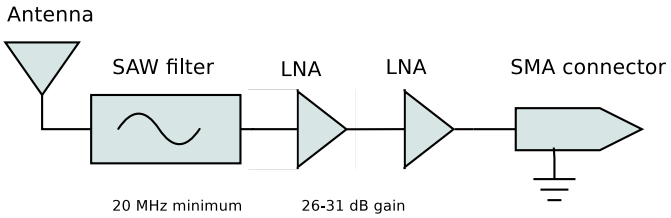

Figure 3.14: Block schematic of the patch antennas internal circuits [9].

GPS receiver monitored its ambient temperature and continuously corrected its oscillator to account for frequency drifts with temperature. If a GPS receiver fails to track at least four satellites required to continuously determine position and time, the receiver enters into a *hold-over* operational mode. During hold-over, the receiver continues to maintain time synchronisation based on its oscillator's frequency stability characteristics. The GTR's GPS receiver used a voltage controlled temperature compensated crystal oscillators (VCTCXO) which offers good phase noise and 100 ppb (over 24 hours) hold-over performance. The receivers also offers an external reference clock utility for external oscillators with greater stability such as an oven controlled crystal oscillators (OCXO) and atomic frequency standards. The use VCTXO oscillator provides sufficient performance for the GPS receiver to comply with the GTR timing requirement stated in Section 3.1.2.

The GPS receiver generates a 1PPS signal that represents the precise time. By default, the 1PPS signal is traceable to the US Naval Observatory (USNO) and additional traceability to the National Metrology Institute of South Africa (NMISA) was established through calibration discussed in Section 3.4.2. By establishing traceability to NMISA, the time difference between the GTR and the radio telescope being tested can be expressed in terms of UTC(ZA). The u-blox M8F GPS timing receiver is based on the LEA-M8F GNSS module and its internal block schematic is given in Figure 3.15. The GTR's u-blox M8F GPS timing receiver provided a special *Time Mode* for stationary antenna setups that used a time determination algorithm that solved for clock errors and clock biases

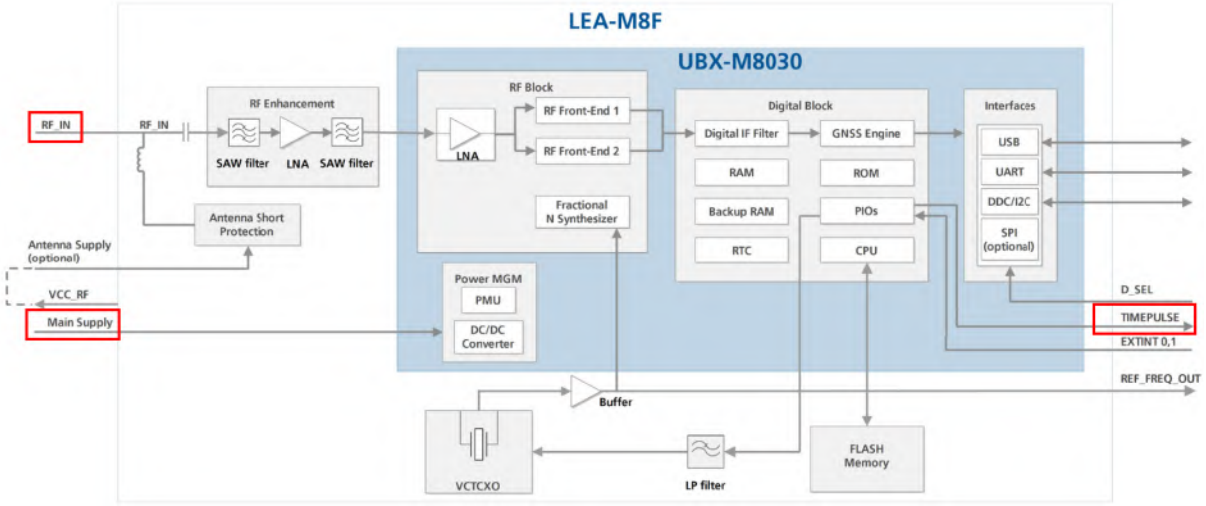

Figure 3.15: Block schematic view of the LEA-M8F module [12].

using all available GPS satellites to determine the most accurate precise time possible. The time mode consisted of three different settings described in Table 3.5. The receiver provided three variants of UTC to which native GPS time was converted. UTC(USNO) was chosen as the UTC variant from which GTR's time reference was derived. Given that the US Naval observatory is responsible for maintaining GPS time and UTC(USNO), the UTC(USNO) variant was chosen in order to avoid contaminating its accuracy with small time offsets between different variants maintained by other institutions and GNSS systems. The u-blox M8F GPS timing receiver came with a GNSS evaluation and visu-

Table 3.5: u-blox M8F GPS timing receiver Time Mode settings [12].

Time mode	**Description**
Disable	A standard mode in which the GPS receiver computes position, velocity and time (PVT).
Survey-In	In this mode, the GPS receiver determines the average antenna position over a predefined period until the required position accuracy is reached. The configurable position accuracy is defined as the standard deviation of the computed position. Upon achieving the required accuracy, the receiver enters into the Fixed Mode.
Fixed mode	A special mode in which the stationary 3D position and standard deviation determined in the Survey-In mode are assumed and the receiver no longer solves for the antenna's position. The use of a fixed or predefined 3D position improves the phase stability of the receiver generated time-pulse signal and eliminates the introduction of timing errors which could result from position errors. The receiver proceeds to unilaterally solve for clock errors and clock biases in order to generate the time-pulse signal as accurate and stable as possible.

alization tool called *u-center*. The software enabled users to conduct performance tests, configure GNSS positioning, and update firmware on u-blox and other GNSS modules. The configuration interface is depicted in Figure 3.16. The navigation mode setting was used to select the appropriate navigation model for the GTR's intended use. The dynamic model was set to stationary, fix mode was set to 3D only, UTC standard was set to USNO(GPS), and the minimum satellite elevation mask was set to between 10° and 20°. The time-pulse setting was used to select the appropriate 1PPS signal behaviour (output frequency and pulse length) depending on whether or not the receiver was locked to a reliable time source. The receiver was configured to generate the 1PPS signal as soon as the receiver calculated a valid time (locked to GPS time). With no GPS frequency lock, the receiver did not output the 1PPS signal, thereby ensuring the GTR remains reliable for accurate timing. The pulses were configured to align to the top of a second. The pulse polarity can be selected as rising or falling edge. The output frequency before and after GPS time lock can be configured. When a 1PPS pulse is required after GPS time lock, a higher frequency can be set during the survey period to provide an unambiguous visual indication to the operator by means of an LED. The time mode provided the special receiver positioning setting depicted in Table 3.5. The *Survey-In* mode ended if both minimum observation time and required position accuracy conditions were met. Since

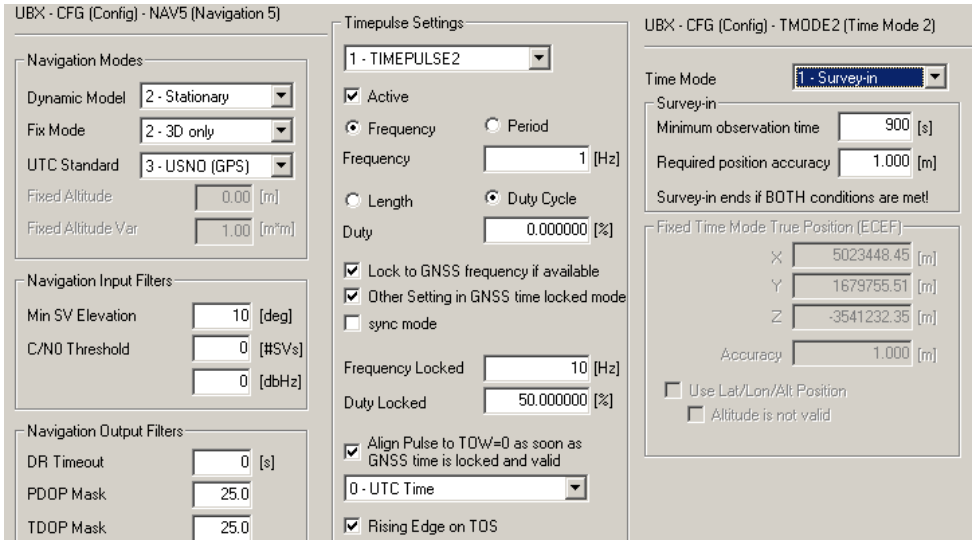

Figure 3.16: Navigation, time pulse and time mode configuration interface of the u-blox GPS receiver.

there was only one reference 1PPS signal, either external or on-board the GPS timing receiver, numerous subsystems shared the signal. The GPS receivers datasheet warned that a low load on its 1PPS (Time Pulse) pin was mandatory in order to avoid prolonging its rise time. A buffer was used in order to distribute the 1PPS signal to each respective subsystem. The OR logic gate was used to select one of the two 1PPS sources, namely, the external source *Aux_PPS_in* typically available in a laboratory or the GPS's time pulse

denoted as *Time Pulse*. The additional delay added by the distribution network was measured and accounted for in the final GTR accuracy. The 1PPS distribution scheme is given in Figure 3.17. The receivers time-pulse output was generated with a configurable

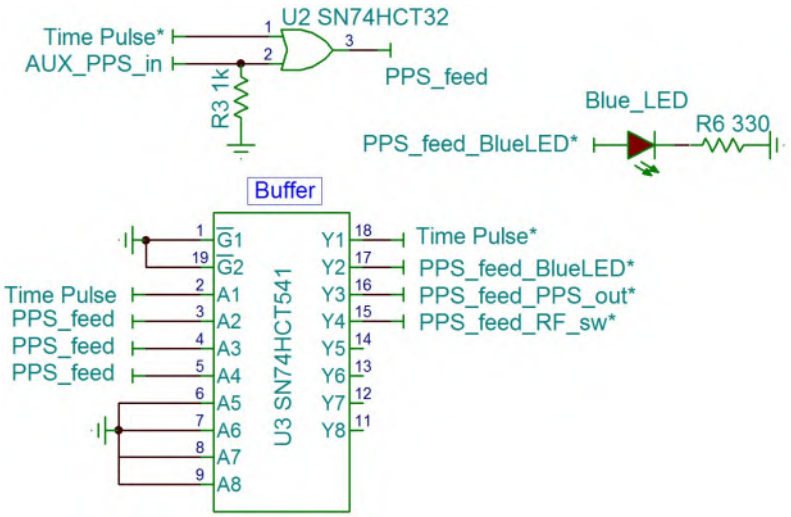

Figure 3.17: 1PPS distribution circuit.

frequency and phase which are aligned to the built-in oscillator. After the initial time acquisition phase, the time-pulse jitter improves and is generated synchronously with the built-in reference oscillator. Small frequency corrections are made to the built-in reference oscillator to achieve step-less time-pulse phase corrections.

3.3.1.4 RF signal conditioner

The SPDT RF switch has two RF inputs and one RF common output. The output of the two way power splitter was connected to one of the SPDT RF switch's RF inputs and the other terminated with a 50 Ω connector. The RF switch had two control bits that are driven by either pulling the control pins high or low to achieve a desired response based on its inputs. The control pins were configured such that the GPS receiver's time pulse controlled the GTR's transmission state as a form of modulation. Given that the time pulse serves as the GTR's time reference, the transmitted timing signals were thereby inherently traceable to UTC(USNO) and consequently UTC(ZA) through the receivers calibration. The SPDT RF switch's control bits were used to select the desired switch state depicted in Table 3.6. The blocks in blue were timing critical components which introduced delays, making the time pulse late with regards to the reference point on GPS receiver's time pulse connector. The delay introduced delay was measure and accounted for in the final GTR accuracy. The RF signal conditioner consisted of two signal generators, namely, a narrowband 1 GHz sine wave signal generator and Zener diode wideband noise signal generator. The frequency spectrum of both signal generators depicted in Figure 3.20 was measured by a Rhode & Schwarz spectrum analyser.

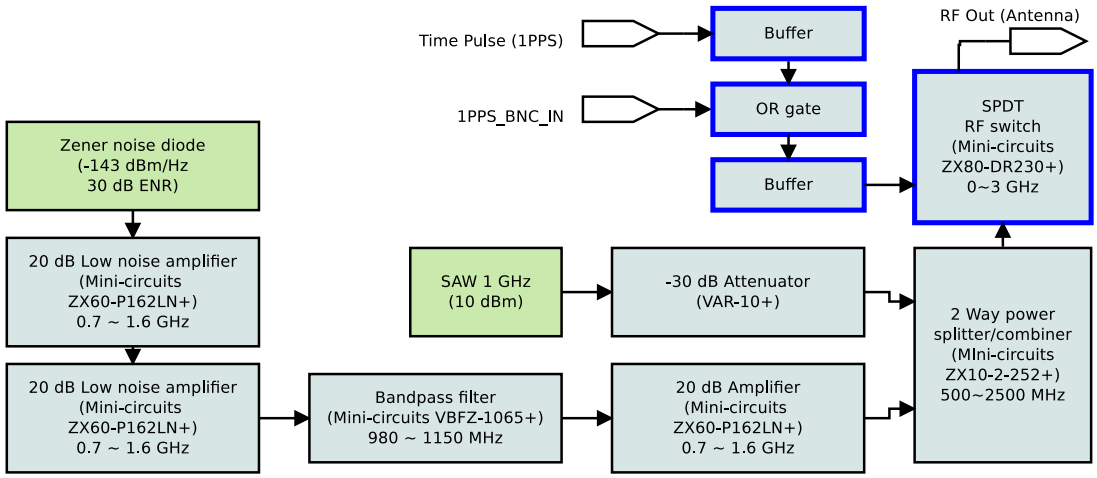

Figure 3.18: RF chain of the signal conditioning subsystem.

Table 3.6: SPDT RF switch truth table.

State	**Control inputs**		**RF input or output**	
	Control 1	**Control 2**	**RF input 1 to RF common**	**RF input 2 to RF common**
1	Low	Low	Off	Off
2	High	Low	On	Off

Narrowband 1 GHz sine wave signal generator: The sine wave generator takes a 3.3 Vdc input and generated a 1 GHz +7 dBm signal into 50 Ohm load. The frequency spectrum of the signal is characterised by a single strong signal at 1 GHz and weak harmonics at integer multiples of the fundamental frequency.

Zener diode wideband noise signal generator: The Zener diode breakdown voltage region was the true source of wideband white noise noise in the design. The noise source produced about -143 dBm/Hz or 30 dB ENR and it was important to ensure that the signal had a Gaussian probability-density function. The white noise generator was based on the avalanche noise generated when the Zener diode's PN junction was operated in the reverse breakdown mode. The avalanche noise had a flat frequency spectrum resembling white noise as expected. The generated noise power was unpredictable and did not have enough power for practical application (± 1 dB typical) [51]. The frequency spectrum of both signal generators depicted in Figure 3.20 was measured by a Rhode & Schwarz spectrum analyser. A cascade of LNA's were used to produce a total gain of 60 dB. The far right image of Figure 3.20 shows the noise signal generator's flat spectrum with a noise floor around -80 dBm and the raised noise floor during active transmission around -18 dBm over L-band frequencies. The noise signal spectrum resembled that of the RF chain's band pass filter as expected. Given the interference potential form the signal generators, the GTR can thus only be operated when the radio telescope is not observing,

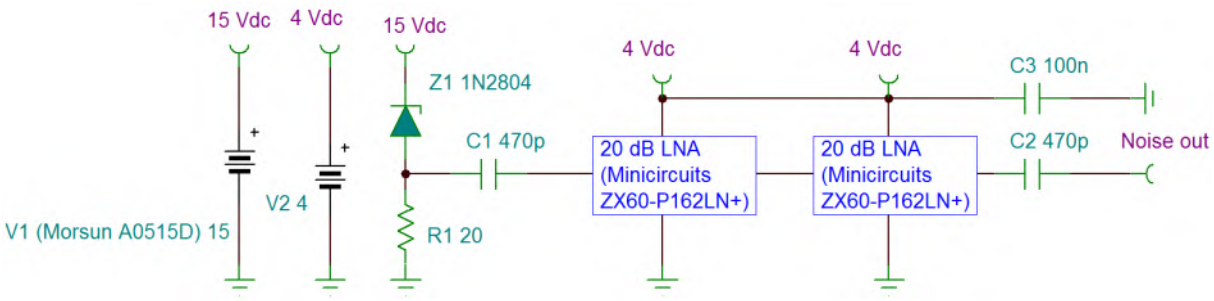

Figure 3.19: White-noise generator circuit.

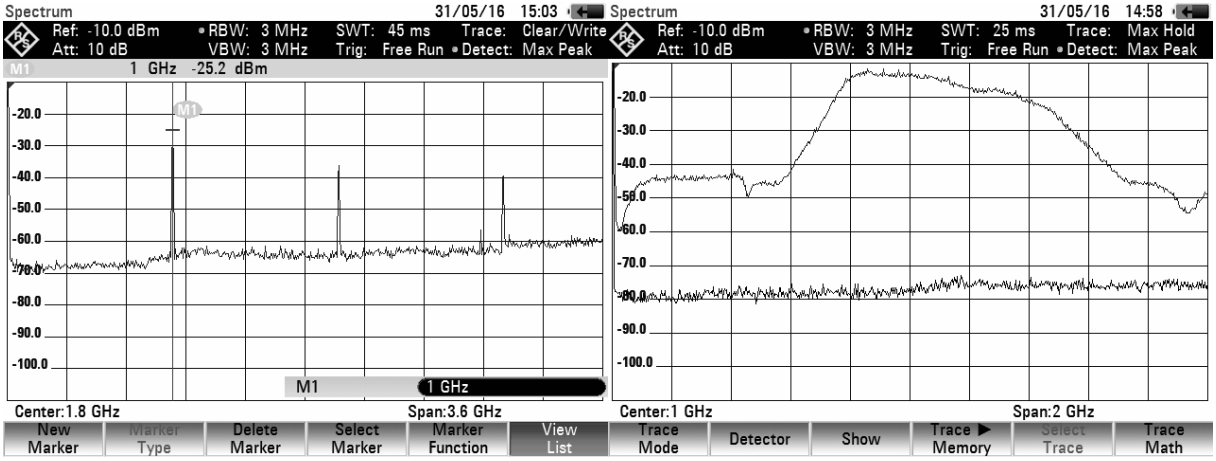

Figure 3.20: Frequency spectrum of the narrowband 1 GHz sine wave (left) and Zener diode wideband noise signal generator (right) in L-band (1–2 Ghz).

or is dedicated to commissioning tasks. The time spent transmitting should be minimised by setting the GTR to a standby mode, which does not transmit any deliberate RFI. In this mode the GTR is effectively far less noisy than a laptop.

3.3.2 System integration and testing

The final GTR system was completed by connecting together all the components given in Section 3.3.1. The veroboard layout was designed to be modular with connectors to electrical components easily accessible with wire to board mounts on either sides depicted in Figure 3.21 and B.1. The modular design allowed for future RF chain upgrades since components could be easily unscrewed from the board mounts and SMA connectors. RF chain upgrades are particularly important when the filter has to be changed to perform timing tests on radio telescope receiver operating in frequency bands other than L-band. A single printed circuit board (PCB) was attractive as the whole product could be a single sheet of PCB, including connectors from the GPS receiver, GPS patch antenna, RF modules, and radiating antenna but there would be real challenges in getting the board right. It could potentially take several iterations to get a PCB design, which takes a long time and would waste many components. The electronics were integrated and

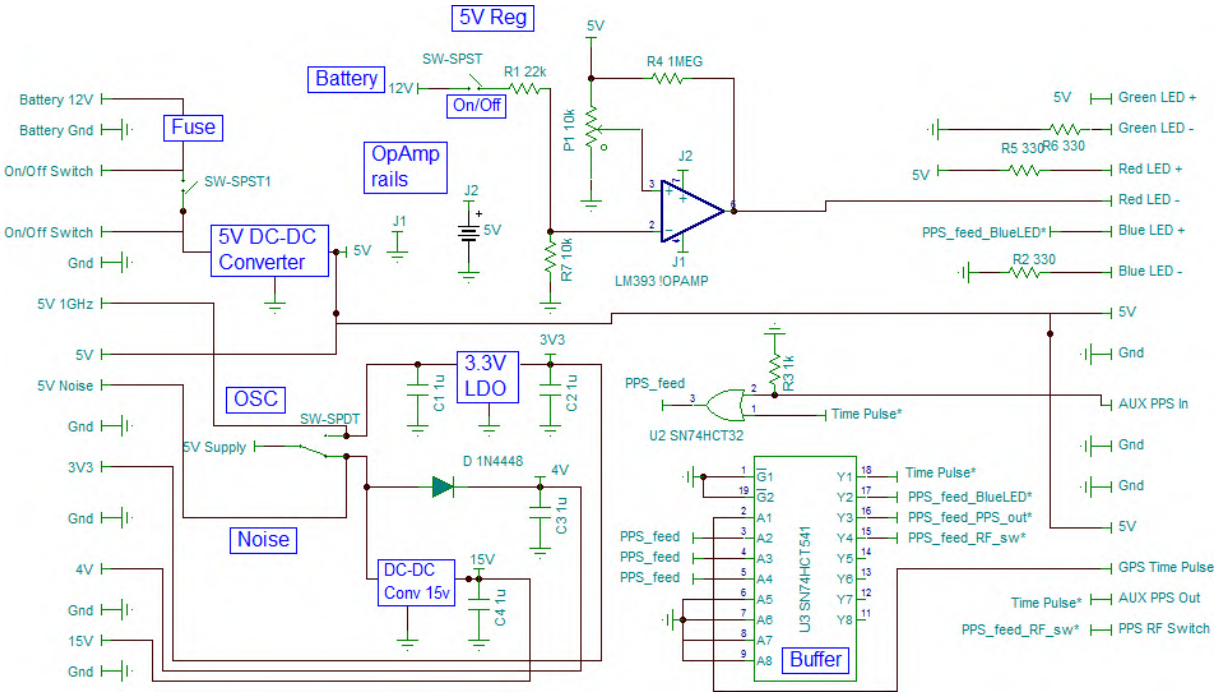

Figure 3.21: Integrated circuit design of the GTR.

assembled into an aluminium enclosure which was easily opened and closed with a hex key. All connectors, LEDs and switches were labelled. The IP68 rated enclosure provided both EMI or RFI shielding and environmental protection from elements such as water and dust. The enclosure was of the dimensions 260 mm x 160 mm x 120 mm and easily packed into a watertight, airtight, and dustproof carry case with pluck foam. The carry case pluck foam was picked and plucked to create a snug fit and additional compartments for all spares (GPS antenna, hex key, battery, RF attenuators and filters) required to operate or service the GTR. A photograph of the GTR instrument in the carry case is depicted in Figure 3.22. The horn antenna was carried in a separate carry case provided by the manufacturer due to its size and weight. Figure 3.22 shows the complete GTR deliverable developed from the work presented in this thesis. Additional images of the GTR instrument's electronics and enclosure are provided in Appendix B.

3.4 GTR system characterisation

In order to certify the GTR as a reliable timing instrument, quantitative measurements were used to determine the GTR's bounded accuracy considering as many sources of errors as possible. This section provides detailed design and discussion of the methods used to measure the timing characteristics of the GTR instrument.

(a) GTR instrument (b) GTR in carry case

Figure 3.22: Complete GTR deliverable.

3.4.1 Statistical error analysis

Statistical data reduction methods were important in determining stability and uncertainty information from data generated in various timing experiments.The probability density function (PDF) and maximum time interval error (MTIE) error analysis methods were used. The computations were performed using Python libraries and were verified by the Stable32 frequency stability analysis software used by the timing community.

3.4.1.1 Probability density function

A probability density function (PDF) is a statistical function applied to a known dataset that describes all possible values and likelihoods a random variable would take [52]. The possible values that a random variable are described in a range that is bounded between the least and most likely possible value. The PDF describes the range in terms of a dataset's mean, standard deviation and skewness. The event from which a dataset is created will dictate its probability distribution. The probability density provides information about the type of phenomenon that influence the events being studied. Typically, systems with good timing stability have a Gaussian distribution that provides information about accuracy in the form of the mean and precision in the form of the standard deviation. In contrast, a none Gaussian or multimodal distribution indicates poor or unpredictable system performance suggesting that there are multiple factors influencing the systems accuracy. For GPS receivers, poor timing performance can be a result of hardware choice, environmental conditions or systematic interference [7]. Through data analysis, sources of errors can be identified and mitigation techniques can be used to improve stability. Probability distributions that were generated from comparing the GTR's GPS timing receiver and other sophisticated timing system's time pulse revealed systematic offsets

that thereby reduced the GTR's timing uncertainties. The influence of variables such as the choice of hardware, time of day and other environmental conditions on the GTR's accuracy can be better understood through the respective experiment's probability distributions. The key variable obtained from the probability distributions of the timing experiments was the mean and standard deviation of the time offset between the GTR's GPS receiver and the reference timing systems. The probability density function of a normal distribution is given by

$$f(x) = \frac{e^{-(x-\mu)^2/(2\sigma^2)}}{\sigma\sqrt{2\pi}} \quad [52] \tag{3.3}$$

where x is a series of phase variation measurements, μ is the mean of the series of phase variation measurements, σ^2 is the variance of the series of phase variation measurements, and σ is the standard deviation of the series of phase variation measurements.

3.4.1.2 Maximum time interval error (MTIE)

Maximum Time Interval Error (MTIE) is a measure of the worst case phase variation of a signal with respect to a reference signal over a particular time interval [52]. It is used to specify clock stability requirements in the timing and telecommunication community. Given a phase variation measurement dataset with a defined observation interval, the MTIE function iterates through the entire dataset keeping note of the peak-to-peak difference between the smallest and largest time interval error. An MTIE graph is effective in revealing the worst case phase transients that are typically expressed conservatively by the probability distribution function. The MTIE was given preference in determining the GPS receiver's uncertainty budget because it gave a more realistic estimate of the short term phase variations which are particularly important for the GTR as it was designed as a short baseline timing instrument. The MTIE function is given by

$$\begin{aligned} MTIE(\tau) &\cong max(max(x_i) - min(x_j)) \quad [52] \\ & MTIE(\tau) : 1 \leq K \leq N - n, \\ & i : K \leq i \leq K + n, \\ & j : K \leq j \leq K + n, \\ & \tau = n\tau_0 \end{aligned} \tag{3.4}$$

where x is a phase variation measurement, τ_0 is the sampling period, τ is the observation time, n is the number of samples, and N is the number of total phase measurements.

3.4.2 GPS receiver calibration

In order to certify the GTR as a reliable timing instrument, the on-board GPS receiver that provides the time and frequency reference was calibrated at NMISA. Before the official calibration was performed, initial calibration were performed using sophisticated GPS timing receiver installed at SARAO's laboratory provided a precise time and frequency reference through which most of the GTR's development and characterisation methodologies evolved. The calibration results are presented in Section 4.2.1.

3.4.2.1 Initial laboratory calibration

The laboratory in SARAO's engineering office, located in Cape Town was equipped with a GPS based Spectracom time and frequency synchronisation System (NetClock 9400 Series). The synchronisation system used the GPS direct time distribution methodology discussed in Section 2.4.5.2 to establish time and frequency traceability to USNO. The system used a Tremble Resolution T GPS timing receiver of which the manufacture guaranteed a 1PPS timing signal accurate to within 15 nanoseconds of GPS or UTC (1 sigma) when using an overdetermined solution in a stationary mode. The receiver provided an automatic self-survey mechanism that tracked temperature, phase and frequency errors for improved timing accuracy. The self-survey data was accessible through a web based interface which provided graphical representations of the overall system health and reports on variables contributing to the real-time timing accuracy. An example of the self-survey web interface showing the system's real-time timing performance is given in Figure A.1 of Appendix A. The self-survey utility was invaluable in identifying the inherent synchronisation system's dynamic timing errors and removing them post calibration for improved timing accuracy. The system had an additional on-board GPS disciplined low phase noise Rubidium atomic oscillator to further enhance the synchronisation systems clock stability. The laboratory was used for various engineering activities that made use of the 1PPS and 10 MHz reference signals generated by the synchronisation system. The laboratory's time distribution set-up is depicted in Figure 3.23. The 1PPS distributor

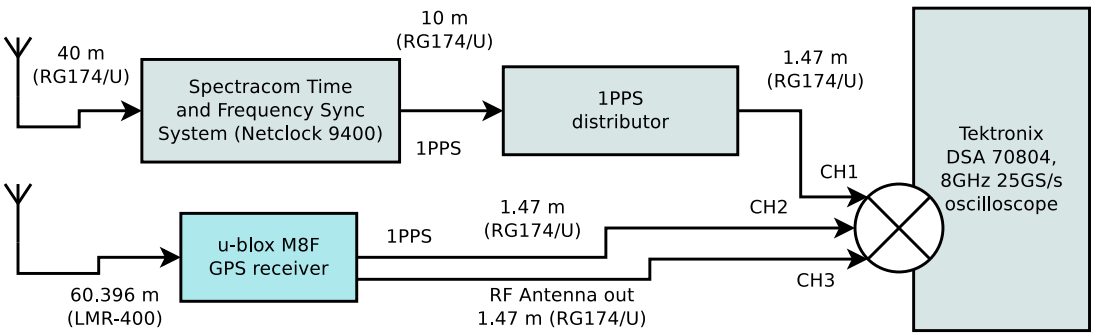

Figure 3.23: Block diagram of the earliest u-blox M8F GPS receiver laboratory calibration set-up.

was used to extend distribution of time and frequency signals to various equipment in the laboratory. All intermediate cable lengths were measured to account for delays that were added to the 1PPS signal from the reference connector to some measurement connector. All cable lengths were subtracted from the final phase difference measurements to accurately characterise the time offset between the GTR's GPS receiver and the Spectracom time and frequency synchronisation System. The delays introduced by cable lengths were determined using the equation

$$Cable\ delay = \frac{L_{mechanical}\sqrt{\varepsilon_r}}{c} = \frac{Cable\ length}{c \times VF} \tag{3.5}$$

where $L_{mechanical}$ is the cable's mechanical length, ε_r is the cable's relative permittivity, VF is the cable's velocity of propagation, and c is the speed of light. A regular inexpensive RG174/U coaxial cable has a velocity factor of 66% and adds time delay of 5.05 ns/meter. A more expensive low loss LMR-400 coaxial cable typically used in specialised timing applications has velocity factor of 84% and adds time delay of only 3.92 ns/meter. The Tektronix DSA 70804 oscilloscope was used to measure phase differences and perform analysis on the GTR's radiated timing signal. The actual calibration and characterisation set-up is depicted in Figure 3.24. The GTR's GPS antenna was mounted on the roof of

Figure 3.24: u-blox M8F GPS timing receiver calibration set-up.

SARAO's office to ensure the antenna maintained full view of the sky ensuring direct line-of-sight with all visible satellites and minimise the influence of multipath. A 60.396 m LMR-400 coaxial cable was used to extend the receivers antenna cable from the roof to the laboratory. A time interval counter was used to measure phase variations of between the GTR's GPS receiver's 1PPS signal and the laboratories 1PPS signal. The phase variation where logged into a file and analysed to extract time offset information. The

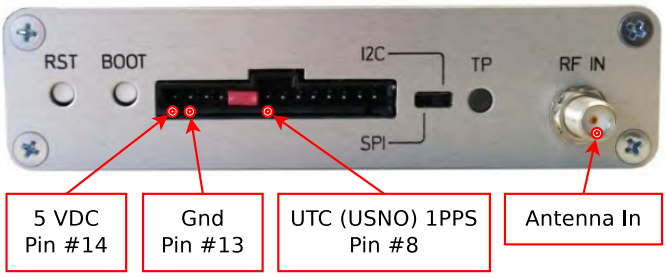

Figure 3.25: Front panels of the u-blox M8F evaluation unit.

GTR's GPS timing receiver (u-blox M8F evaluation unit) had a 1PPS output pin that was accessible with the use of jumper cable depicted by Figure 3.25. The receiver was configurable through a USB interface, provided an SMA connector for the antenna and jumper pins for power.

3.4.2.2 Official metrology laboratory calibration (NMISA)

The National Metrology Institute of South Africa (NMISA) is accountable for upholding, developing and maintaining the primary scientific standards of South Africa. The institution is mandated to maintain South African national measurement standards and ensure their laboratory standards are calibrated, verified to global standards. NMISA maintains a local variant of UTC known as UTC(ZA) and contributes to the realisation of the international reference time standard UTC. The International Bureau of Weights and Measures (BIPM) calculates UTC based on data provided by NMISA and other internationally recognised metrology institutions. NMISA maintains traceability of UTC(ZA) to UTC BIPM by regularly exchanging clock information with the BIPM. The clock information of participating metrology institutions is published in monthly BIPM Circular T. The GTR's GPS receiver (u-blox M8F) responsible for providing frequency and time reference was calibrated at NMISA. The calibration set-up is depicted in Figure 3.26. NMISA provided UTC(ZA) as an ultra-stable 1PPS signal generated from an ensemble

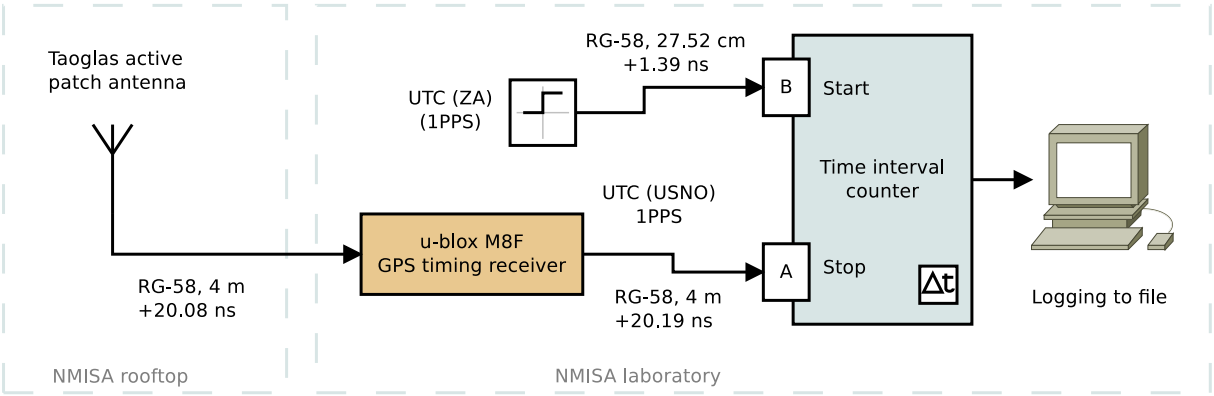

Figure 3.26: u-blox M8F GPS timing receiver calibration set-up.

of atomic clocks. This calibrator signal was a square wave with a rising edge represent-

ing the top of the second. The u-blox M8F GPS timing receiver being calibrated also produced a 1PPS signal with a rising edge representing the top of the second traceable to UTC(USNO). The aim of the calibration was to determine the phase offset or delay between the two 1PPS signals. The UTC(ZA) 1PPS signal was set as the reference to which the GPS receiver's UTC(USNO) 1PPS signal was compared. The comparison was performed with the use of a time interval counter which took phase measurements of the two signals. Each conservative phase measurement was taken exactly one second apart over a 24 hour period. The calibration test consisted of the calibrator signal extended over a 27.52 cm coaxial cable, two 4 m (RG-58) coaxial cables for the receiver's antenna and 1PPS extension, two BNC to SMA connector adapters for the receiver's antenna and 1PPS signal, receiver patch antenna, and the time interval counter. The time offset between the u-blox M8F GPS timing receiver and NMISA is given by Equation 3.6. The time offset between the u-blox M8F GPS timing receiver and UTC is given by 3.7.

$$M8F\text{–}UTC(ZA) = \mu + \beta_{UTC(ZA)} - (\times 2\ cable + \tau_{M8F} + \alpha_{M8F} + \iota_{M8F}) \tag{3.6}$$

$$M8F\text{–}UTC = M8F\text{–}UTC(ZA) + \Delta_{UTC(ZA)-UTC} \tag{3.7}$$

where μ is the mean of all phase measurements, $\beta_{UTC(ZA)}$ is the delay added to UTC(ZA) by the short extension cable, $\times 2$ *cable* is the delays introduced by the two RG-58 coaxial cables, τ_{M8F} is the M8F's antenna group delay, α_{M8F} is the short cable leading to the M8F's antenna, ι_{M8F} is the delay added by the M8F's SMA to jumper adapter, and $\Delta_{UTC(ZA)-UTC}$ is the time difference between UTC(ZA) and UTC. Figure 3.27 shows the GPS receiver's electrical connections with the programmable power supply and laptop. The laptop ran the u-center GNSS evaluation software that provided a graphical user interface through which the GPS receiver could be configured. In addition, the software provided visualisation capabilities through which GNSS data such as position, velocity, time, and satellite tracking were monitored in real-time. To maintain full view of the

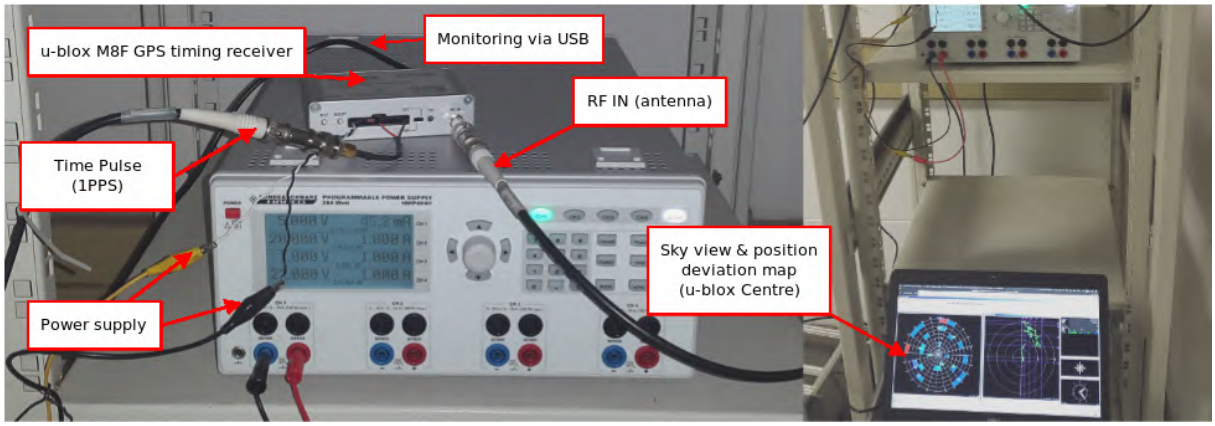

Figure 3.27: u-blox M8F calibration set-up at NMISA.

sky, the GPS receiver's patch antenna was mounted on the roof, 4m from the labora-

tory through a cable conduit, to ensure direct line-of-sight with all visible satellites. The antenna remained stationary for the duration of the calibration exercises. The patch antenna placement is depicted in Figure 3.28. NMISA precise timing infrastructure includes,

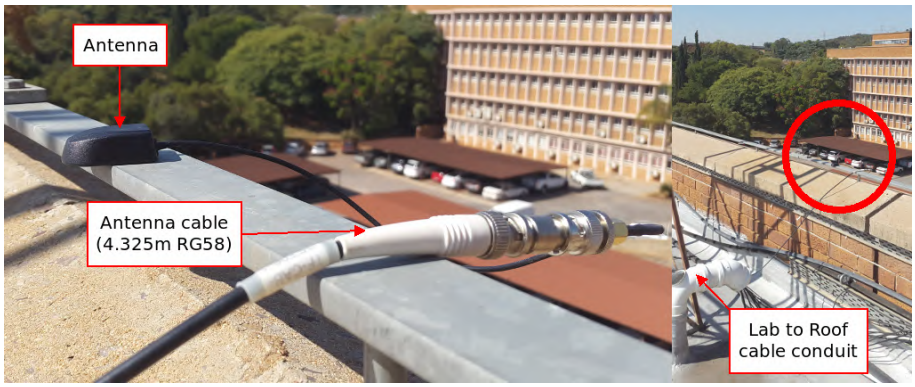

Figure 3.28: u-blox M8F antenna positioning on NMISA building rooftop.

three Hydrogen masers, six Caesium clocks, and multiple dual frequency GNSS receiver. UTC(ZA)is steered to within a few nano seconds of UTC. Figure 3.30 shows a graph

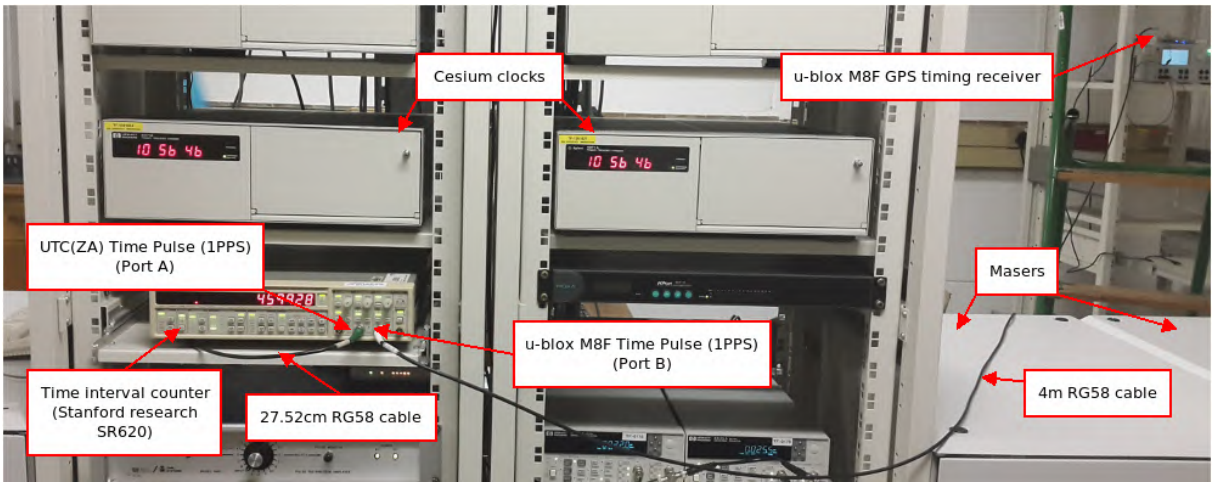

Figure 3.29: NMISA precise timing infrastructure and calibration set-up.

of the BIPM Circular T records showing the differences between true UTC maintained by BIPM and the NMISA laboratory that publishes UTC(ZA) around the GTR's u-blox M8F GPS timing receiver calibration day. The calibration was performed on 10 May 2018. Each point on the graph below is 5 days apart. NMISA UTC(ZA) was late to true UTC by around 2.7 ns on the day of the calibration. The GTR's GPS receiver (uBlox M8F) configurations are given in Table 3.7. GPS satellites at low elevations (horizon) are often excluded from a GPS solution because their signals experience considerable ionospheric delays and multipath effects. Excluding such satellites can degrade the overall satellite geometry for the calculations, resulting in greater errors. In contrast, signals from high elevation satellites experience less ionospheric delays and multipath effects. A balance in the choice of elevation mask is required to reduce the propagation delays and multipath

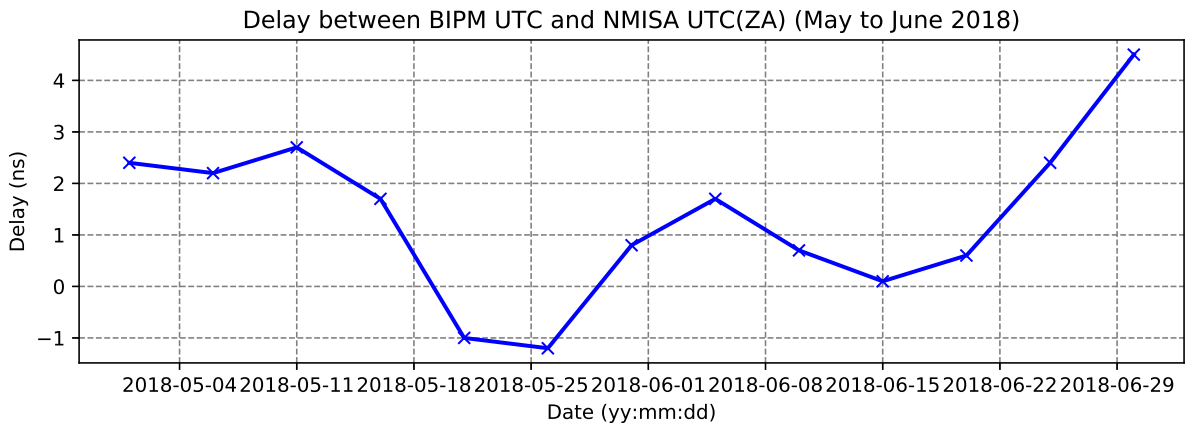

Figure 3.30: Differences between true UTC maintained by BIPM and UTC(ZA) maintained by NMISA laboratory on the day of calibration. Clock comparison data published regularly on the BIPM Time Department website [13].

Table 3.7: uBlox M8F GPS receiver calibration settings.

Receiver parameter	**Configuration**
Time Pulse	- Frequency locked: 1 Hz - Align pulse on GPS time lock - Duty cycle on lock: 50% - Rising edge on top of second
GNSS constellation	- GPS constellation only - Dynamic mode: Stationary - UTC standard: UTC(USNO) - Fix mode: 3D only - Minimum SV elevation: 20°
Calibration duration	- 24 hour calibration time - 900 seconds survey time - 1 m position accuracy (*Survey-In mode persisted throughout calibration)

whilst maintaining good satellite geometry. A study done by [53] recommended that GPS timing receivers deployed in relatively mobile timing applications as presented in this thesis, are most accurate when satellites at lower elevations continue to be included with an elevation mask in the range 10° to 20°. It should be mentioned that it was a good thing that the GPS receiver maintained the *Survey-In* mode during the calibration because the GTR was designed to be portable instrument capable of dynamically determining its stationary position. In practise, the instrument was expected to redetermine its 3D position every time the operator tested various telescope receivers located at varying distances

apart. If the on-board GPS receiver went into a *Fixed mode* with a 3D position of some radio telescope dish, all subsequent tests performed on dishes located in different locations would be invalid because the GPS receiver's time-pulse would be determined from a redundant position. Alternatively, the *Fixed mode* would be desirable in a single receiver or non array based radio telescope experimental set-up where a fixed 3D location is know resulting in better timing stability. In such a case, the GTR's GPS receiver would need be recalibrated in the *Fixed mode* however, the time it takes for the receiver to successfully survey its position with the required accuracy can be considerably long especially if affected by poor visibility, poor satellite geometry or multipath. If a field test requires that the GTR operates in the *Fixed mode*, the precise 3D position coordinates should be provided or adequate time should be allocated to guarantee that the GPS receiver determines the average antenna position with the required position accuracy.

3.4.3 Timing related subsystem characterisation

Given that the GPS receiver's time accuracy was traceable to UTC(ZA) and UTC by extension through calibration, the components that manipulate the receiver's 1PPS signal to radiate an RF timing signal required characterisation. In order to quantify the overall timing accuracy of the GTR instrument, each time critical component was accounted for by measuring the time delay that the respective components added to the calibrated GPS receiver's 1PPS reference signal. The following components and associated aspects were measured

1. Antenna group delay measurements.
2. RF switch characterisation.
3. Impact of 1PPS signal polarity on timing.
4. Antenna sensitivity.
5. Survey-In and Fixed mode comparison.
6. Impact of antenna placement on position and time accuracy.
7. Time to first fix test.

3.4.3.1 Antenna group delay measurements

In GPS applications, the antenna receiving signals from satellites needs to have a uniform group delay response over all angles of incident for maximum accuracy [54]. If the group delay varies over different elevation and azimuth incident angles, the angles will experience timing errors. In addition to the incident angle, group delay is a function of frequency. Receiving antennas consist of filters and LNAs depicted by Figure 3.14, have a response that varies with the incident signal's frequency. As part of characterising the receiver's antenna, the group delay was measured for GPS L1 frequency of 1575.42 MHz using the Rohde & Schwarz FSH8 spectrum analyser. The near field measurements conducted were

performed to obtain an indication of the impact of the filters and LNAs in the two active patch antennas compared however the measured delays were not accounted separately in the final result. The overall group delay of the chosen antenna was accounted for in the final larger offset determined through calibration. The spectrum analyser had S-parameter measurement capability which included antenna group delay measurements over a wide range of frequencies. The experiment consisted of two antennas, namely the receiving antenna being tested and a short stub transmitter antenna. The group delay measurement required that the stub antenna transmit a wideband signal and the group delay readings of receiving antenna be recorded for the frequency of interest. The experiment set-up is depicted in Figure 3.31. The two antennas were kept at close proximity and rotated in

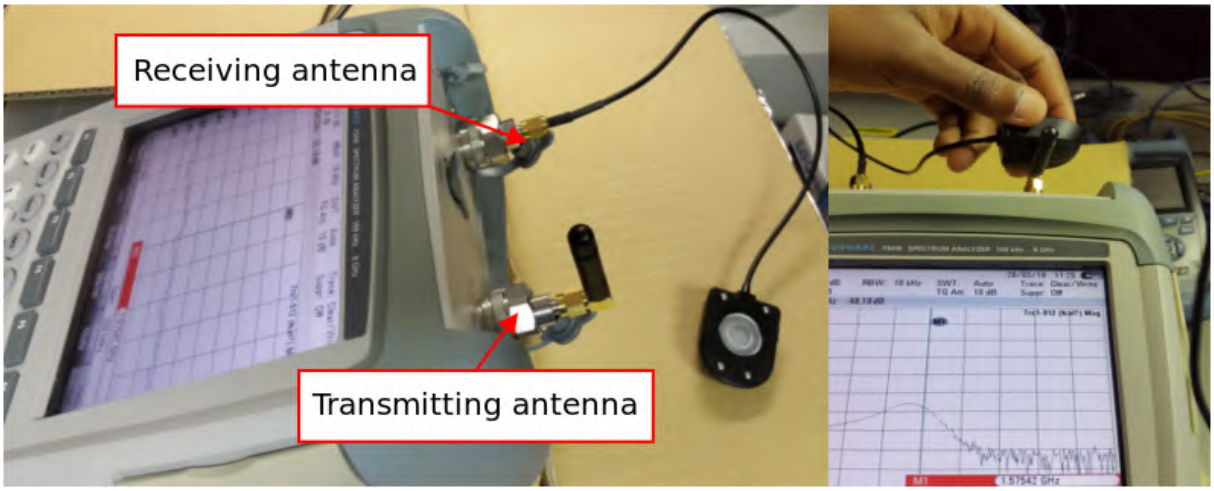

Figure 3.31: Antenna group delay measurements with the Rohde & Schwarz FSH8 spectrum analyser.

different elevation and azimuth incident angles to observe the overall impact on group delay. The experiment was performed for both u-blox ANN-SM and Taoglas active GPS patch antenna. The antenna group delay measurement results are presented in Section 4.2.2.

3.4.3.2 RF switch characterisation

The precision of the GTR's RF timing signal was broadly influenced by the RF switch that synchronously modulated the noise signal with the GPS receiver's 1PPS reference signal to produce the timing signal. The receiver generated 1PPS signal had a rise and fall time in the order of a few nanosecond which improves timing precision. By using the 1PPS signal as a digital logic driver to control the RF switch, traceability between the modulated RF signal and 1PPS signal was established. In contrast, the rise and fall time of the modulated RF signal is hardware dependent and significantly differs from that of the signal that controls the switch's internal control driver. The 1PPS and RF signal phase difference or delay was measured by an oscilloscope. The measurement was configured

to trigger on the GTR's BNC output 1PPS signal. The GTR generated RF noise timing signal's shape was determined by the oscilloscope's envelope detection algorithm. The phase measurement between the reference 1PPS signal and the half power mark of the RF signal was determined using the oscilloscope's vertical cursor utility. The results where recorded and the time offset between the receiver's 1PPS signal and RF switch's output signal was determined. The RF switch characterisation experimental set-up is depicted in Figure 3.32. The RF switch characterisation results are presented in Section 4.2.3.

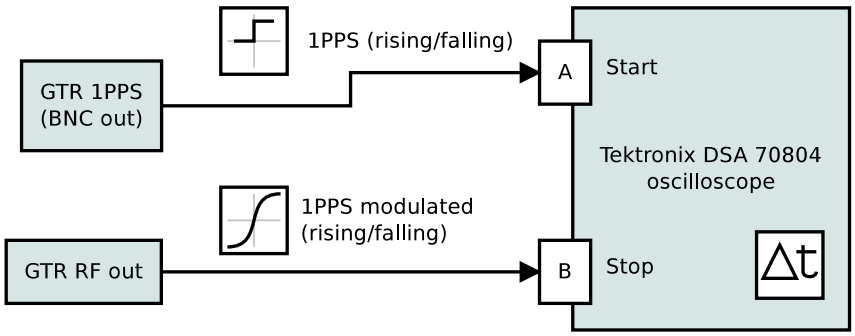

Figure 3.32: RF switch characterisation experimental set-up.

3.4.3.3 Impact of 1PPS signal polarity on timing

The GTR's GPS receiver 1PPS signal had a configurable pulse period, pulse length and polarity (rising or falling edge). The polarity was configured to mark the top of a second, thereby providing a utility through which amplitude modulation could be achieved. By controlling the RF switch's internal control driver with the 1PPS signal, amplitude modulation was achieved. While both polarities valid markers for precise time, the 1PPS polarity comparison experiment was conducted to determine whether there were timing errors introduced by using either a rising or falling edge. The experimental set-up consisted of a reference Rubidium standard 1PPS signal with rising edge polarity from the Spectracom time and frequency synchronisation System, 1PPS signal from the GTR's GPS receiver, and the Pendulum CNT-91 time interval counter. The polarity and frequency of the receiver's 1PPS signal were changed whilst the reference 1PPS signal remained unchanged. The phase difference was recorded as the polarity of the receiver's 1PPS signal was changed. Special attention was taken by ensuring that phase measurements were taken immediately after the polarity was changed to minimise the phase drift errors from both GPS discipled systems, thereby isolating the polarity time offset. The 1PPS signal polarity test experimental set-up is depicted in Figure 3.33. The impacts of 1PPS signal polarity on timing measurement results are presented in Section 4.2.4.

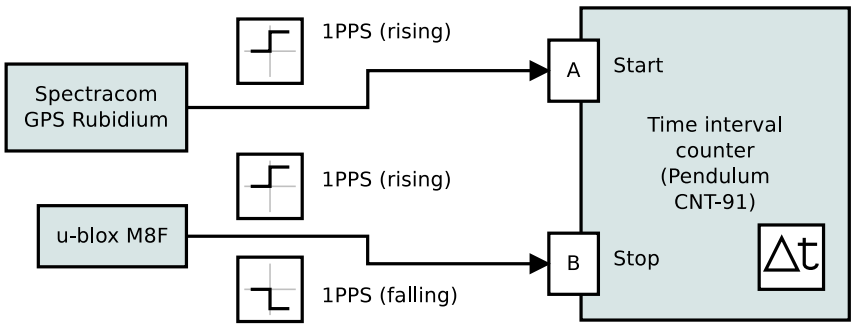

Figure 3.33: 1PPS signal polarity test experimental set-up.

3.4.3.4 Antenna sensitivity

The accuracy of GPS receivers in real-time is often much worse due to large noise in the GPS signal. The two antennas considered (u-blox ANN-SM active GPS antenna and Taoglas active GPS antenna) in the design where very similar with a difference in amplifier noise figure. The u-blox and Taoglas antennas had amplifier noise figures of 0.9 dB and 2.6 dB respectively. The antenna specifications are depicted in Table 3.3. A 24 hour experiment was performed to quantify the influence of antenna amplifier noise figure on the overall GPS receiver timing accuracy. Both antenna were mounted on the same platform with full view of the sky depicted by Figure 3.24. The receiver's time mode was set to the *Fixed mode* in which fixed position coordinates of the antenna were provided. The antenna position coordinates estimate was obtained from Google Maps®. The fixed position mode was use in order to eliminate position wondering errors in the time solution. The antenna sensitivity measurement results are presented in Section 4.2.5.

3.4.3.5 Survey-In and Fixed mode performance comparison

While the GTR was designed to be a short baseline test instrument, it was crucial to determine the GPS receiver's time error when operated in the *Survey-In* and *Fixed* dynamic mode. The short term accuracy was measured over 15 minutes (900 seconds) for both *Survey-In* and *Fixed* mode. The results obtained from the experiment were used to provide a better uncertainty budget estimate for the GTR's time accuracy. The time mode setting dialogs are shown in Figure 3.34. The *Survey-In* and *Fixed* mode comparison results are presented in Section 4.2.6.

3.4.3.6 Impact of antenna placement on position and time accuracy

The position of a GPS receiver antenna placement is crucial for optimal pseudorange measurements. The determination of the impact of obstructed satellite visibility and multipath was crucial on the accuracy of position and time. The antenna placement experiment was crucial in determining the real-time degradation in position and time accuracy. The experimental set-up was performed from two locations, one from a window

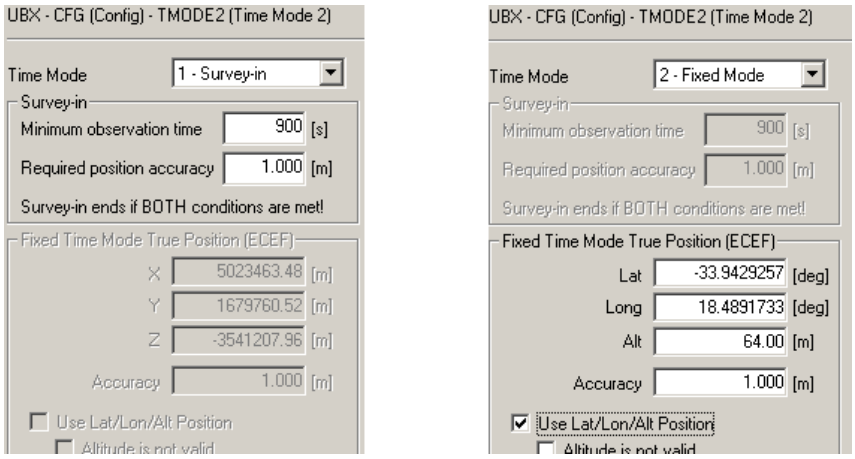

Figure 3.34: Time mode setting dialogs.

in a building with poor sky visibility and the other from the roof with an unobstructed sky view. The antenna placement experimental set-up is depicted in Figure 3.35. The

Figure 3.35: Antenna placement experimental set-up. Window test on the left and roof test on the right.

GPS receiver antenna placement influence on position and time accuracy measurement results are presented in Section 4.2.7.

3.4.3.7 Time to first fix test

Time to first fix refers to the time required for a GPS receiver to acquire satellite signals and navigation data in order to determine the antennas position. Manufacturers typically state that receivers require a minimum of 15 minutes after the start of the synchronization to adjust the clock to settle to a required accuracy [55]. The waiting period gives the GPS receiver enough time to receive complete navigation messages from all available GPS satellites in order to determine correction parameters and generate a precise time-pulse. The aim of the experiment was to determine the receiver's time to first fix in order to determine the minimum waiting time before an operator could set the GTR to begin transmitting a reliable timing signal. The experiment set-up consisted of the GPS receiver

and a stop watch. The stop watch was used to measure the duration between a receiver cold start and GPS time lock. The time to first fix test results are presented in Section 4.2.8.

3.4.4 Electromagnetic reverberation chamber test

The GTR was RFI tested in SARAO's electromagnetic reverberation chamber located in Cape Town. Based on the measurements, the separation distance required to attenuate the GTR's radiated signal to a level that did not saturate MeerKAT's receivers was determined. The electromagnetic reverberation chamber experimental set-up is depicted in Figure 3.36. The South African Radio Astronomy Service (SARAS) determines the levels

Figure 3.36: GTR electromagnetic reverberation chamber test set-up.

of radio frequency interference capable of degrading the performance of radio telescopes, generated by devices operating in locations surrounding the radio telescope receivers. The interference impact are referenced at the input of a low noise amplifier (LNA). The SARAS protection levels was based on the International Telecommunication Union's (ITU) Protection criteria for radio astronomical measurements [56]. The most severe impact of radio frequency interference causes saturation in parts of the receiver resulting in loss of sensitivity which renders astronomical signals unobservable. The reverberation chamber test results are presented in Section 4.2.9.

3.5 MeerKAT timing experiments

Each of the MeerKAT radio telescope dishes was equipped with an L-band receiver and digitiser mounted on a pivoting indexer platform used to select the frequency band. The digitiser units were responsible for digitising the astronomical signals at 1712 MHz sam-

pling frequency. The MeerKAT time and frequency (TFR) subsystem was responsible for transmitting the digitiser sample clock and synchronisation pulse. In addition, the TFR subsystem was also responsible for measuring the delay to each digitiser unit in order to determine the synchronisation pulse's offset to the telescope time. The sample clock and synchronisation pulse are transmitted over optical fibre links in order to keep the time error to a minimum. The delay offsets were determined by measuring the round trip delay of the reflected light pulse, and the offset was used to correct the apparent time of arrival (TOA). The time at each digitiser relative to the telescope reference time was calculated as half of the round trip delay plus other known systematic offsets. The corrected apparent time was used to ensure absolute timestamping of astronomical signals. Pulsar timing and fast radio transient observations have become a leading science area for MeerKAT. Detecting individual sources above the gravitational wave background was

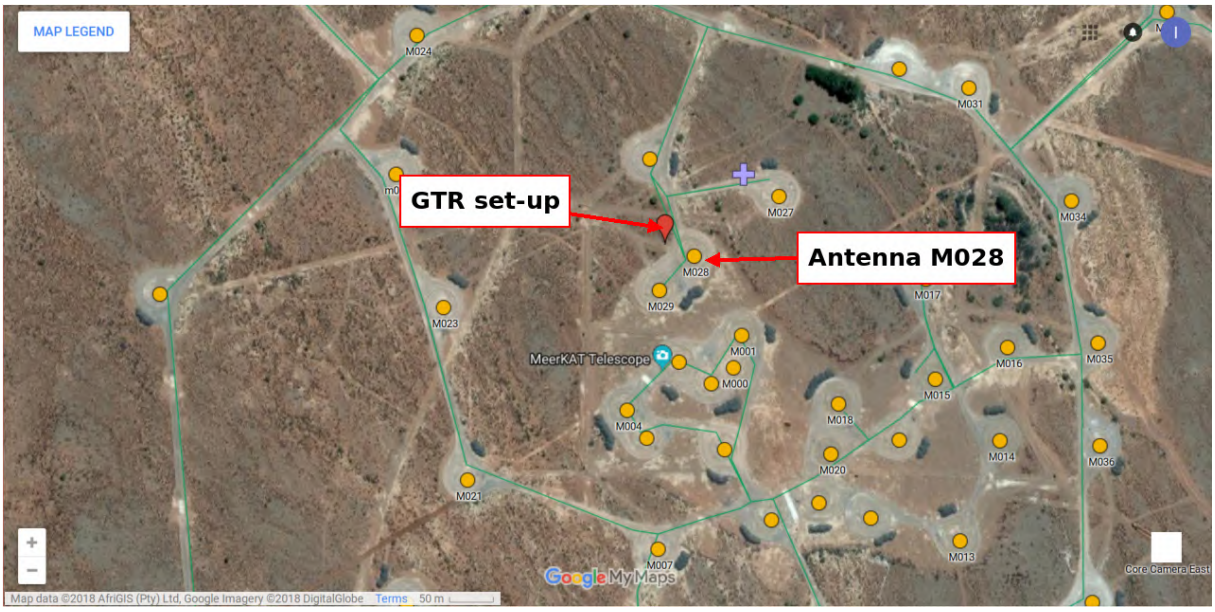

Figure 3.37: Layout of MeerKAT antennas on Google Maps®.

predicted to require timing precision of 5 ns to 50 ns [57]. Consequently, there was a requirement imposed on Meerkat data products to achieve a timing uncertainty of less than 5 ns with regards to UTC. The GTR instrument was designed to determine the delay offset between the data products timestamps and UTC. Timing uncertainty in MeerKAT is attributed to the stability of atomic clock ensemble, and the associated control and monitoring system. The MeerKAT field test set-up consisted of the GTR instrument, double ridge horn antenna and a single dish belonging to the MeerKAT radio telescope array. The GTR and antenna were placed North West of the M028 MeerKAT dish at a distance of 26.2 m to the L-band receiver and 28.36 m distance to the dish pedestal as measured by a BOSCH PLR 50C range finder. The field test set-up is depicted in Figure 3.37 and 3.38. The receiver positioner was configured to use the L-band receiver with the dish pointing in the direction of 238° azimuth and 30° elevation depicted in Figure B.5 in

Figure 3.38: GTR and horn antenna set-up during MeerKAT field test.

Appendix B. The Meerkat timing experiment results are presented in Section 4.3.

3.5.1 1PPS edge polarity based timing

The 1PPS signal is used as the definition of a second. The choice of polarity is arbitrary although the generally adopted convention in the timing community is the rising edge. The 1PPS polarity based timing test was designed to transfer time over RF whilst maintaining the familiar convention of a 1PPS signal in the time domain. It furthermore simplified the method of determining time offset on the radio telescope by enabling the use of simple envelope detection in the time domain raw digitiser voltage data products to determine the 1PPS pulse transition time. The accuracy in determining the RF 1PPS pulse transition time on MeerKAT was improved by averaging a set of captured pulses. Given that the RF 1PPS pulse was derived from a random noise generator, special attention should be paid to the integration time as noise averages to zero if averaged long enough. The time domain raw digitiser voltage data products captured by the radio telescope where squared and expressed as positive voltages in order improve the 1PPS signal's envelope and mitigate integration time limitations. The rising edge 1PPS polarity based timing test is summarised in Figure 3.39. The clock comparison data published in the BIPM Time Department website was used to determine the delay between UTC and UTC(ZA). The delay between the u-blox M8F GPS receiver and UTC(ZA) was determined by calibration. The delay between the GPS receiver reference on its 1PPS connector and the pulse distribution buffer was measured with a time interval counter. The delay between the rising edge of the buffered 1PPS signal and RF switch's output was measured with an oscilloscope. The delay between the rising edge of the GTR's RF 1PPS signal and that

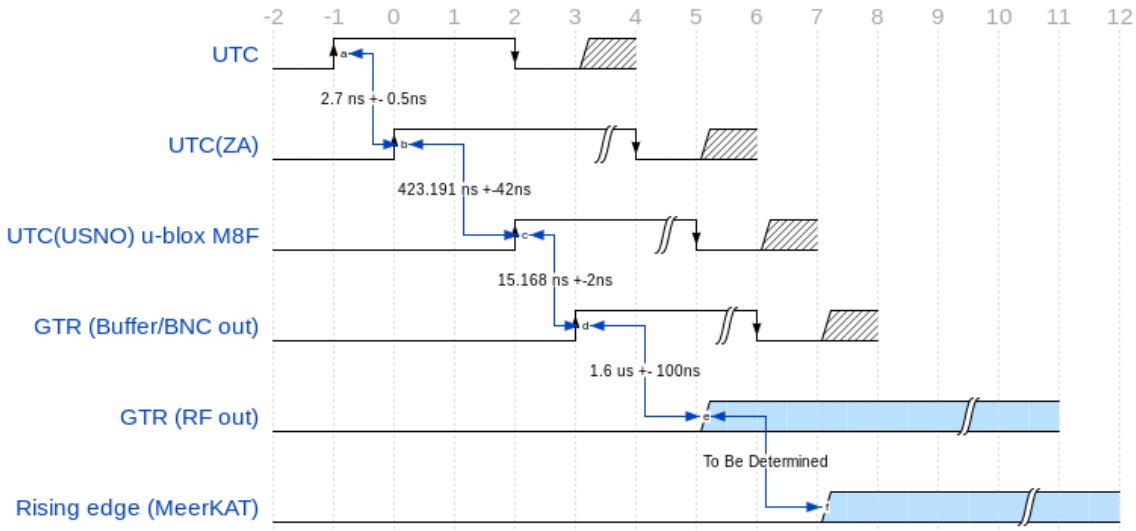

Figure 3.39: 1PPS rising edge timing diagram.

captured by the MeerKAT radio telescope was determined by calculating the difference between the expected edge transition timestamp and the timestamp reported by the telescope. The values shown in the timing diagram in Figure 3.39 and 3.40 were obtained from the calibration and characterisation experiments. The graphs from which the values are derived are given in the respective experiment in Chapter 4.

In contrast, a falling edge 1PPS signal can also be used for timing. The falling edge was preferred because the RF switch's response showed a sharper edge when compared to the rising edge. The edge transition shape was crucial in the effectiveness of envelope detection algorithms used in determining the edge transition time. The GTR's RF conditioning subsystem responded differently to the 1PPS signal polarity, special attention should be paid when deciding on the polarity for consistency. The falling edge 1PPS polarity based timing test is summarised in Figure 3.40. The clock comparison data published in the BIPM Time Department website was used to determine the delay between UTC and UTC(ZA). The delay between the u-blox M8F GPS receiver and UTC(ZA) was determined by calibration. The delay introduced by using the falling edge was measured with a time interval counter. The delay between the GPS receiver's 1PPS connector and the pulse distribution buffer was measured with a time interval counter. The delay between the falling edge of the buffered 1PPS signal and RF switch's output was measured with an oscilloscope. The delay between the falling edge of the GTR's RF 1PPS signal and that captured by the MeerKAT radio telescope was determined by calculating the difference between the expected edge transition timestamp and the timestamp reported by the telescope. The GTR's GPS receiver (u-blox M8F) settings for MeerKAT timing test on dish M028 for 1PPS polarity based timing test is summarised in Table 3.8. The time ambiguity $T_{ambiguity}$ of a 1 Hz 1PPS rising edge signal with a 10% duty cycle is given by Equation 3.8. The time ambiguity of the 1PPS signal is equal to 100 ms. The time

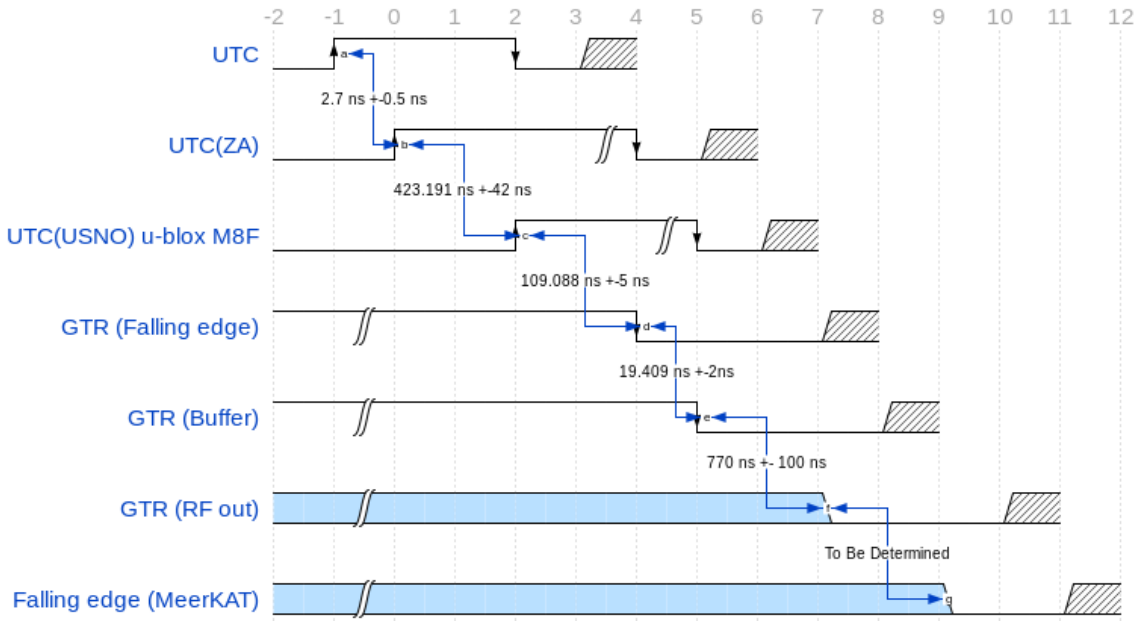

Figure 3.40: 1PPS falling edge timing diagram.

ambiguity is the maximum absolute time delay between the radio telescope time and GTR time such that there is no ambiguity on which of the two is late or early with respect to the other. The time ambiguity of a 1PPS falling edge signal with a 90% duty cycle is also equal to 100 ms. According to Equation 3.8, an increase in duty cycle increases the time ambiguity. If a large delay is expected between the telescope time and UTC, the GTR's 1PPS duty cycle can be increased in order to accommodate large delays whilst maintaining certainty in determining whether or not the telescope time is late or early.

$$T_{ambiguity} = \frac{duty\ cycle}{f_{GPS\ lock}} = \frac{10\%}{1\ Hz} = 100\ ms \tag{3.8}$$

The receiver was configured to generate a 1PPS signal upon locking to GPS time traceable to UTC(USNO). The 1PPS polarity and duty cycle were changed accordingly. The GPS constellation was used exclusively with tracking limited to satellites that were above the horizon by 10°. Given that the GTR was designed to be a portable instrument, the survey duration was set to 24 hours to prevent the receiver from setting a persistent position during the test. The 1PPS polarity based timing field test set-up is depicted in Figure 3.41. The GTR and horn antenna were placed North West of the M028 MeerKAT dish at a distance of 26.2 m to the L-band receiver. Summary of transmission delays and cable loss:

- Total cable loss: 0.449 dB + 2.694 dB + 1.158 = 4.301 dB
- Total attenuator block loss: 10 dB + 3 dB = 13 dB
- Total attenuation in transmit path: 17.301 dB
- Total transmit path delay: 2.58 ns + 15.174 ns + 13.158 ns = 30.912 ns

Table 3.8: u-blox M8F GPS receiver settings for MeerKAT timing test on dish M028 for 1PPS polarity based timing test.

Receiver parameter	**Rising edge on top of second**	**Falling edge on top of second**
1PPS	- Frequency on lock: 1 Hz - Align pulse on GPS time lock - Duty cycle on lock: 10% - Rising edge on TOS	- Frequency locked: 1 Hz - Align pulse on GPS time lock - Duty cycle on lock: 90% - Falling edge on TOS
GNSS constellation	- GPS constellation only - Dynamic mode: Stationary - UTC standard: UTC(USNO) - Fix mode: 3D only - Minimum SV elevation: 10°	- GPS constellation only - Dynamic mode: Stationary - UTC standard: UTC(USNO) - Fix mode: 3D only - Minimum SV elevation: 10°
Survey-In duration	- 24 hours/86400 seconds - 1 m position accuracy	- 24 hours/86400 seconds - 1 m position accuracy

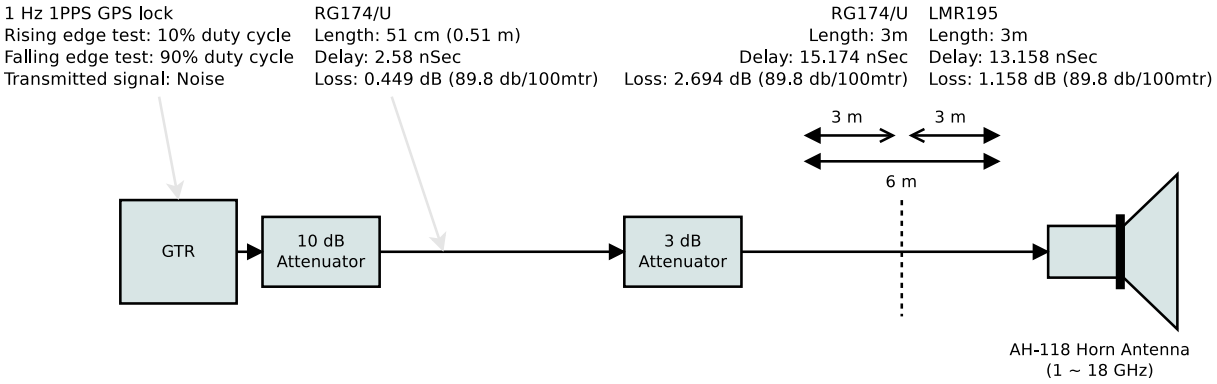

Figure 3.41: 1PPS polarity based MeerKAT timing experimental set-up.

- Signal propagation delay over 26.2 m = 87.33 ns

It was crucial that all delays and cable losses introduced by cables and RF components external to the GTR instrument were recorded in order to give the most accurate time audit of the radio telescope under test as possible.

3.5.2 1 kHz pulse edge polarity based timing

Although similar to the PPS based timing test, the 1 kHz pulse test was specifically designed to reduce the integration or folding time by generating a thousand of pulses per second. The telescope can fold a larger number of pulses per second thereby improving the measurement accurate over a short period of time without generating large volumes of

data. The 1 kHz pulse based timing test identical to the PPS rising edge timing diagram depicted in Figure 3.39. The u-blox M8F GPS receiver settings for MeerKAT timing test on dish M028 for 1PPS polarity based timing test is summarised in Table 3.9. The time

Table 3.9: uBlox M8F GPS receiver settings for MeerKAT timing test on dish M028 for 1 kHz digitiser.

Receiver parameter	**Configuration**
1PPS	- Frequency on lock: 1 kHz - Align pulse on GPS time lock - Duty cycle on lock: 10% - Rising edge on top of second
GNSS constellation	- GPS constellation only - Dynamic mode: Stationary - UTC standard: UTC(USNO) - Fix mode: 3D only - Minimum SV elevation: 10°
Survey-In duration	- 24 hours/86400 seconds - 1 m position accuracy

ambiguity $T_{ambiguity}$ of a 1 kHz 1PPS rising edge signal with a 10% duty cycle is given Equation 3.9. The time ambiguity of the 1 kHz 1PPS signal is equal to 100 μs. An increase in 1PPS frequency reduces the time ambiguity resulting in a shorter unambiguous range suitable for shorter telescope time to UTC delays. In contrast, by using a 1 kHz 1PPS signal, there is a thousand pulses within a one second period, a special attention must be paid if the 1PPS polarity based timing test is used. The definition of a second can be lost since the device under test cannot unambiguously determine the first UTC aligned pulse in a set of thousands.

$$T_{ambiguity} = \frac{duty\ cycle}{f_{GPS\ lock}} = \frac{10\%}{1\ kHz} = 100\ \mu s \tag{3.9}$$

The receiver was configured to generate a 1k Hz 1PPS signal upon locking to GPS time traceable to UTC(USNO). The 1PPS polarity and duty cycle were changed accordingly. The GPS constellation was used with tracking limited to satellites that were above the horizon by 10°. Given that the GTR was designed to be a portable instrument, the survey duration was set to 24 hours to prevent the receiver from setting a persistent position during the test. A team of engineers and scientists qualified to drive the radio telescope configured the receiver and took measurements. The 1 kHz pulse based timing field test set-up is depicted in Figure 3.42. The GTR and horn antenna were placed North West of the M028 MeerKAT dish at a distance of 26.2 m to the L-band receiver.

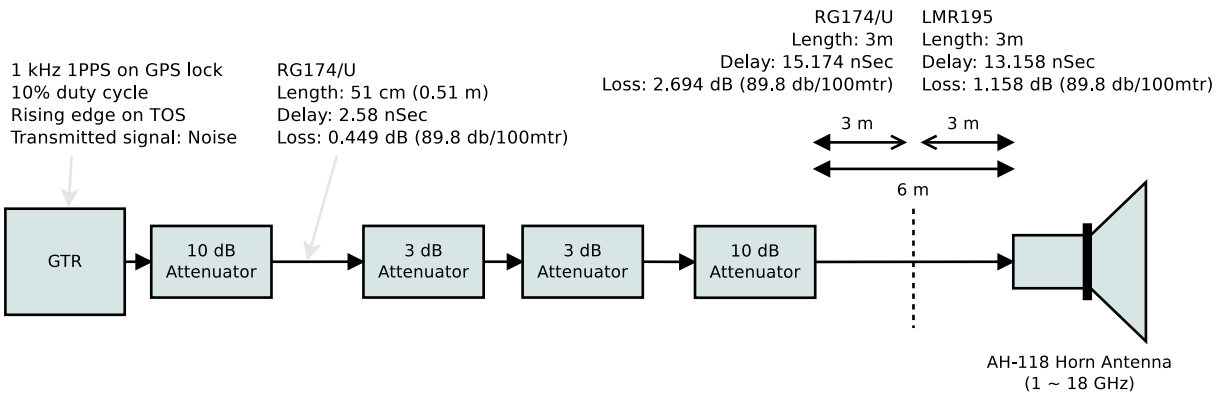

Figure 3.42: 1 kHz pulse MeerKAT timing experimental set-up.

Summary of transmission delays and cable loss:

- Total cable loss: 0.449 dB + 2.694 dB + 1.158 dB = 4.301 dB
- Total attenuator block loss: 10 dB + 3 dB + 3 dB + 10 dB = 26 dB
- Total attenuation in transmit path: 30.301 dB
- Total transmit path delay: 2.58 ns + 15.174 ns + 13.158 ns = 30.912 ns
- Signal propagation delay over 26.2 m = 87.33 ns

It was crucial that all delays and cable losses introduced by cables and RF components external to the GTR instrument were recorded in order to give an the most accurate time audit of the radio telescope under test as possible.

3.5.3 Non PPS edge polarity based timing

The 1 kHz pulse presents an innovative and potentially more accurate method for testing timestamps in radio telescopes through the use of pulsar timing principles. This method was proposed because the GTR's RF signal edges were not sharp enough to see below 1 us, while the entire pulse might be useful for timing with an accuracy down to 10 ns or better. The objective of pulsar timing as discussed in Section 2.2.2.3, is to determine the time argument that corresponds to the maximum peak in the output of the cross-correlation function of pulses. Preliminary work was performed in determining the delay between the receiver's 1PPS signal and RF switch output pulse's center. The delay was measured with a high resolution oscilloscope, and accurately calculated numerically in Python using Equation 3.10 there by establishing traceability to UTC(ZA) and UTC. The concept on which TOA estimation of pulsar signals is based on is depicted in Figure A.19 in Appendix A. The center of a pulse, also refereed to as center of gravity is determined by

$$Center\ of\ gravity = \frac{\sum x_N y_N}{\sum y_N} \tag{3.10}$$

where N is the total number of pulse samples, x_N is the timestamp of each sample and y_N is the magnitude of each sample. The center of gravity result is the timestamp that corresponds to the center of the pulse with units in seconds. The TOA of a pulsar signal is determined as [58]

$$TOA = t_{ref} + t_{dif} - t_{group} \tag{3.11}$$

where t_{ref} is the reference clock, t_{dif} is the time delay of the filtered signal relatively to the cross-correlation peak of the pulsar template, and $tgroup$ is the group delay of the radio telescope's filter. The TOA timestamp that corresponds to the center of the pulse as described by Equation 3.11 can be used to calculate the difference to the expected timestamp to determine the delay between the GTR and telescope time standard. The timing diagram on which the center of gravity concept is based is depicted by Figure 3.43. The center of gravity concept was an independent invention to allow more accurate

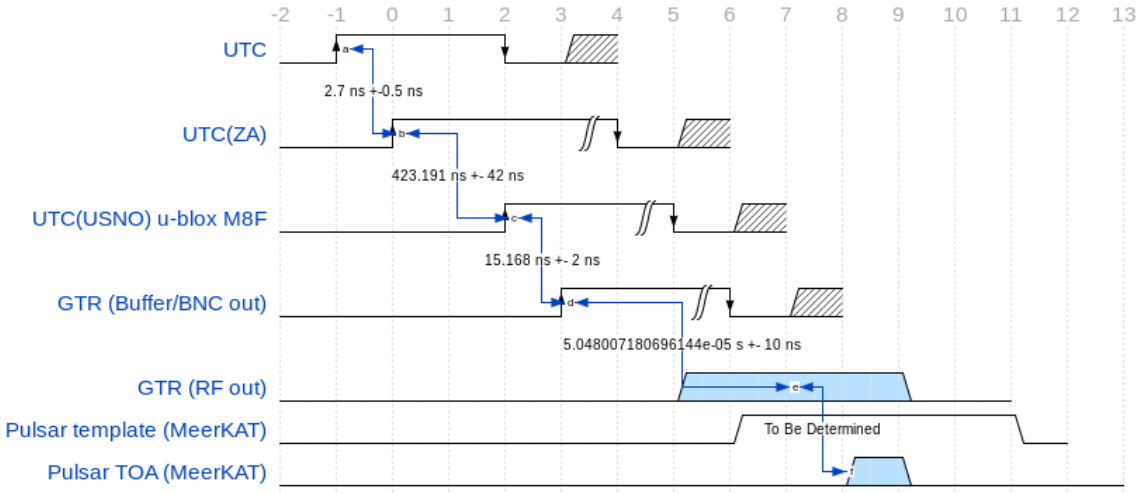

Figure 3.43: 1 kHz pulse timing diagram.

transfer of the time from the GTR RF output to the MeerKAT detected power input. The concept was not considered as the primary timing technique in this thesis although future work is planned to compare the technique's accuracy in timing against the 1PPS edge polarity based technique.

3.6 Design summary

Table 3.10 summarises the system requirements (SR), associated user requirements (UR), and how the system requirements were implemented and verified to ensure they satisfy the user requirements. The summary serves as an indication of the high level explanation of the experiments and methods used to verify each capability of the GTR. Some of the derived requirements of system requirement 4 and 5 required a survey from the two main users, namely, MeerKAT system engineers and commissioning scientists to verify the

requirements through visual inspections and demonstration. Quantifiable results obtained from the experiments are detailed in Chapter 4.

Table 3.10: Summary of System Requirements for the GTR and the associated verification procedures.

SR	**Description**	**UR**	**Experiment or verification**
1	Radiate a periodic timing signal that coincide with UTC.	UR1, UR2	Experiment 1–8: The on-board GPS receiver that provides the time and frequency reference was calibrated at NMISA. The result where analysed to verified the performance.
2	Timing signal comply with radio frequency interference (RFI) restriction imposed by the radio astronomy observatory.	UR4	Experiment 9: The frequency spectrum of the RF timing signal was measured with a spectrum analyser and the reverberation chamber. The frequency response was analysed to verify compliance with SARAS standards and results used to apply for a permit.
3	The GTR instrument shall be portable.	UR2, UR5, UR6	The instrument was designed to operate from a battery. A rechargeable battery with a common voltage rating and high current capacity was chosen. The instrument was designed to fit into a back pack sized carry case..
4	The GTR instrument's design shall use human factors and ergonomics principles.	UR5, UR6	The instrument was designed using the turn key principle. LEDs, markers, modular connectors and tactile switches were used to provide a clear visual indication for status and purpose. Electrical protection components were used for electrical shock and fire hazard protection.
5	The GTR shall operate successfully in both dry and wet weather conditions.	UR5	The instrument was assembled and enclosed in a IP68 rated aluminium enclosure which provides protection from water and dust.

Chapter 4

Results

The results obtained from experiments 1 through 9 are documented in this chapter. The design details of the experiments are discussed in Section 3.4. The results obtained from the calibration performed at the National Metrology Institute of South Africa (NMISA) are presented in Section 4.2.1. The antenna group delay measurement results are presented in Section 4.2.2. To determine the delay introduced by modulating the calibrated 1PPS signal to a radio frequency (RF) signal, the RF switch characterisation results are presented in Section 4.2.3. The results from the investigation into whether or not setting the u-blox GPS receiver's 1PPS polarity as rising or falling edge influenced the GPS time-pulse radiator's (GTR) accuracy is presented in Section 4.2.4. The results from the 24 hour experiment performed to quantify the influence of the noise figure on the overall GPS receiver timing accuracy is presented in Section 4.2.5. The GPS receiver's timing uncertainty results when operated in the *Survey-In* and *Fixed* position mode is presented in Section 4.2.6. The results obtained from operating the GTR's in two different environments affecting satellite visibility are presented in Section 4.2.7. In order to determine how long the GTR would take to acquire GPS time lock, the results obtained from the time to first fix are presented in Section 4.2.8. The results form the reverberation chamber that measured the signal power radiated by the GTR is presented in Section 4.2.9. Compelling results obtained from performing timing experiments on the MeerKAT radio telescope are presented in Section 4.3. The timing accuracy investigated by the GTR instrument characterisation experiments was of the GTR device and not of the device under test such as the MeerKAT radio telescope. The GTR was designed to be a verification tool and the timing uncertainties discovered from the radio telescope's data products were assumed to be of the radio telescope being tested.

4.1 Summary of results achieved

The GTR was successfully characterised using a series of rigorous experiments. Each experiment was performed to determine the impact that each subsystem and configuration

had on the GTR's timing accuracy. All delays mentioned in this section emanate from the results of the characterisation experiments. The GTR's timing accuracy with respect to UTC(ZA) and UTC is given in Table 4.1. A positive delay meant that the time standard being tested was ahead (late) whereas a negative delay means the time standard was behind (early). The GTR's 1 Hz falling edge RF timing signal with a 90% duty cycle ($GTR_{1Hz–fall–90\%}$) was 1.31 μs ahead of UTC(ZA) and 1.32 μs ahead of UTC. The GTR's 1k Hz rising edge RF timing signal with a 10% duty cycle ($GTR_{1kHz–rise–10\%}$) was 2.10 μs ahead of UTC(ZA) and 2.10 μs ahead of UTC. The GTR time conversion table was

Table 4.1: GTR time conversion table.

	UTC(ZA)	**UTC**
u-blox M8F GPS receiver	423.191 $\pm$ 42ns (3σ)	425.891 $\pm$ 42 ns (3σ)
$GTR_{1Hz–fall–90\%}$	1.31 $\pm$ 0.1 μs (1σ)	1.32 $\pm$ 0.1 μs (1σ)
$GTR_{1kHz–rise–10\%}$	2.10 $\pm$ 0.1 μs (1σ)	2.10 $\pm$ 0.1 μs (1σ)

derived from Equation 4.1, 4.2, 4.3, and 4.4. The delay between the GTR's 1 Hz falling edge RF timing signal with a 90% duty cycle with respect to UTC(ZA) is given by

$$\begin{aligned} GTR–UTC(ZA)_{1Hz–fall–90\%} &= M8F–UTC(ZA) + T_{rise–fall\ 1PPS} \\ &\quad + T_{buffer–fall} + T_{1Hz–fall–90\%} \\ &= (423.191 + 104.847 + 19.409 + 770)\ \text{ns} \\ &= 1317.447 \pm 100\ \text{ns}\ (1\sigma) \end{aligned} \tag{4.1}$$

where $M8F–UTC(ZA)$ is the calibrated delay between the u-blox GPS receiver and UTC(ZA) determined by Experiment 1, $T_{rise–fall\ 1PPS}$ is the average phase difference between the GPS receiver's 1PPS rising and falling edge determined by Experiment 4, $T_{buffer–fall}$ is the PPS buffer delay determined by Experiment 4, and $T_{1Hz–fall–90\%}$ is the RF timing signal's falling edge delay determined by Experiment 3. The delay between the GTR's 1 Hz falling edge RF timing signal with a 90% duty cycle with respect to UTC is given by

$$\begin{aligned} GTR–UTC_{1Hz–fall–90\%} &= GTR–UTC(ZA)_{1Hz–fall–90\%} + \Delta_{UTC(ZA)–UTC} \\ &= 1317.447\ \text{ns}\ + 2.7\ \text{ns} \\ &= 1.32 \pm 0.1\ \mu s\ (1\sigma) \end{aligned} \tag{4.2}$$

where $GTR–UTC(ZA)_{1Hz–fall–90\%}$ is the delay between the GTR's 1 Hz falling edge RF signal with a 90% duty cycle with respect to UTC(ZA) determined by Equation 4.1, and $\Delta_{UTC(ZA)–UTC}$ is the delay between UTC(ZA) and UTC on the day of calibration determined by Experiment 1. The delay between the GTR's 1k Hz rising edge RF timing

signal with a 10% duty cycle with respect to UTC(ZA) is given by

$$\begin{aligned} GTR\text{–}UTC(ZA)_{1kHz\text{–}rise\text{–}10\%} &= M8F\text{–}UTC(ZA) + T_{buffer\text{–}rise} + T_{rise\text{–}\ frequencies} \\ &= 423.191 \text{ ns} + 15.168 \text{ ns} + 1.665\ \mu s \\ &= 2.10 \pm 0.1\ \mu s\ (1\sigma) \end{aligned} \tag{4.3}$$

where $M8F\text{–}UTC(ZA)$ is the calibrated delay between the u-blox GPS receiver and UTC(ZA) determined by Experiment 1, $T_{buffer\text{–}rise}$ is the PPS buffer delay determined by Experiment 4, and $T_{rise\text{–}\ frequencies}$ is the rising edge delay for all PPS frequencies due to the RF switch determined by Experiment 3. The delay between the GTR's 1k Hz rising edge RF timing signal with a 10% duty cycle with respect to UTC is given by

$$\begin{aligned} GTR\text{–}UTC_{1kHz\text{–}rise\text{–}10\%} &= GTR\text{–}UTC(ZA)_{1kHz\text{–}rise\text{–}10\%} + \Delta_{UTC(ZA)-UTC} \\ &= 2103.359 \text{ ns} + 2.7 \text{ ns} \\ &= 2106.059 \pm 100 \text{ ns}\ (1\sigma) \end{aligned} \tag{4.4}$$

where $GTR\text{–}UTC(ZA)_{1kHz\text{–}rise\text{–}10\%}$ is the delay between the GTR's 1k Hz rising edge RF timing signal with a 10% duty cycle with respect to UTC(ZA) determined by Equation 4.3, and $\Delta_{UTC(ZA)-UTC}$ is the delay between UTC(ZA) and UTC on the day of calibration determined by Experiment 1. Compelling GTR field test results of a single MeerKAT telescope antenna are presented in Section 4.3.

4.2 GTR characterisation experiments

4.2.1 Experiment 1: Calibration results

The aim of the calibration was to determine the delay between the GTR's GPS receiver's 1PPS pulse traceable to UTC(USNO) and NMISA's official 1PPS pulse referred to as UTC(ZA). The calibration experiment set-up is depicted in Figure 3.26 and the GPS receiver's settings used are given in Table 3.7. The measurements were taken with a time interval counter and recorded into a file over a 24 hour period. The receiver did not achieve the 1 m position accuracy and maintained the survey mode during the duration of the calibration. Shortly after the calibration began, the receiver encountered a timing error in which the delay between the receiver and UTC(ZA) reduced from 450 ns (2018-05-10 14:57:26) to -3 ns (2018-05-10 15:19:16) in 1310 seconds (21 minutes) depicted in Figure 4.1. Since the time interval counter used UTC(ZA) as the measurement reference, during the error in which the receiver 1PPS was leading UTC(ZA), the time interval counter reported delays in the order of 1 second. This persisted for 510 seconds (8 minutes) after which the receiver recovered from the timing error, began to lag UTC(ZA) as expected and the delay increased from 23 ns to 400 ns in 29 seconds. Typically when a receiver failed to

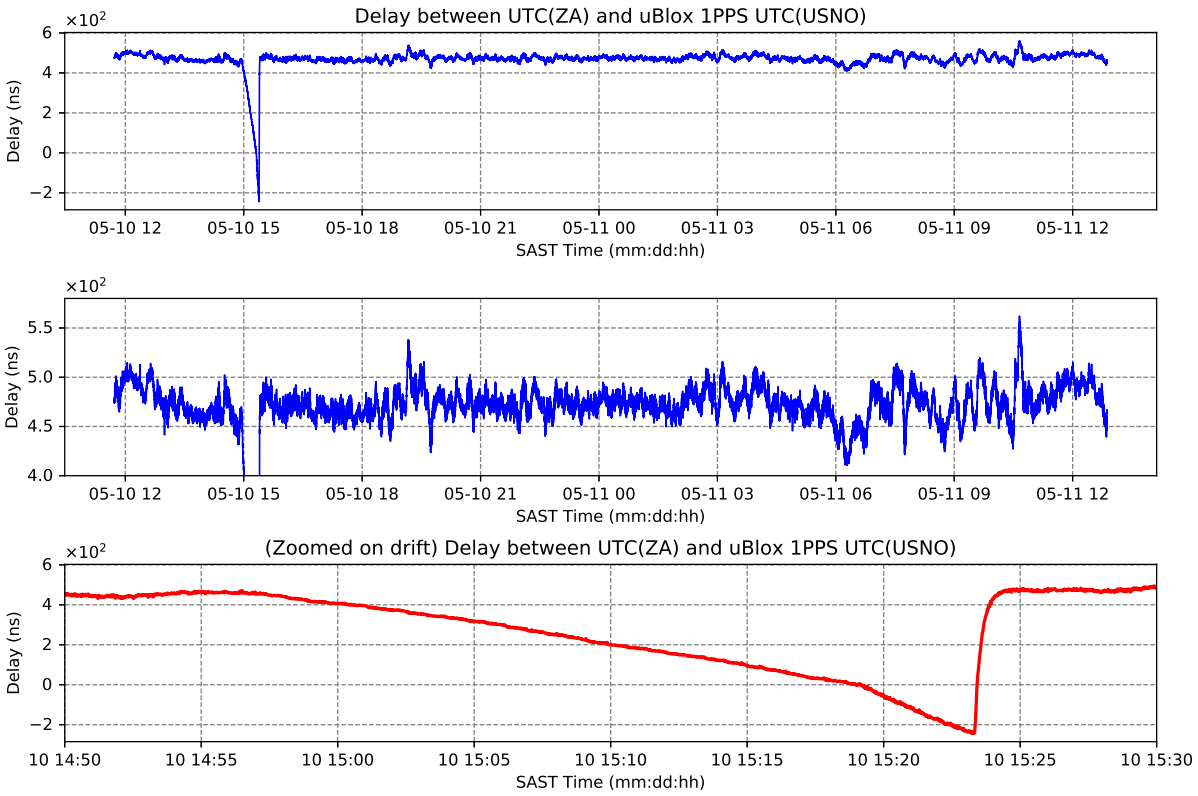

Figure 4.1: Calibration measurements with outliers.

track a minimum of four satellites whilst in the *Survey-In* mode, the receiver goes in to a *Hold-over* mode where it maintains time synchronisation with the stability of the reference oscillator. Whilst in this mode, the receiver time solution drifts and thereby remains the suspect cause of the error as experienced by [55]. Table 4.2 depicts the list of all available satellites at time of error to support evidence that there were enough satellite at the time of error resulting in outlier phase drift. Considering that the receiver remained in the *Survey-In* mode for the duration of the calibration experiment, the cause of the GPS receiver's 1PPS outlier phase drift was not found. As discussed in Section 2.4.5, the receiver's position, velocity and time is determined by taking pseudorange measurements from four or more satellites. Sophisticated survey grade GPS timing receivers generate data based on the Consultative Committee for Time and Frequency (CCTF) Group on GNSS Time Transfer Standards (CGGTTS) specification, and present data for each satellite tracked. The data file header consists of information about the GPS time transfer equipment, and the institution operating the equipment. PRN is the satellite vehicle PRN number, CL is the hexadecimal number that corresponds to the Common View class of the track, MJD the five digit Modified Julian Date of the start of the track, STTIME is the hour, minute, and second of the start of the track in UTC, TRKL is the track length in seconds (a full track is 780 seconds), ELV is the elevation of the satellite at the midpoint of the track, AZTH is the azimuth of the satellite at the midpoint of the track REFSV is the time difference (measured in .1 nanosecond) between the laboratory reference clock and satellite

Table 4.2: CGGTTS GPS data from NMISA's Septentrio PolaRx3eTR receiver.

PRN	CL	MJD	STTIME	TRKL	ELV	AZTH	REFSV
			hhmmss	s	.1dg	.1dg	1ns
21	FF	58248	125400	780	581	2647	+3968664
20	FF	58248	125400	780	569	1980	-5078375
24	FF	58248	125400	780	772	506	+495510
15	FF	58248	125400	780	486	1545	+3544089
21	FF	58248	131000	780	581	2804	+3968619
20	FF	58248	131000	780	630	1903	-5078403
24	FF	58248	131000	780	787	893	+495521
15	FF	58248	131000	780	445	1466	+3544087
21	FF	58248	132600	780	558	2950	+3968571
20	FF	58248	132600	780	692	1801	-5078400
24	FF	58248	132600	780	748	1210	+495513
15	FF	58248	132600	780	405	1392	+3544085

time, referred to the midpoint of the pass via a linear fit. GPS satellites are identified by PRN numbers range from 1 to 66. The Modified Julian Date 58248 corresponds to the date 10 May 2018. The STTIME time 125400 corresponded to the time 12:54.00 UTC+0. South African standard time (SAST) was 2 hours ahead of UTC+0, denoted as UTC+2. The time used in the time axis of the calibration plots was in SAST. The records in Table 4.2 are extracts from NMISA's Septentrio PolaRx3eTR receiver CGGTTS data filtered to only reflect GPS satellites as the receiver under calibration (u-blox M8F) made use of GPS satellites exclusively. After the outliers were removed, the delay measurements in Figure 4.2 were obtained. The receiver had a delay in the order of hundreds of nano

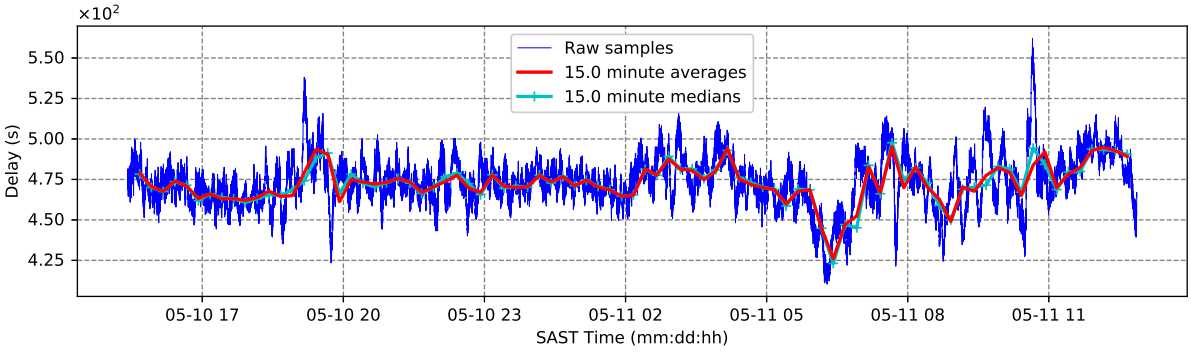

Figure 4.2: Calibration measurements with no outliers.

seconds as expected. The receiver had an average delay of 472.57 ns, median delay of 472.22 ns, and standard deviation of 15.899 ns. According to Figure 3.26, the 27.52 *cm* extension cable added a 1.39 ns delay to the calibrator's signal. Each of the two 4 m (RG-

58) introduced delays to the receiver's time solution by 20.08 ns and 20.19 ns respectively. NMISA UTC(ZA) was late to true UTC by around 2.7 ns on the day of the calibration. Using Equation 3.6 and 3.7, the measured delay was corrected for cable length delays and

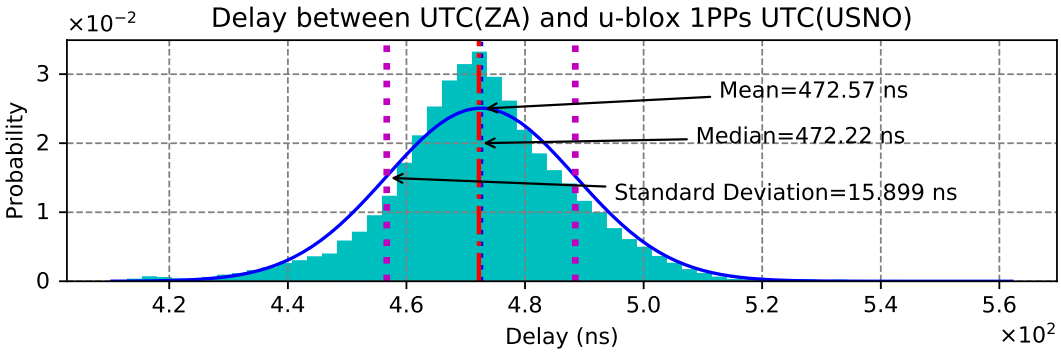

Figure 4.3: Delay between UTC(ZA) and u-blox 1PPS.

the absolute receiver to UTC(ZA) and UTC delay is given by

$$\begin{aligned} M8F\text{–}UTC(ZA) &= \mu + \beta_{UTC(ZA)} - \ (\times 2\ cable + \tau_{M8F} + \alpha_{M8F} + \iota_{M8F}) \\ &= 472.57\ \text{ns} + 1.39\ \text{ns} \ - (20.08\ \text{ns} + 20.19\ \text{ns} + 8.4\ \text{ns} \\ &+ 1.644\ \text{ns} + 0.48\ \text{ns}) \\ &= 423.191\ \text{ns} \end{aligned} \tag{4.5}$$

$$\begin{aligned} M8F\text{–}UTC &= M8F\text{–}UTC(ZA) + \Delta_{UTC(ZA)-UTC} \\ &= 423.191\ \text{ns} + 2.7\ \text{ns} \\ &= 425.891\ \text{ns} \end{aligned} \tag{4.6}$$

The 24 hour measurements were further reduced and analysed over 6 hour sets, and the results are depicted in Figure A.3 and A.4 in Appendix A. The Maximum Time Interval Error (MTIE) was calculated to determine the receiver's uncertainty budget. Since the GTR would be used repeatedly over short periods, the MTIE was calculated over a 15 minute period. The MTIE was calculated for each 15 interval over the 24 hours calibration period. The average MTIE was then determined and used as the receiver's uncertainty budget. The MTIE results are depicted in Figure 4.4. The receivers uncertainty budget was rounded off to 42 ns which was approximately three times the delay standard deviation. The final receiver accuracy to UTC(ZA) and UTC is given by

$$M8F\text{–}UTC(ZA) = 423.191 \ \pm 42\text{ns}\ (3\sigma) \tag{4.7a}$$

$$M8F\text{–}UTC = 425.891 \ \pm 42\ \text{ns}\ (3\sigma) \tag{4.7b}$$

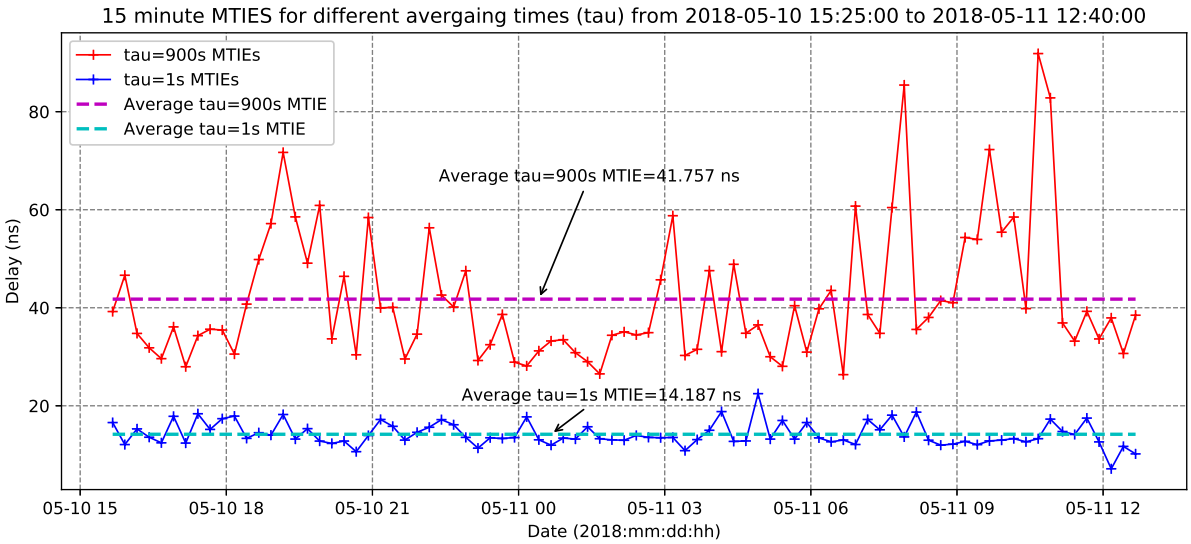

Figure 4.4: 15 minute MTIES for different averaging times (tau) over the calibration period.

4.2.2 Experiment 2: Antenna group delay measurements

The single frequency u-blox M8F GPS timing receiver was only capable of receiving the L1 GPS signal. The group delay was measured for GPS L1 frequency of 1575.42 MHz using the Rohde & Schwarz FSH8 spectrum analyser. The spectrum analyser radiated an L1 signal, and concurrently measured the radiated signal power and delay on an adjacent receiving antenna. The u-blox ANN-SM and Taoglas active GPS antenna group delays were measured and the resulsts presented in Figure 4.5 and 4.6. The Taoglas antenna had

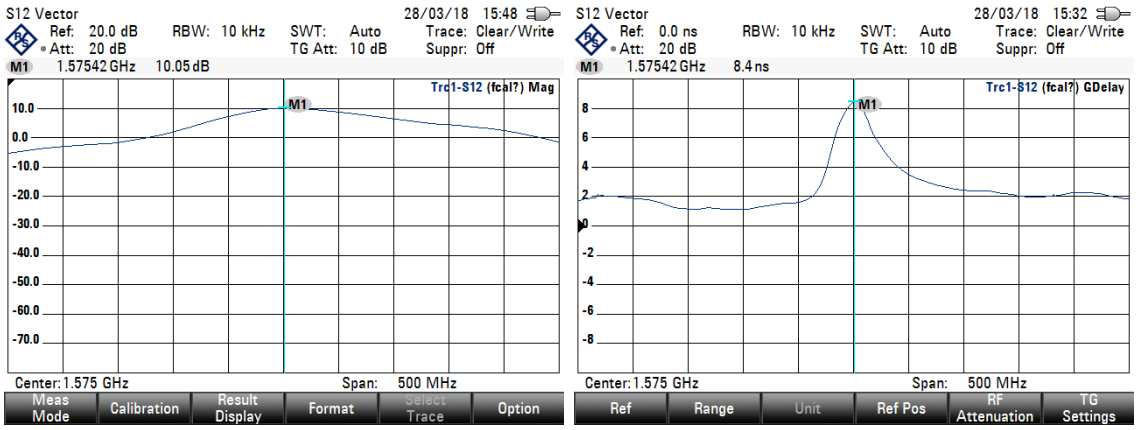

(a) Magnitude (b) Group delay

Figure 4.5: Taoglas active GPS antenna group delay measurement.

a group delay of 8.4 ns with a signal power of 10.05 dB. This antenna was used in the calibration and the measured group delay corresponding to ι_{M8F} was accounted for in the receiver's time accuracy. The measured signal power and group delay generally decrease with the increase in separation distance between the radiating and receiving antenna. The

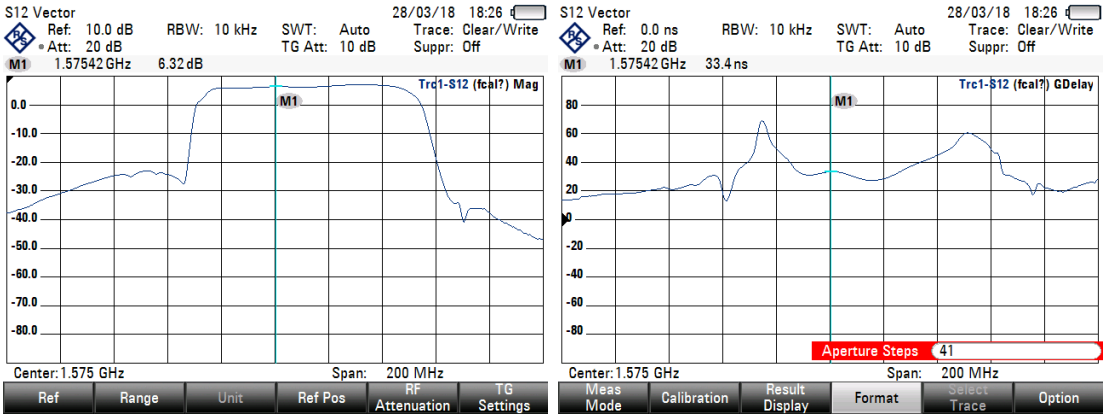

(a) Magnitude (b) Group delay

Figure 4.6: u-blox ANN-SM active GPS antenna group delay measurement.

u-blox ANN-SM antenna had a group delay of 33.4 ns with a signal power of 6.32 dB. The measurement results from both antennas is summarised in Table 4.3.

Table 4.3: Group delay measurements of the u-blox ANN-SM and Taoglas active GPS antennas.

	u-blox antenna	**Taoglas antenna**
Magnitude	6.32 dB	10.05 dB
Group delay	33.4 ns	8.4 ns

4.2.3 Experiment 3: RF switch characterisation

The precision of the GTR's RF timing signal was broadly influenced by the switching characteristics of the RF switching. The GPS receiver's 1PPS signal was used as the RF switch's switching logic driver, and the delay between the 1PPS signal and RF signal were measured in order to maintain traceability. The amplitude modulation scheme is depicted in Figure 4.7. The blue curve denoted as *GTR 1PPS BNC out* resented the receiver's 1PPS signal whilst the magenta and orange curves denoted as *GTR 1PPS Ant. out* represented the modulated RF signal. The RF signal response showed that the rising and falling edge were significantly stretched compared to the 1PPS signal. The Tektronix DSA 70804 oscilloscope was configured to trigger on the 1PPS signal and the delay was measured at 50% of each signal's amplitude. The rising edge delay was measured to be 1.665 μs consistent over all 1PPS signal frequencies as depicted in Figure 4.8 and given in Equation 4.9. The delay coincided closely with the switch's manufacturer switching time of 2.0 μs, implying that the switch required a digital logic driver signal with a duty cycle of at least 2 μs to switch on thereby radiating an RF signal. Careful attention was be paid to the 1PPS signal's duty cycle to ensure the GTR radiated the timing signal.

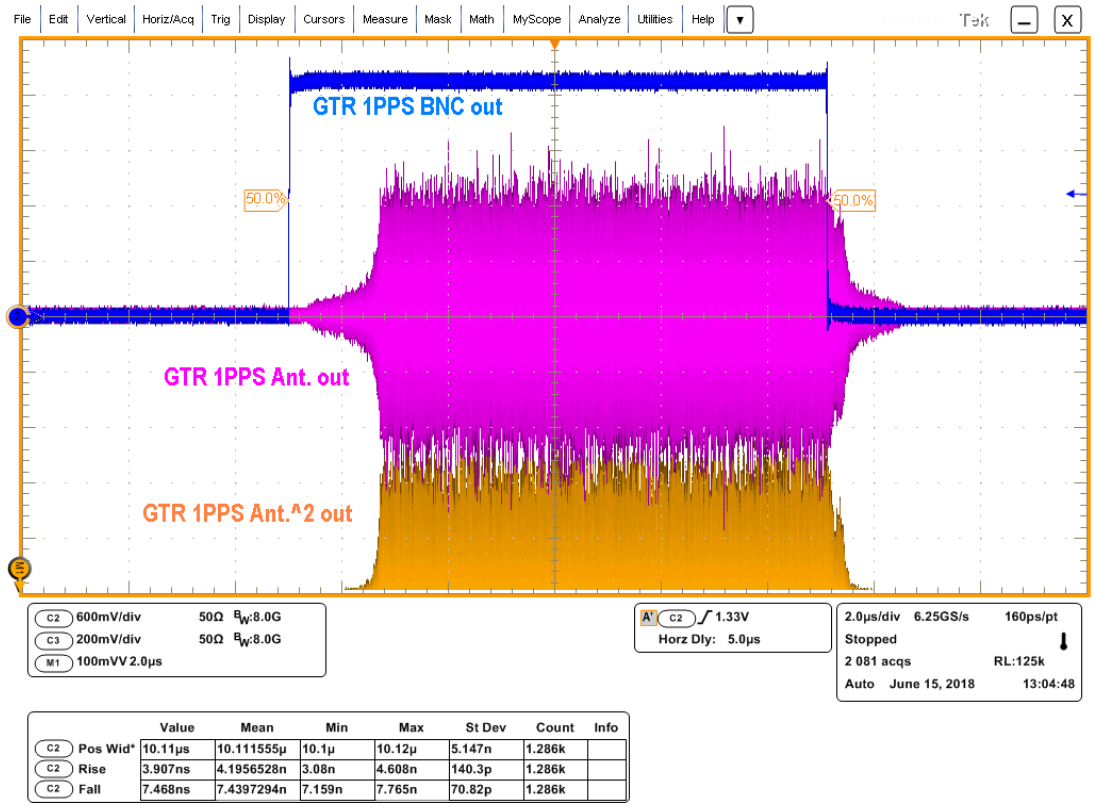

Figure 4.7: GTR's modulated RF timing signal.

The falling edge delay varied with the 1PPS signal's duty cycle and frequency. A rigorous test was conducted to measure the falling edge delay as the 1PPS signal's frequency was changed. The results are summarised in Table 4.4. The results showed that the falling edge delay decreased with an increase in frequency and duty cycles. Since the GTR operates independent of the radio telescope being tested, the crucial challenge in using high frequency 1PPS signals in timing is in determining the first pulse that is aligned to UTC(USNO) within the thousands. A 1 Hz falling edge 1PPS signal with a 90% duty cycle was chosen for the 1PPS polarity based timing test. The falling edge delay was measured to be equal to 770 ns.

$$T_{1Hz-fall-90\%} = 770 \text{ ns} \tag{4.8}$$

$$T_{rise-frequencies} = 1.665\ \mu s \tag{4.9}$$

The center of gravity technique could also be used as an alternative method to the polarity based timing signal. The technique could be useful for pulsar timing although radiating thousand of pulses per second introduces time ambiguities with regards to traceability. The time of arrival (TOA) corresponds to the pulse's maximum peak which is located at 50% of the modulating pulse width as depicted in Figure A.19. The center of gravity of the 1 kHz pulse was calculated from an oscilloscope generated file containing samples of

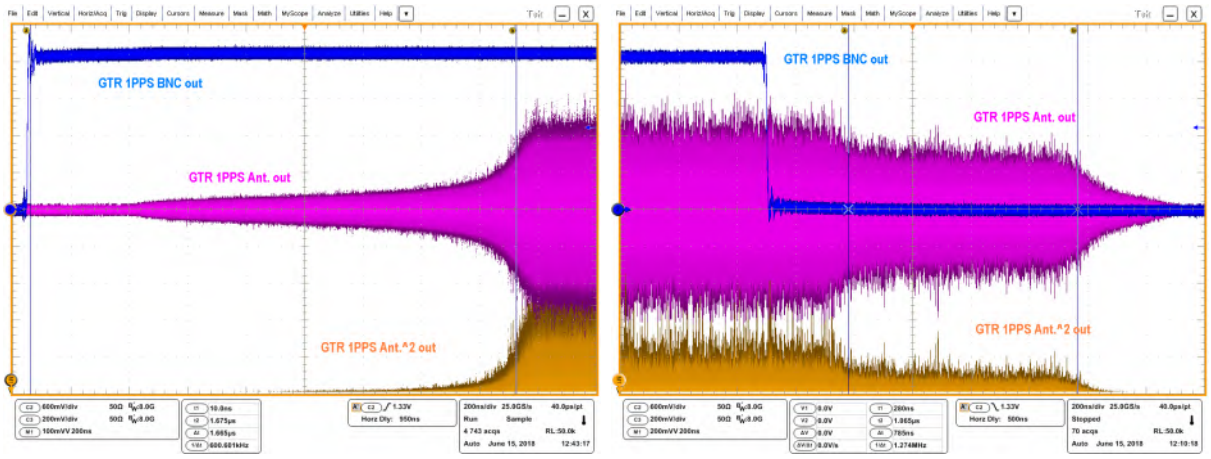

(a) Rising edge (b) Falling edge

Figure 4.8: Oscilloscope 1PPS rise and fall time measurements.

Table 4.4: Measurements of RF timing signal fall time with change in 1PPS frequency.

Frequency (Hz)	**Duty cycle (%)**	**Fall time**	**Frequency (Hz)**	**Duty cycle (%)**	**Fall time**
1	50	1.09 μs	10k	50	375 ns
1	90	770 ns	10k	90	355 ns
1	10	1.21 μs	10k	10	375 ns
1k	50	422.5 ns	25k	50	375 ns
1k	90	365 ns	25k	90	335 ns
1k	10	395 ns	25k	10	375 ns
5k	50	395 ns	50k	50	335 ns
5k	90	375 ns	50k	90	175 ns
5k	10	375 ns	50k	10	355 ns

the pulse and the results are given in Figure A.7 located in Appendix A. The challenge lies in determining the first pulse in the thousand that is aligned to UTC(USNO). Similar to the GTR's modulated RF timing signal depicted in Figure 4.7, the oscilloscope time stamped waveforms of the RF signal's are depicted in Figure A.5. The oscilloscope sampled the 1 kHz signal with a 160 ps resolution. The oscilloscope was in principle preforming the same role as a radio telescope except it was synchronised to the GTR via a 1PPS signal obtained via the BNC connector and the RF signal via a coaxial cable. The signal envelope is shown relative to the modulating 1PPS signal. The fine resolutions improved the characterisation precision, and the generated waveform data was invaluable in enabling analyses using various mathematical libraries in Python and other mathematical modelling software. An example of envelope detection used as a pulse edge transition time detector is depicted in Figure A.11 and A.12 in Appendix A.

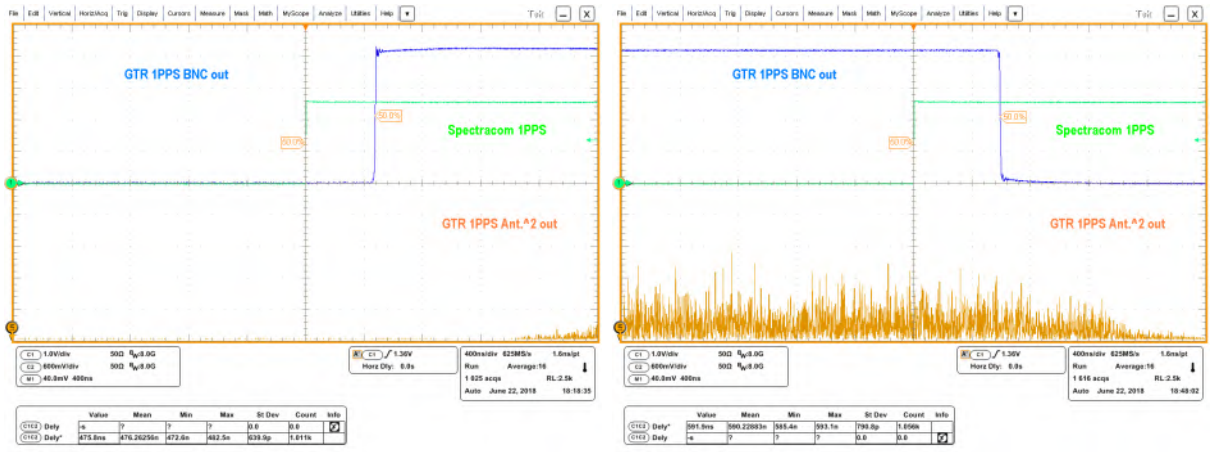

(a) 1 Hz rising edge

(b) 1 Hz falling edge

Figure 4.9: Oscilloscope phase measurement set-up.

Since the noisy timing signal has an irregular profile, a balance between envelope detection algorithm parameters such distance to look ahead from a peak candidate, and minimum distance between peaks and successive points must be chosen such that the pulse profile clearly distinguishes the pulse's on and off state in order for the detected pulse edge transition time to be as accurately as possible.

4.2.4 Experiment 4: Impact of 1PPS signal polarity on timing

The test was conducted to investigate whether or not setting the u-blox GPS receiver's 1PPS polarity as rising or falling edge influences the GTR's accuracy. The polarity and frequency of the receiver's 1PPS signal were changed whilst the reference 1PPS signal remained unchanged. The phase difference was recorded as the polarity of the receiver's 1PPS signal was changed. The phase measurements were measured against the Spectracom synchronisation System configured as the reference. The measurements where measured directly from the u-blox GPS receiver's 1PPS connector and after the buffered output leading to the BNC output connector, this way the buffer and polarity delay were measured simultaneously. The average phase difference between the GPS receiver's 1PPS rising and falling edge was 104.847 ns as measured directly from the receiver's time-pulse connector. The average phase difference between the GPS receiver's 1PPS rising and falling edge was 109.088 ns as measured directly from the receiver's time-pulse connector.

Table 4.5: Results obtained from the phase delay measurements between the rising edge and falling edge.

u-blox 1PPS frequency	**u-blox 1PPS polarity (less 0.48 ns)**	**Phase delay (TP port)**	**Phase delay (BNC port)**	**Delta (BNC-TP)**
1 Hz	Rising	193.246 ns	208.203 ns	14.957 ns
1 Hz	Falling	297.24 ns	317.837 ns	20.597 ns
1 kHz	Rising	191.612 ns	206.991 ns	15.379 ns
1 kHz	Falling	297.312 ns	315.533 ns	18.221 ns

$$T_{rise-Fall\ 1PPS\ TP\ port} = 104.847 \text{ ns} \tag{4.10a}$$

$$T_{rise-Fall\ 1PPS\ BNC\ out} = 109.088 \text{ ns} \tag{4.10b}$$

$$T_{buffer-rise} = 15.168 \text{ ns} \tag{4.10c}$$

$$T_{buffer-fall} = 19.409 \text{ ns} \tag{4.10d}$$

It was evident from the results presented in Table 4.5 that the GPS receiver's 1PPS polarity influenced GTR's accuracy. Possible future test would investigate whether the behaviour is common to other GPS receivers.

4.2.5 Experiment 5: Antenna sensitivity

A 24 hour experiment was performed to quantify the influence of the antenna amplifier noise on the overall GPS receiver timing accuracy. The u-blox ANN-SM antenna had a three times lower noise figure compared to the Taoglas antenna. The receiver was configured with a static position to eliminate position wandering errors in the time solution. The results showed that the GPS receiver determined a more accurate time solution when used with an antenna that had a lower noise figure. The ANN-SM antenna measurements showed an average delay of 413.87 ns, although higher than Taoglas's, the delay was a better estimate when compared to the calibration delay. The Tagloas antenna showed an average delay of 393.02 ns and higher standard deviation resulting in a broader phase delay spread shown in Figure 4.11 when compared to the u-blox ANN-SM antenna with lower amplifier noise shown in Figure 4.10. The results are summarised in Table 4.6.

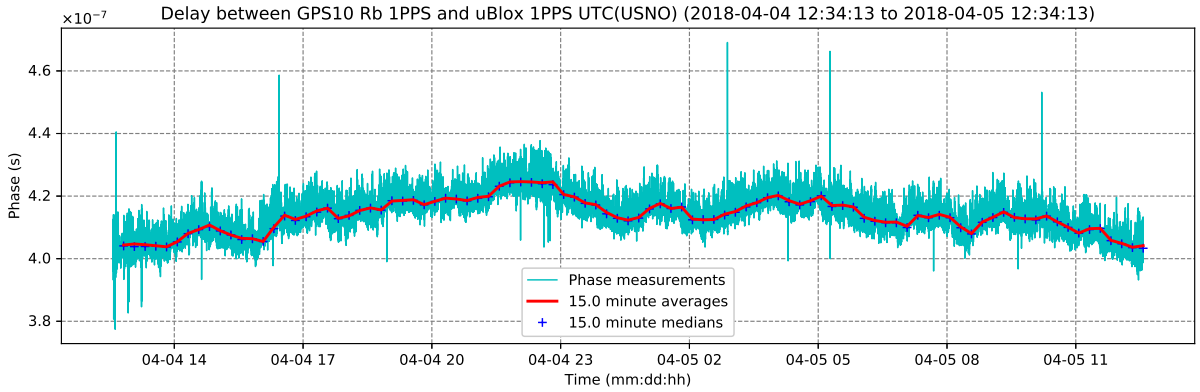

Figure 4.10: 24 hour delay measurements between GPS10Rb and u-blox M8F with a u-blox ANN-SM antenna.

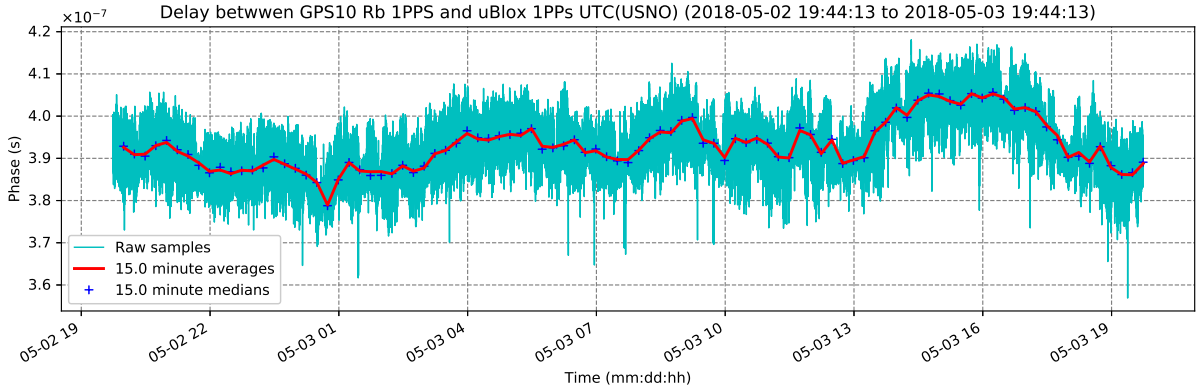

Figure 4.11: 24 hour delay measurements between GPS10Rb and u-blox M8F with a Taoglas antenna.

4.2.6 Experiment 6: Survey-In and Fixed mode performance comparison

The short term accuracy was measured over 15 minutes (900 seconds) for both *Survey-In* and *Fixed* mode. The performance of both timing modes was performed in the same experimental set-up and mounting position. The receiver antenna was placed by the laboratory window, such antenna placement rendered the experiment as a worst case measurements given the poor visibility. Both modes would have an improved standard deviation or narrower delay spread if placed in an area with an unobstructed sky view and minimal potential for multipath as highlighted in Section 4.2.7 and Experiment 7. The results depicted in Figure 4.12 and 4.13 showed that the receiver operating in the *Fixed* mode generated a 1PPS signal which was more stable and accurate compared to the *Survey-In* mode even when the antenna was subjected to poor satellite visibility and multipath. The average delay of both modes was 100–200 ns lower than the expected delay of 423.191 *ns* as determined through calibration and early laboratory experiment experiment conducted when the antenna was placed in an area with an unobstructed sky

Table 4.6: Results of the 24 hour antenna sensitivity survey experiment.

	u-blox ANN-SM antenna	**Taoglas antenna**
Amplifier noise figure	0.9 dB	2.6 dB
Average delay	413.87 ns	393.02 ns
Standard deviation	5.9517 ns	7.137 ns

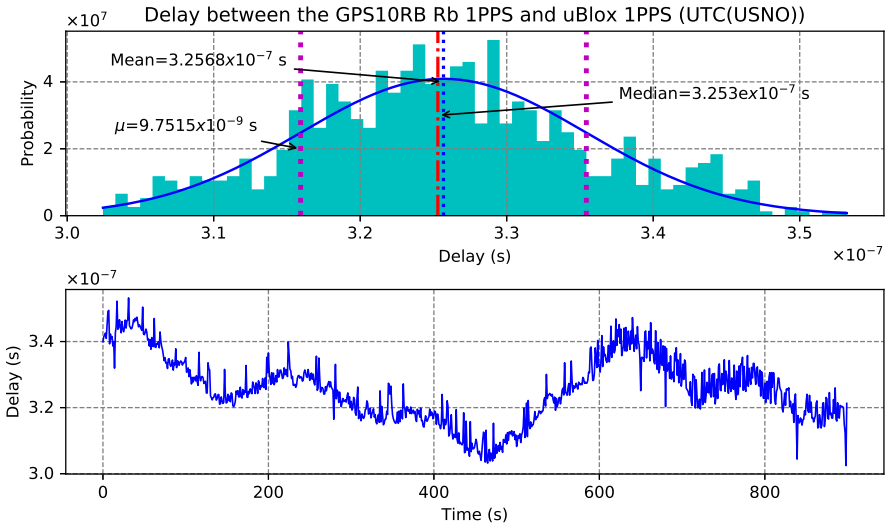

Figure 4.12: 15 minute Survey-In mode experiment results.

view and minimal potential for multipath. In order to ensure that the GTR radiates an accurate time-pulse, it is crucial to ensure that the GTR is placed in an area with a wide unobstructed sky view and minimal potential for multipath. Guidelines on mitigating multipath are discussed in Section 2.3.7. The results are summarised in Table 4.7. In contrast, if the antenna was placed on the roof, the receiver would generate a time solution accurate to within a few tens of nanoseconds of the calibrated delay as depicted in Experiment 7.

Table 4.7: Results of the Survey-In and Fixed mode performance comparison experiment.

	Survey-In mode	**Fixed mode**
Average delay	325.68 ns	209.32 ns
Standard deviation	9.751 ns	4.622 ns

4.2.7 Experiment 7: Impact of antenna placement on position and time accuracy

The experiment was aimed at determining the impact of multipath and satellite visibility on position and time accuracy with regards to antenna placement. The receiver was

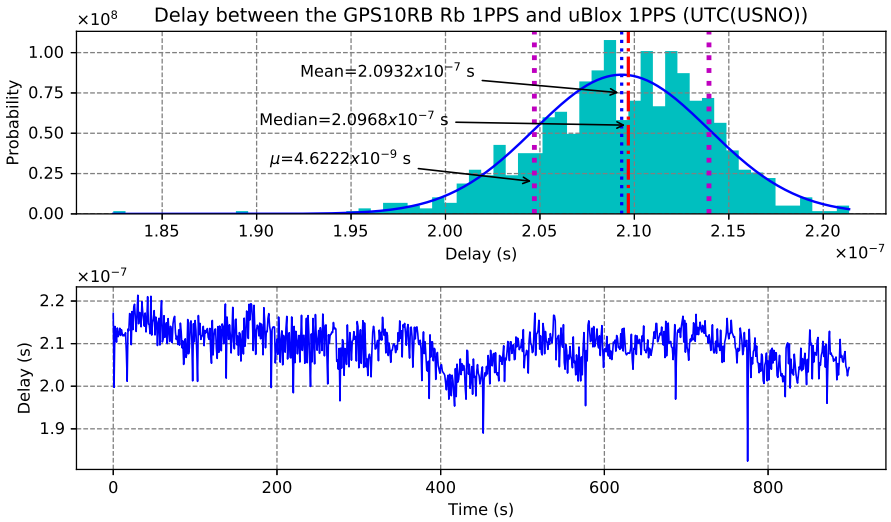

Figure 4.13: 15 minute Fixed mode experiment results.

configured to use the special *Fixed* timing mode in order to mitigate position wandering and maximise the time solution accuracy, thereby isolating the environmental bias on the time solution. The antenna was placed by the laboratory window and on the roof.

Similarly, the average delay determined when the antenna was placed by the window

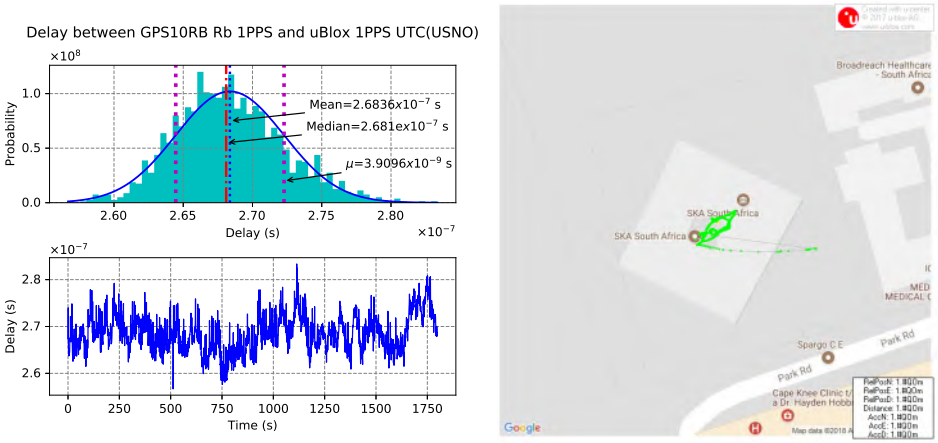

(a) Statistical measure (b) Deviation map

Figure 4.14: 30 minute window antenna placement experiment results.

was 100–200 ns lower than the expected delay of 423.191 ns evident in Experiment 6. The adverse impact of poor satellite visibility and multipath was evident in the position deviation of approximately 19 m over a 30 minute period. The average delay determined when the antenna was placed on the roof was 408.36 ns, accurate to within the expected value. The outstanding performance of good satellite visibility and multipath suppressed environments is evident in the position deviation of approximately 2.5 m over a 30 minute period. The experiment's results are summarised in Table 4.8. Detailed position deviation maps of the experiment are depicted in Figure A.13 in Appendix A.

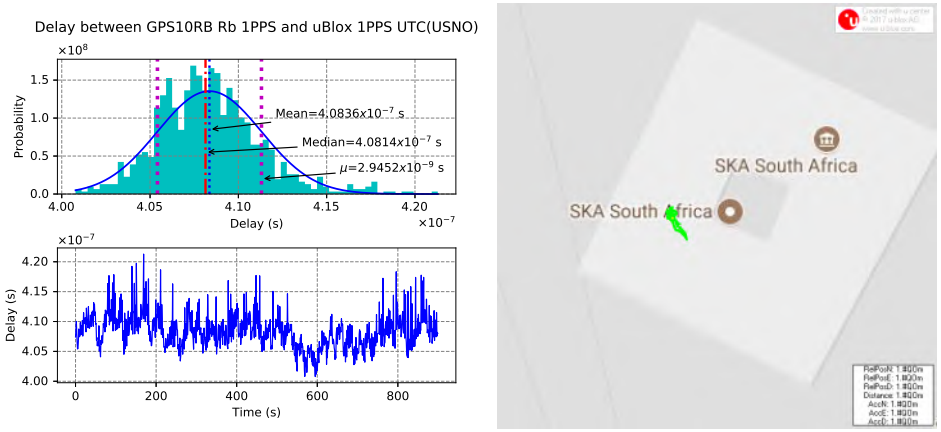

(a) Statistical measure (b) Deviation map

Figure 4.15: 30 minute roof top antenna placement experiment results.

Table 4.8: Impact of antenna placement influence on position and time accuracy.

	Window	**Roof**
Average delay	268.36 ns	408.36 ns
Standard deviation	3.91 ns	2.945 ns
Position deviation	19 m	2.5 m

4.2.8 Experiment 8: Time to first fix test

The experiment measured the time taken by the GPS receiver to obtain GPS time lock and generate a 1PPS signal after a cold start. Each test involved resetting the GPS receiver in a cold start. A cold start refers to a start-up procedure in which a receiver has inaccurate estimates of position, velocity, and time, after which the receiver begins a lengthy process of searching and acquiring GPS satellite. A stop watch was used to measure the duration between a receiver cold start and GPS time lock. Test 1 and 7 had

Test	**Time to GPS time lock (minutes:seconds)**	**Test**	**Time to GPS time lock (minutes:seconds)**
1	04:14.82	8	10:25.64
2	12:10.67	9	10:28.17
3	12:14.13	10	12:16.85
4	12:14.53	11	12:13.21
5	10:10.44	12	12:19.40
6	12:15.29	13	12:19.18
7	05:40.84	14	12:24.54

the lowest time to first fix because the receiver was powered up from a normal start in which the receiver had valid estimates of the position, time and velocity from a recent

history. Typically the GTR will be regularly switched on and off during the field tests thereby guaranteeing quicker fix time as the receiver keeps cache of recent records of valid position, time and velocity estimates. The result clearly demonstrate that the time it takes for a GPS receiver to acquire GPS time lock from a cold start coincided with the time it takes for any GPS receiver to receive the entire navigation message. The navigation message contains satellite almanac, health status, orbit information and clock bias information required to determine accurate position and time. It takes 12.5 minutes for each satellite to transmit the entire message. The minimum start-up time for the GTR was set to 15 minutes in order to allow the GTR to acquire all visible satellites and determined its position, velocity and time accurately regardless of the validity of cached data. The start-up time allowed the instrument's temperature to gradually reach the ambient temperature. The impact of temperature on the GTR on timing performance is proposed in future. Although it was not the focus of this study, the fix time can be significantly reduced by the use of augmented GPS systems.

4.2.9 Experiment 9: Electromagnetic reverberation chamber test

The GTR was set-up in the reverberation chamber as depicted in Figure 3.36 and the electromagnetic emissions where measured. The radiating antenna was terminated with a 50 Ω load in order to measure the instrument's baseline RFI emission without the intentional RFI timing signal. That way, the GTR's shielding effectiveness was measured against the reverberation chamber's RFI baseline. The results showed that the GTR was well shielded. The red curve represented the limits for RFI pass and fail criteria. There were frequency artefacts below 600 Mhz due to self generated EMI from electronic components such as switching logic gates, amplifiers, RF switch and GPS receiver. The frequency artefacts were not detrimental to the GTR or MeerKAT because they were no in the telescope's receiver L-band frequency range on within which timing signal bandwidth occupied. The reverberation chamber's system noise dominated towards higher frequencies depicted by apparent artefacts and increase in power in the 3–4 GHz range. The spectrum of the GTR radiating shown in Figure 4.17 was similar to the spectrum generated by the spectrum analyser depicted in 3.20. The reverberation chamber measurement confirmed that the GTR radiated the desired signal within the design frequency band (L-band). The GTR was designed to radiate a timing signal with high signal-to-noise (SNR) for clear visibility in the raw voltage time domain without lengthy integration times typical in pulsar radio astronomy. The radiated signal intentionally interfered with radio astronomy signals. The compliance limits provided by the South African Radio Astronomy Service (SARAS) are primarily aimed at mitigating radio astronomy signal interference [56]. That meant that SARAS imposed limits on RFI sources (transmitter

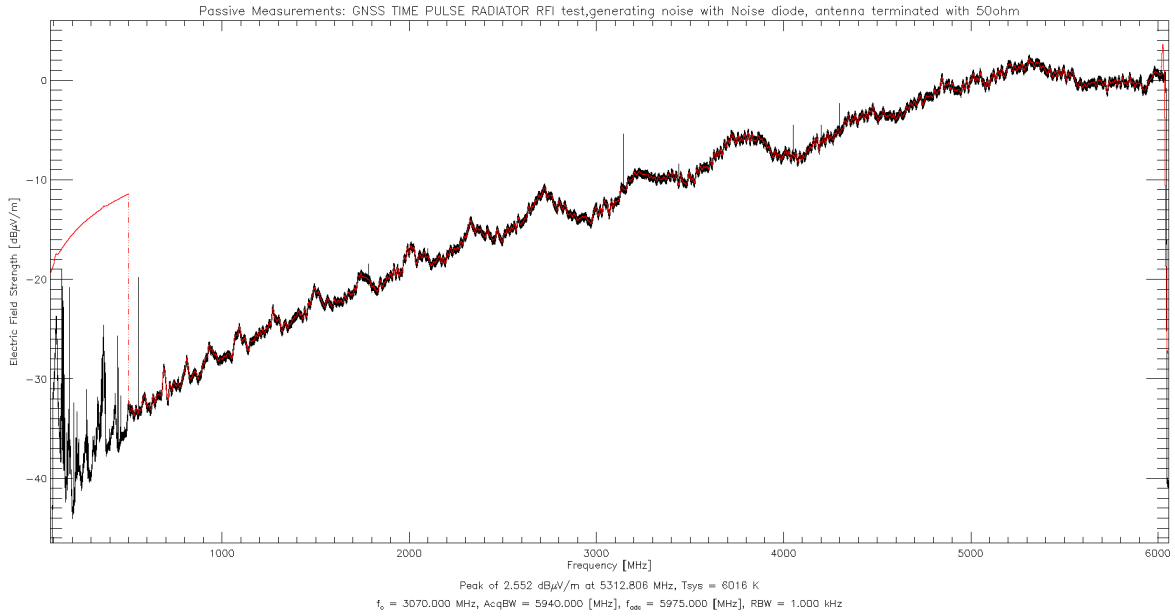

Figure 4.16: RFI measurement of the GTR radiating a modulated timing signal through an antenna terminated with a 50 Ω load.

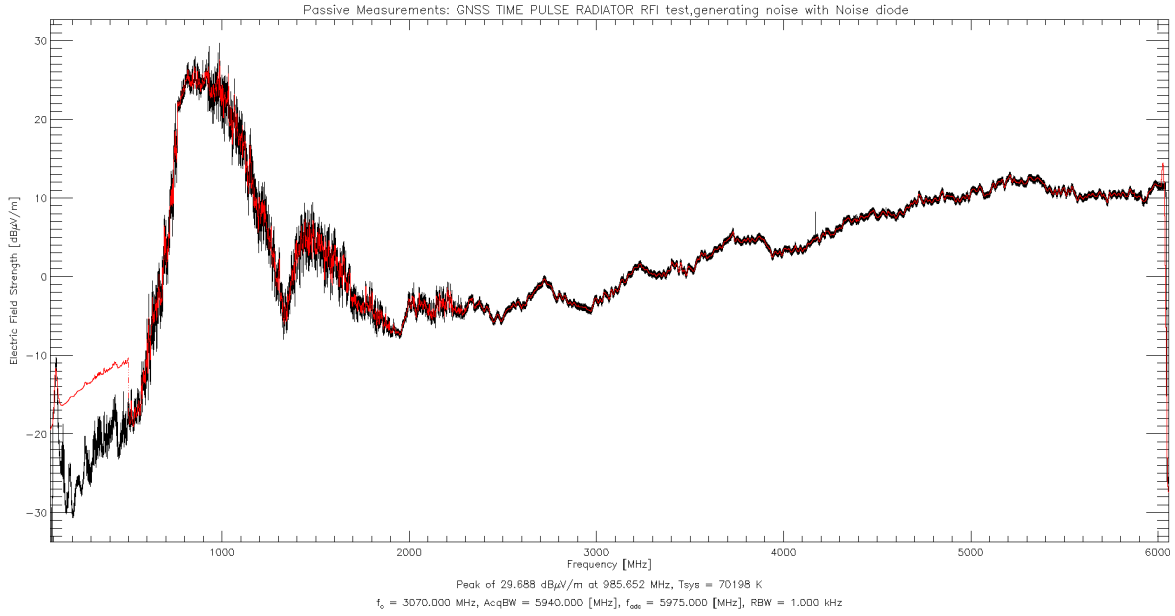

Figure 4.17: RFI measurement of the GTR radiating a modulated timing signal with the noise diode.

limits) with the assumption of an active radio astronomy observation. The GTR was designed as a special use tool, exclusively permissible when no astronomical observation were active. The instrument would definitely render the astronomical signal unobservable given the stringent specifications. The GTR was assigned a permit by the South African Radio Observatory (SARAO) bearing permission for use when no astronomical observation were active. The RFI measurement results of the 1 GHz tone is depicted in Figure

A.14 of Appendix A.

4.3 Meerkat timing experiment

SARAO has built an ensemble of clocks to provide timing to MeerKAT traceable to UTC. The master clock timing edge distributed across the radio telescope array is called Karoo Telescope Time (KTT). The MeerKAT timing experiment's main objective was to compare the GTR's timing edge to KTT. MeerKAT uses a precise time measurement and transfer system called Karoo Array Timing System (KATS). The KATS system provides precise transfer of time in the form of an optically modulated 1PPS signal to the telescope's digitisers. The KATS system measures the round trip delay to each digitiser of the telescope's phased array located tens of kilometers from the master clock transmitter in real time. The measured delay is used post-facto to correct the telescope time for more accurate timestamping [23]. The KATS system measurements are compared with the GTR's measurements to independently verify the delays spanning science processing, correlator and digitiser systems. Time correction techniques based on KATS measurements are applied to steer the Karoo Telescope Time (KTT) to within tens of nanoseconds of UTC. It should be noted that the KATS system measures and post-facto corrects for the delays between the KTT and UTC time standard. The delays measured by the KATS system are related to the KTT-GTR delays depicted in Figure 4.18 and 4.19 because both systems are traceable to UTC. The KTT-GTR delays determined by the Meerkat timing experiment are denoted as edge transition time.

4.3.1 1PPS edge polarity based timing

The GTR transmitted 1PPS modulated RF timing signal with a 90% duty cycle and falling edge on the top of a second was captured by the L-band receiver of MeerKAT antenna M028. The raw digitiser voltage are depicted in Figure A.15 and A.16 in Appendix A. The captured dataset was operated on by a rolling window function that produced rolling window shaped data resembling variations in signal power from which a threshold was used to detect the RF timing signal's edge TOA with respect to the telescope time (KTT). The detected RF timing signals falling edge is depicted in Figure 4.18. The time of arrival of the GTR's falling time edge with respect to the KTT ($KTT - GTR$) time standard was determined to be 17.489 μ s. A positive delay meant that the time standard being tested by the GTR was late whereas a negative delay meant that the time standard was early. Furthermore, the TOA represents the delay between the two time standards. Since traceability of the GTR time standard to UTC(ZA) and UTC was established through calibration, the delay between KTT and UTC(ZA) with respect to the GTR time standard

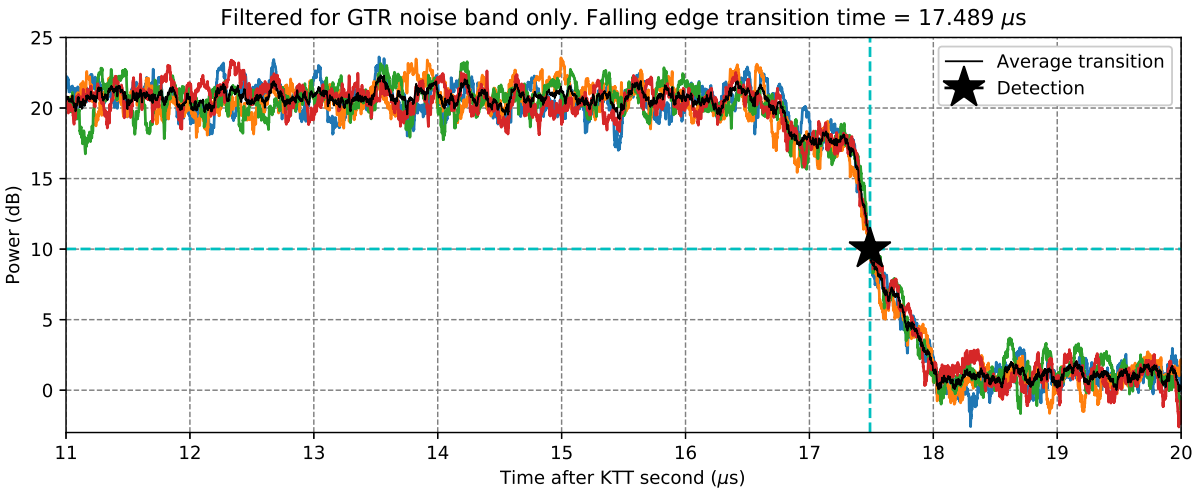

Figure 4.18: Detection of falling edge transition time of the folded GTR 1 Hz timing signals.

is given by

$$\begin{aligned} KTT - GTR_{UTC(ZA)\ 1Hz\text{–}fall\text{–}90\%} &= (GTR\text{–}UTC(ZA)_{1Hz\text{–}fall\text{–}90\%} + T_{GTR\text{–}horn\text{–}cable} \\ &\quad + T_{propagation\text{–}delay\text{–}26.2m}) - T_{1Hz\text{–}edge\text{–}detection} \\ &= (1317.447 + 30.912 + 87.33)\ \text{ns} - 17.489\ \mu s \\ &= -16053.311\ \text{ns} \\ &= -16.05\ \pm 0.1\ \mu s\ (1\sigma) \end{aligned} \tag{4.11}$$

where $KTT - GTR_{UTC(ZA)\ 1Hz\text{–}fall\text{–}90\%}$ is the delay between the KTT and UTC(ZA) time standard, $GTR\text{–}UTC(ZA)_{1Hz\text{–}fall\text{–}90\%}$ is the delay between the GTR and UTC(ZA) time standard, $T_{GTR\text{–}horn\text{–}cable}$ is the horn antenna cable delay, and $T_{propagation\text{–}delay\text{–}26.2m}$ is the RF signal's propagation delay over a 26.2 m distance. The delay between KTT and UTC with respect to the GTR time standard is given by

$$\begin{aligned} KTT - GTR_{UTC\ 1Hz\text{–}fall\text{–}90\%} &= GTR\text{–}UTC_{1Hz\text{–}fall\text{–}90\%} + T_{GTR\text{–}horn\text{–}cable} \\ &\quad + T_{propagation\text{–}delay\text{–}26.2m}) - T_{1Hz\text{–}edge\text{–}detection} \\ &= (1320.147 + 30.912 + 87.33)\ \text{ns} - 17.489\ \mu s \\ &= 16050.611\ \text{ns} \\ &= -16.05\ \pm 0.1\ \mu s\ (1\sigma) \end{aligned} \tag{4.12}$$

where $KTT - GTR_{UTC\ 1Hz\text{–}fall\text{–}90\%}$ is the delay between the KTT and UTC time standard, and $GTR\text{–}UTC_{1Hz\text{–}fall\text{–}90\%}$ is the delay between the GTR and UTC time standard.

4.3.2 1 khz pulse edge polarity based timing

The GTR transmitted 1 khz pulse modulated RF timing signal with a 10% duty cycle and rising edge on the top of a second was captured by the L-band receiver of MeerKAT antenna M028. The raw digitiser voltages are depicted in Figure A.17 and A.18 in Appendix A. The captured dataset was operated on by a rolling window function that produced rolling window shaped data resembling variations in signal power from which a threshold was used to detect the RF timing signal's edge with respect to KTT. The detected RF timing signals rising edge is depicted in Figure 4.19. The time of arrival of the GTR's

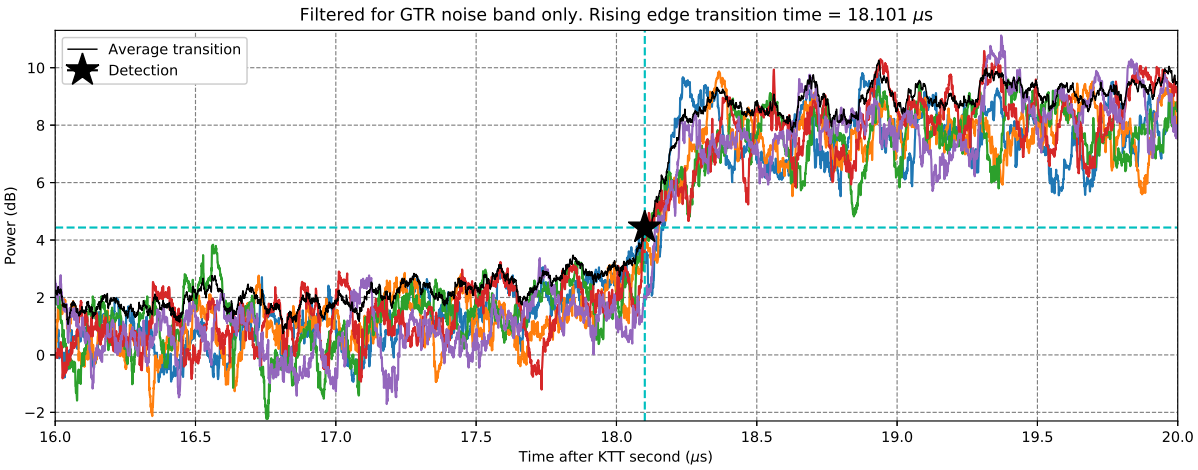

Figure 4.19: Detection of rising edge transition time of the folded GTR 1 kHz timing signals.

falling time edge with respect to the KTT time standard is given by

$$KTT - GTR = T_{1kHz\text{–}edge\text{–}detection} = 18.101\ \mu s \tag{4.13}$$

where $KTT - GTR$ is the time of arrival of the GTR time edge denoted as rising edge transition time. The delay between KTT and UTC(ZA) with respect to the GTR time standard is given by

$$\begin{aligned} KTT - GTR_{UTC(ZA)\ 1kHz\text{–}rise\text{–}10\%} &= (GTR\text{–}UTC(ZA)_{1kHz\text{–}rise\text{–}10\%} + T_{GTR\text{–}horn\text{–}cable} \\ &\quad + T_{propagation\text{–}delay\text{–}26.2m}) - T_{1kHz\text{–}edge\text{–}detection} \\ &= (2103.359 + 30.912 + 87.33)\ \text{ns} - 18.184\ \mu s \\ &= -15962.399\ \text{ns} \\ &= -15.96\ \pm 0.1\ \mu s\ (1\sigma) \end{aligned} \tag{4.14}$$

where $KTT - GTR_{UTC(ZA)\ 1kHz\text{–}rise\text{–}10\%}$ is the delay between the KTT and UTC(ZA) time standard, $GTR\text{–}UTC(ZA)_{1kHz\text{–}rise\text{–}10\%}$ is delay between the GTR and UTC(ZA) time standard, $T_{GTR\text{–}horn\text{–}cable}$ is the horn antenna cable delay, and $T_{propagation\text{–}delay\text{–}26.2m}$ is

the RF signal's propagation delay over a 26.2 m distance. The delay between KTT and UTC with respect to the GTR time standard is given by

$$\begin{aligned} KTT - GTR_{UTC\ 1kHz\text{–}rise\text{–}10\%} &= (GTR\text{–}UTC_{1kHz\text{–}rise\text{–}10\%} + T_{GTR\text{–}horn\text{–}cable} \\ &\quad + T_{propagation\text{–}delay\text{–}26.2m}) - T_{1kHz\text{–}edge\text{–}detection} \\ &= (2106.059 + 30.912 + 87.33)\ \text{ns} - 18.184\ \mu s \\ &= -15959.699\ \text{ns} \\ &= -15.95\ \pm 0.1\ \mu s\ (1\sigma) \end{aligned} \tag{4.15}$$

where $KTT - GTR_{UTC\ 1kHz\text{–}rise\text{–}10\%}$ is the delay between the KTT and UTC time standard, and $GTR\text{–}UTC_{1kHz\text{–}rise\text{–}10\%}$ is the delay between the GTR and UTC time standard.

4.3.3 Verification

The results presented in Table 4.9 shows a summary of delays between KTT and GTR timescales with respect to UTC(ZA) and UTC for MeerKAT antenna M028. The 1 kHz timing signal can be used confidently provided there is evidence that the delay of the radio telescope master clock being tests does not exceed the signal's time ambiguity. As a rule of thumb, the 1Hz pulse has a larger time ambiguity and should be always be used first in order to determine whether the telescope is late or early with respect to the GTR. A positive delay meant that the time standard being tested by the GTR was ahead (late) whereas a negative delay meant that the time standard was behind (early). Similar to the GTR time standard, KTT is traceable to UTC and UTC(ZA). The telescope's timestamp results showed that KTT was -16.05 μs behind UTC(ZA) and -16.05 μs behind UTC with respect to the GTR's 1 Hz RF signal. The results also showed that KTT was -15.96 μs behind UTC(ZA) and -15.95 μs behind UTC with respect to the GTR's 1 kHz RF signal. The precise time measurements of antenna M028 situated 4.8 km from

Table 4.9: KTT-GTR delay for MeerKAT antenna M028.

	UTC(ZA)	**UTC**
$KTT - GTR_{1Hz\text{–}fall\text{–}90\%}$	$-16.05\ \pm 0.1\ \mu s\ (1\sigma)$	$-16.05\ \pm 0.1\ \mu s\ (1\sigma)$
$KTT - GTR_{1kHz\text{–}rise\text{–}10\%}$	$-15.96\ \pm 0.1\ \mu s\ (1\sigma)$	$-15.95\ \pm 0.1\ \mu s\ (1\sigma)$

the master clock transmitter were analysed and compared to the GTR measurements. There were outliers in the KATS delay measurements of antenna M028 with delays equal to 0 ns. Such values were outliers because an optical signal transmitted several kilometers away from a transmitter experiences a delay much larger than 0 ns over a 4.8 km optical fibre link. The KATS system reports the precise time measurements through a graphical user interface system called Karoo Array Telescope Graphical User Interface (KATGUI). The KATGUI measurements with outliers are depicted in Figure A.20 in Appendix A. The

outliers were removed and the precise time delay measurements from the KATS system are depicted in Figure 4.20. The delay experienced by the PPS signal with respect to KTT over the 4.8 km distance was measured to be

$$\Delta KTT\text{–}M028_{KATS\ system} = -16.008\ \mu s \pm 160.890\ \text{ns} \tag{4.16}$$

The delay is given as a negative value to signify that the synchronisation PPS signal

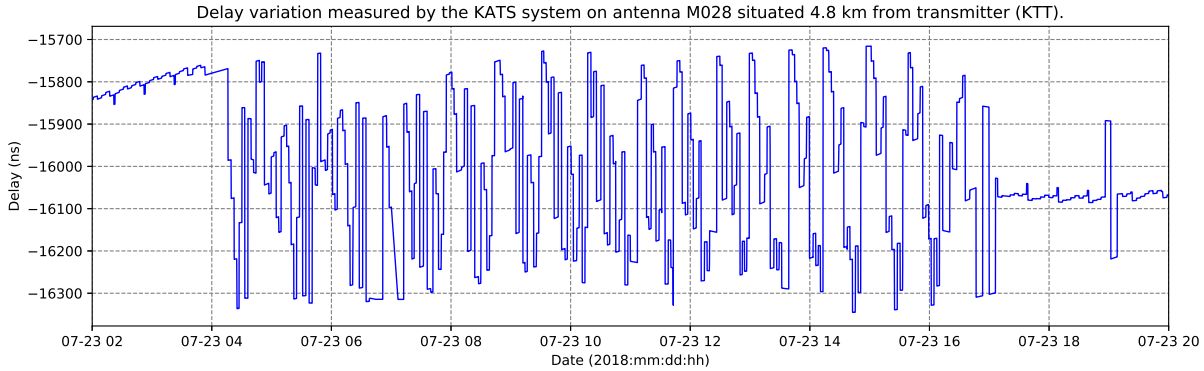

Figure 4.20: 24 hour KATS system delay variation measurements on antenna M028 situated 4.8 km from transmitter (KTT).

would have to be transmitted 16.008 μs before the master clock timing edge (KTT) in order to correct for the delay experience by the signal over the 4.8 km optical fibre link. The 1PPS and 1 khz pulse signal are compared in Table 4.10. The KATS system delay

Table 4.10: Comparison between 1 Hz and 1 kHz 1PPS.

1 Hz 1PPS signal	**1 kHz 1PPS signal**
1 pulse per second	1000 pulses per second
Maximum pulse power per duty cycle	Power reduces with duty cycle and frequency
Long integration or pulse folding	Short integration or folding time
Telescope generates large data volumes with longer observations	Telescope generates smaller data volumes with shorter observations
Large storage capacity required	Smaller storage capacity required

measurements confirmed that the GTR successfully determined the telescope time delay on antenna M028 to within 100 ns. The typical sources of errors in estimating the GTR RF pulse transition time from the telescope data includes:

- Uncertainty in the detected transition time with regards to the detection algorithm used.

- Errors introduced to the PPS edge as the signal is transformed from an unblemished square wave pulse to an RF signal with profile variations generated from the noise diode.
- The fibre links used to distribute the precise telescope time (KTT) are affected by environmental conditions such as temperature and seasonal variation which induces variation in the KATS round trip delay measurements.
- Offsets introduced by clock drifts influence delays in KTT-UTC and KTT-UTC(ZA).

By comparing the antenna delay determined with the use of the GTR as depicted in Table 4.9 and the delay measured by the KATS system given by Equation 4.16, the direct relationship between the telescope's timestamps and its masker clock was revealed. The telescope generated timestamps associated with the detected RF signal edges coincided with the expected delay measured from antenna M028 of approximately 16 μs $\pm$ 100 ns. Furthermore, the GTR successfully verified that the KATS precise time system distrusted and measured the telescope time (KTT) to the antenna precisely and accurately. The GTR and telescope master clock (KTT) spanning science processing, correlator and digitiser systems were aligned to within a 100 ns uncertainty. The GTR effectively determined the KTT-UTC(ZA) and KTT-UTC delay. Since the GTR and KTT time standards were aligned, this was confirmation that KTT was aligned to UTC(ZA) and UTC. The GTR was therefore a valid and effective tool, capable of accurately verifying the timestamp accuracy of each telescope antenna.

Chapter 5

Discussion and conclusion

5.1 Interpretation of results

A GPS time-pulse radiator (GPS) timing instrument was iteratively developed, built, tested and successfully used for testing time-stamp accuracy of the MeerKAT radio telescope. The overall timing accuracy and uncertainty was determined through a series of experiments and calibration. The GTR's GPS timing receiver was calibrated at the National Metrology Institute of South Africa (NMISA) to ensure validity of the GTR time standard and field test results. International standards such as ISO 17025 required that all equipments used for test having a significant effect on validity of results be calibrated before being put to service. The calibration established traceability between the GTR, UTC(ZA) and UTC time standards, thereby ensuring that the results obtained from a radio telescope timestamp test were valid. During the course of the calibration, the receiver encountered a timing error for a short period in which the 1-pulse-per-second (1PPS) signal drifted significantly resulting in outliers. Although the cause of the timing error was not found, receivers typically use a built in mechanism (*Hold-over*) to maintain time synchronisation when they loose track of satellites. The 1PPS drifts at a rate attributed to the reference oscillator stability. The error only occurred briefly over a 24 hour period but could seriously degrade the accuracy of certain time critical applications. The calibration results showed that the receiver was 423.191 ns ahead of UTC(ZA) and 425.891 ns ahead of UTC with an error budget of 42 ns. This offset was crucial in establishing the time reference for the instrument.

The precision of the GTR's RF timing signal was influenced by the RF switch that synchronously modulated the noise signal with the GPS receiver's 1PPS reference signal to produce the timing signal. The center of gravity concept was an independent invention to allow more accurate transfer of the time from the GTR RF output to the radio telescope detected power input. This method was proposed because the GTR's RF signal edges were not sharp enough to see below 200 μs. The entire pulse might be useful for timing

with an accuracy down to 10 ns or even better. After all possible delays were considered, the GTR's 1 Hz RF timing signal was measured to be 1.31 μs ahead of UTC(ZA) and 1.32 μs ahead of UTC with an uncertainty of 100 ns. The GTR's 1 kHz RF timing signal was measured to be 2.10 μs ahead of UTC and UTC(ZA) with an uncertainty of 100 ns.

The timestamp field test showed that the 1 Hz and 1 kHz GTR timing signals were equally adequate for timing. The telescope generated timestamps associated with the detected RF signal edges coincided with the expected delay measured from antenna M028. Through calibration, the GTR effectively determined the KTT-UTC(ZA) and KTT-UTC delay. The results showed that the GTR and telescope master clock (KTT) were aligned to within a 100 ns uncertainty. Furthermore, the GTR test confirmed that KTT spanning science processing, correlator and digitiser systems was aligned to UTC to within the GTR's accuracy. The GTR instrument successfully verified that the KATS precise time system and measured the telescope time (KTT) to the antenna precisely and accurately. The GTR was therefore a valid and effective tool capable of accurately verifying the timestamp accuracy of each telescope antenna.

5.2 Aspects to be improved in current design

The RF switch used in the design had a slow switching time in the order of $0.5-1.6$ μs. The physical properties of the materials and switching mechanisms of the switch are typically the speed limiting factor. The radio telescope timestamp field tests were based on the detection of the RF signal rising and falling edges. Although both edge polarities were used, the falling edge was preferred because the RF switch's response showed a sharper edge when compared to the rising edge. The pulse recovery algorithm in the receiver under test predominately depends on the pulse profile, therefore poor switching speeds will introduce greater uncertainties when recovering the 1PPS edges in the RF signal. Solid state RF switches with nanosecond range switching speed can be considered.

Since a short baseline was analysed, the phase variances measured from the u-blox M8F GPS timing receiver calibration were likely affected by satellite visibility, multipath and antenna choice (noise figure) which translate to errors in the time solution. Survey-grade GPS antennas with multipath suppression and uniform group delay response over all angles of incident can be used for maximum accuracy. It has been shown that the survey-grade antennas can significantly improve the performance for the inexpense receivers [59].

It was a good thing that the GPS receiver maintained the *Survey-In* mode during the calibration because the GTR was designed to be portable instrument capable of dynamically determining its stationary position. In practise, the instrument was expected to redetermine its 3D position every time the operator tested various telescope receivers located at varying distances apart. If the onboard GPS receiver went into a *Fixed mode* with a 3D position of some radio telescope receiver, all subsequent tests performed on

receivers located at different locations would be invalid because the GPS receiver's time-pulse would be determined from a redundant position. Alternatively, the *Fixed mode* would be desirable in a single receiver or non array based radio telescope experimental set-up where a fixed 3D location is known resulting in better timing stability. Attention should be paid to the errors in the fixed position as position errors will translate into additional timing errors.

While the GTR was constructed from various electronic components with wide temperature tolerance, an environmental chamber experiment is suggested in future in order to determine the impact of temperature on the instrument's timing performance.

5.3 Strong points of current design

The 1PPS polarity based timing test was designed to transfer time over RF whilst maintaining the familiar convention of a 1PPS signal in the time domain. It enabled the use of simple envelope detection in the time domain raw digitiser voltage data products to determine the 1PPS arrival time. The GTR was attractive in that it remained independent to the timing infrastructure of the experimental radio telescope. In addition to being an independent system to the radio telescope, the GTR device was desirable in that being a portable time fault finding instrument, it enabled users to isolate and individually test radio telescope receivers that formed part of the larger system. A single Global navigation satellite system (GNSS) system was used to calibrate the GTR instrument and maintain a known timing accuracy in order to avoid contaminating its accuracy with small time offsets between different GNSS systems. Given the inherent benefits of GPS, the GTR is capable of providing reliable and accurate timing performance from virtually any location world wide.

The chosen batteries were rechargeable, disposable and easily replaceable. The instrument design was modular to ease servicing and upgrading. The instrument was easy to set-up and use, an operator simply connected a GPS antenna, transmitter antenna, and battery. The experiments begin by switching the instrument on and waiting for the GPS ready signal on the LED, after which the RF timing signal is turned on with a second switch. The instrument was equipped with a low battery indicator for an early recharge warning. The 12 V 4000 mAh chosen battery provided up to 26 hours runtime between recharges. Two rechargeable batteries were purchased to extend the runtime to up to 2 days between charges. The enclosure was based on an IP68 rated lightweight aluminium enclosure with EMI or RFI shielding and environmental protection from dust and water. The GTR will continue to allow for the evaluation of MeerKAT's time accuracy as its atomic clock ensemble evolves and number of receivers increases. Time and frequency reference (TFR) engineers will be able to monitor the systematic impact of upgrading the telescopes timing infrastructure on the telescope's final data products.

5.4 Circumstances in which current system fails

The instrument requires a 12 V battery with a minimum current rating of 1200 mAh in order to operate over an 8 hour period between charges. If the battery is low enough, there will not be enough electric power to operate the instrument reliably. A functional GPS antenna needs to receive signals from as many visible GPS satellite as possible. The GPS receiver needs to receive navigation information from the satellites in order to determine the position and time required for achieving the GTR's mission critical objective of timing. Objects that may obstruct the antenna's line-of-sight with the satellite, attenuate the weak GPS signals, degrade the overall satellite geometry and induce multipath that introduces errors in the position and time solution. The performance of the most sophisticated receivers will suffer due to a poor antenna. The operator needs to pay special attention where the GTR is set-up in order to mitigate obstructions and multipath.

The wideband noise timing signal is capable of jamming other signals in the 980 MHz to 1150 MHz bandwidth including the GTR instrument itself. While GPS signal frequencies are within the GTR's transmission bandwidth, special attention should be paid to isolate the antenna and transmitter to avoid jamming the weak satellite signals. Position wandering and time errors resulting from jamming will translate into unpredictable time errors. A directive transmitter antenna such as a horn antenna should be used to avoid unintentionally jamming the instrument.

5.5 Design ergonomics

The instrument was securely stored in a plastic pluck foam carry case for ease carry and protection. The carry case pluck foam created a snug fit and additional compartments for all spares (GPS antenna, hex key, battery, RF attenuators and filters) required to operate and service the GTR. Tactile toggle switches were used to turn the instrument on or off and to activate the RF timing signal. The operator interface was easy to use without need for rigorous training. The interface had clearly visible markers of name, purpose, frequency, output and other items visible on the enclosure. The LEDs provided an effective method of providing visual indication when the instrument was on and operational status. The modular design allowed for future RF chain upgrades since components could be easily unscrewed from the board mounts and SMA connectors. RF chain upgrades are particularly important when the filter has to be changed to perform timing tests on radio telescope receiver operating in frequency bands other than L-band.

5.6 Health and safety aspects of the design

A fuse is an electrical circuit breaker that was used to protect the GTR from excessive current or short circuits that could permanently damage the electronics and potentially deliver harmful electrical shock to the instrument's operator. In the event a fuse is damaged, a replacement should be installed before the instrument is used for subsequent tests. The batteries should always be stored away in such a way that the positive and negative terminals do not short which can cause fire hazards or electrical shocks. The instrument's enclosure is IP68 rated and provides protection from elements such as water and dust. Although the enclosure provides protection from liquids, operators should avoid exposing the instrument's connectors (battery, antenna and BNC) to liquids to avoid unintended short circuiting. Like mobile phones, two-way radios and other microwave gadgets, the GTR instrument emitted microwaves generally considered too weak to affect living tissue, thereby not harmful to human beings. Ethical clearance was obtained prior to commencement of design and testing.

5.7 Social and legal impact and benefits of the design

The GTR design approach was based on a L-band frequency design within the range of 1 GHz to 2 GHz. The carrier frequencies were assigned to microwave communications, television broadcasts, mobile phones, two-way radios and radio astronomy are defined by the Radio Regulations of the International Telecommunication Union (ITU) and IEEE standards. The instrument designed complied with the RFI restrictions imposed by SARAO for use at the MeerKAT radio telescope site. The instrument transmitted, horn antenna directive signal not interfering with un-intended devices.

One of the major social concerns with the use of the GTR instrument was inherent jamming capabilities on civilian communication systems. The instrument was intended to be used for special radio astronomy applications, carefully controlled environment, radio quiet zone, with compliance to such sites, thereby did not interfere with regular day to day communication systems found in regular residential areas. The instrument was capable of jamming L-band signals, special attention should be paid to avoid operating the device in unauthorised locations. The instrument can be used for timing experiments with other radio telescopes provided their receivers frequency bands include the carrier frequency of the signals transmitted by the GTR instrument.

5.8 Environmental impact and benefits of the design

While rechargeable batteries cost more than disposable batteries, they are far more cost effective and least impact the environmental, as they can be recharged inexpensively many

times before they need replacing. Recycling is an important consideration for the recovery of valuable materials and protection of the environment. All forms of batteries used are to be recycled in a facility that treats the acid, lead, plastic, and metals to protect the local environment. The instrument can be easily disassembled and electronic components can be salvaged for alternative use to reduce electronic waste. The RF waves radiated by the instrument are not harmful to the animals, people or the environment. No acoustic noise is produced from the system.

5.9 Summary of the work

In this thesis, we investigated the GPS time-pulse radiator for testing time-stamp accuracy of a radio telescope. The GTR's GPS receiver's timing performance was evaluated through calibration by measuring the phase difference against the National Metrology Institute of South Africa's (NMISA) UTC(ZA) precise time-pulse. The comparison was needed in order to determine the timing accuracy of the GTR device and establish time traceability to UTC. We also demonstrated that a low-cost, single frequency GPS receiver can give competitive timing results and as a result, the GTR offers an independent method for testing time accuracy in radio telescopes. A special attention should be paid to the set-up of the GTR, keeping in mind what field performance is expected given the choice of hardware sophistication in mitigating disturbances in the GPS signal during the timing experiments. A GPS time-pulse radiator for testing time-stamp accuracy for radio astronomy was successfully developed. The instrument is capable of delivering the accuracy needed for time-critical applications when a microsecond or better level of accuracy is required.

5.10 Summary of the results and conclusions

The GTR has been tested on MeerKAT and successfully identified delays in the radio telescope's receiver chain, specifically with the digitiser timestamping state machine. The greatest proof of the success of the GTR is that it has already been used by SARAO's time and frequency reference department, and pulsar timing astronomers for testing time-stamp accuracy of a radio telescope. It has been useful in providing a holistic method of verifying the Karoo telescope time to UTC and testing the radio telescopes pulsar timing units. As the radio telescope timing infrastructure becomes sophisticated, the GTR will provide an independent and reliable method for investigating and validating precise timing in MeerKAT and other radio telescopes around the world.

5.11 Suggestions for future work

An extension of the GTR characterisation experiment is suggested to investigate the use of higher frequency PPS signals based on pulsar timing principles. The timing precision can further be improved by using an ultra-fast switching RF switch for modulation, survey-grade receiver antennas and dual frequency timing receivers to achieving sub-microsecond level of accuracy. Unlike the 1PPS edge polarity based technique, using the entire timing signal presents a potentially more accurate method for testing timestamps in radio telescopes through the use of pulsar timing principles. Different modulation schemes, such as linear frequency modulated chirp signals, can be investigated.

Bibliography

[1] D. W. Allan, N. Ashby, and C. C. Hodge, "The science of timekeeping," tech. rep., 07 1997.

[2] P. Misra, "The role of the clock in a gps receiver," *GPS World, Innovation column*, vol. 7, pp. 60–66, 04 1996.

[3] A. Lyne, "A new pulsar survey," *Publications of the Astronomical Society of Australia*, vol. 3, no. 2, p. 118120, 1977.

[4] D. R. Lorimer, "Binary and millisecond pulsars," *Living Reviews in Relativity*, vol. 11, p. 8, 11 2008.

[5] M. McLaughlin, "Pulsar timing arrays," *Proceedings of the International Astronomical Union*, vol. 11, no. A29B, p. 321328, 2015.

[6] B. Hofmann-Wellenhof, H. Lichtenegger, and E. Wasle, *GNSS-global navigation satellite systems: GPS, GLONASS, Galileo, and more. Springer, Vienna.* Springer-Verlag Wien, 01 2007.

[7] P. Misra and P. Enge, *Global Positioning System: Signals, Measurements, and Performance.* Ganga-Jamuna Press, 1 ed., 2011.

[8] u-Blox, *EVK-M8F-0-01 Evaluation Kit time and frequency reference products.*

[9] Taoglas Ltd, *Magnet Mounted GPS-GLONASS-GALILEO Antenna.*

[10] Com-Power Corporation, *Model AH-118 Horn Antenna.*

[11] Deltron, *IP66/IP67/IP68 Deltron 486 series Diecast Aluminium Boxes.*

[12] u Blox, *LEA-M8F u-blox M8 time and frequency reference GNSS module.*

[13] The International Bureau of Weights and Measures (BIPM), *Values of the differences between UTC and its local representation by the given laboratory, including relevant notes and, since January 2007, the respective uncertainties.*, 10 2018.

[14] United States Department of Defence, *GPS Precision Positioning Service (PPS) Performance Standard*, 02 2007.

[15] u-blox, *ANN-MS High performance active GPS antenna.*

[16] O. Nnadih, U. A.C, and B. Okere, "Calibration of radio telescope using a satellite dish," *The International Journal of Engineering and Science*, vol. 4, pp. 38–44, 07 2015.

[17] R. Siebrits, J. Burger, G. Adams, R. Gamatham, F. Kapp, T. Abbott, N. Mnyandu, C. van der Merwe, and Z. Ramudzuli, "Robust time scale design and implementation for telescope time in a remote desert environment," in *Proceedings of the 2018 IEEE International Frequency Control Symposium (IFCS)*, pp. 55–60, IEEE, 2018.

[18] Y. Xinying, Z. Xia, D. Ran, L. Di, and H. jie, "Data processing and synchronization of the digital backend for fast," in *2015 IEEE International Symposium on Precision Clock Synchronization for Measurement, Control, and Communication (ISPCS)*, pp. 48–48, Oct 2015.

[19] C. Matthee, "Using gps for establishing frequency traceability in a time and frequency laboratory," 09 2013.

[20] *Time Synchronization over a Free-Space Optical Communication Channel*, IEEE, 2018.

[21] *Portable Picosecond Synchronization Technique Based on Optical Free-space Time Transfer*, IEEE, 2018.

[22] *Preliminary Evaluation of NRC-FCs2 Fountain Clock at the National Research Council Canada*, IEEE, 2018.

[23] R. Siebrits, J. Burger, G. Adams, R. Gamatham, F. Kapp, T. Abbott, T. Gibbon, S. Malan, E. Bauermeister, L. Boyana, H. Kriel, M. Welz, N. Mnyandu, A. Otto, C. van der Merwe, and S. Tshongweni, "Dissemination of reference signals for a next generation radio telescope," in *Proceedings of the 2018 IEEE International Frequency Control Symposium (IFCS)*, pp. 70–75, IEEE, 2018.

[24] B. Wang, X. Zhu, C. Gao, Y. Bai, J. W. Dong, and L. J. Wang, "Square kilometre array telescopeprecision reference frequency synchronisation via 1f-2f dissemination," *Scientific Reports*, vol. 5, pp. 38–44, 07 2015.

[25] W. Shillue, "Fiber distribution of local oscillator for atacama large millimeter array," in *OFC/NFOEC 2008 - 2008 Conference on Optical Fiber Communication/National Fiber Optic Engineers Conference*, pp. 1–3, Feb 2008.

[26] S. Schediwy, D. Gozzard, C. Gravestock, S. Stobie, R. Whitaker, J. Malan, P. Boven, and K. Grainge, "The mid-frequency square kilometre array phase synchronisation system," 05 2018.

[27] M. Soffel and R. Langhans, *Introduction*, pp. 1–10. Berlin, Heidelberg: Springer Berlin Heidelberg, 2013.

[28] J. Fisher, "Astronomical times."

[29] M. Kramer, J. Bell, R. Manchester, A. Lyne, F. Camilo, I. Stairs, N. DAmico, V. Kaspi, G. Hobbs, D. Morris, F. Crawford, A. Possenti, B. Joshi, M. McLaughlin, D. Lorimer, and A. Faulkner, "The parkes multibeam pulsar survey - iii. young pulsars and the discovery and timing of 200 pulsars," *Monthly Notices of the Royal Astronomical Society*, vol. 342, pp. 1299–1324, 2003.

[30] M. Burgay, B. Joshi, N. DAmico, A. Possenti, A. Lyne, R. Manchester, M. McLaughlin, M. Kramer, F. Camilo, and P. Freire, "The parkes high-latitude pulsar survey," *Monthly Notices of the Royal Astronomical Society*, vol. 368, pp. 283–292, 2006.

[31] F. Camilo and F. Rasio, "Binary radio pulsars," vol. 328, pp. 147–169, Astronomical Society of the Pacific Conference Series, 2005.

[32] A. Hewish, S. Bell, J. Pilkington, P. Scott, and R. Collins, "Observation of a rapidly pulsating radio source," *Nature*, pp. 217,709–713, 1968.

[33] M. Davis, J. Taylor, J. Weisberg, and D. Backer, "High-precision timing observations of the millisecond pulsar psr 1937+21," *Nature*, pp. 315,547–550, 1985.

[34] G. C. Hunt, "The rate of change of period of the pulsars," vol. 153, p. 119, 08 1971.

[35] B. W. Stappers, "Pulsars," *Proceedings of the International Astronomical Union*, vol. 7, no. S285, p. 103103, 2011.

[36] D. N. Matsakis and R. S. Foster, "Application of millisecond pulsar timing to the long-term stability of clock ensembles," pp. 445–462, 1996.

[37] M. Ryba and J. Taylor, "High precision timing of millisecond pulsars. i. astrometry and masses of the psr 1855+09 system," *Astrophysical Journal*, vol. 371, pp. 739–748, 991.

[38] J. Verbiest, M. Bailes, W. van Straten, G. Hobbs, R. Edwards, R. Manchester, N. Bhat, J. Sarkissian, B. Jacoby, and S. Kulkarni, "Precision timing of psr j0437-4715: An accurate pulsar distance, a high pulsar mass, and a limit on the variation of newtons gravitational constant," *Astrophysical Journal*, vol. 679, pp. 675–680, 2008.

[39] V. Kaspi, J. Taylor, and M. Ryba, "High-precision timing of millisecond pulsars. iii. long-term monitoring of psrs b1855+09 and b1937+21," *Astrophysical Journal*, vol. 428, pp. 713–728, 1994.

[40] R. N. Manchester, G. Hobbs, M. Bailes, W. A. Coles, W. van Straten, M. J. Keith, R. M. Shannon, N. D. R. Bhat, A. Brown, S. G. Burke-Spolaor, and et al., "The parkes pulsar timing array project," *Publications of the Astronomical Society of Australia*, vol. 30, p. e017, 2013.

[41] Naval Research Lab Washington DC, *Application of Millisecond Pulsar Timing to the Long-Term Stability of Clock Ensembles*, Astrophysical Journal, 1994.

[42] R. B. Langley, "Dilution of precision," *GPS World*, pp. 52–59, 04 1999.

[43] D. Wells, N. Beck, A. Kleusberg, E. J. Krakiwsky, G. Lachapelle, R. B. Langley, K. peter Schwarz, J. M. Tranquilla, P. Vanicek, D. Wells, D. Delikaraoglou, A. Kleusberg, E. J. Krakiwsky, G. Lachapelle, R. B. Langley, K. peter Schwarz, J. M. Tranquilla, and P. Vanicek, "Guide to gps positioning," in *Canadian GPS Association*, 1987.

[44] J. K. Ray, E. Cannon, and P. C. Fenton, "Mitigation of static carrier-phase multipath effects using multiple closely spaced antennas," *Navigation*, vol. 46, 09 1999.

[45] R. Langley, *Orbit Data and Resources on Active GNSS Satellites*.

[46] R. Prasad and M. Ruggieri, *Applied satellite navigation using GPS, GALILEO, and augmentation systems*. Artech House, 2005.

[47] T. Creel, A. Dorsey, P. Mendicki, J. Little, R. Mach, and B. Renfro, "New, improved gps: The legacy accuracy improvement initiative," *GPS World*, vol. 17, pp. 20–22+24+26, 03 2006.

[48] E. Kaplan and C. Hegarty, *Understanding GPS: Principles and Applications*. Artech House, 2005.

[49] Department of the Air Force, *Approved Lexicon of Signal Abbreviations*.

[50] u-blox, *GPS Antennas RF Design Considerations for u-blox GPS Receivers*.

[51] Maxim Integrated, *Application Note: Building a Low-Cost White-Noise Generator*, 03 2005.

[52] W. Riley, "Handbook of frequency stability analysis," vol. 1065, pp. 1–123, 01 2007.

[53] J. Rose, J. Tong, D. Allain, and C. Mitchell, "The use of ionospheric tomography and elevation masks to reduce the overall error in single-frequency gps timing applications," *Advances in Space Research*, vol. 47, pp. 276–288, 1 2011.

[54] W. Kunysz, "Effect of antenna performance on the gps signal accuracy," 01 1998.

[55] V. Ogrizovi, J. Marendic, S. Renovica, S. Delev, and J. Gucevic, "Testing gps generated 1pps against a rubidium standard," vol. 2, p. 7, 08 2013.

[56] A. Jessner, R. Lord, H. van der Marel, R. Millenaar, H. Reader, and F. Schlagenhaufer, "Emi protection and threshold levels for the ska," 2014.

[57] A. Sesana and A. Vecchio, "Gravitational waves and pulsar timing: Stochastic background, individual sources and parameter estimation," *Classical and Quantum Gravity*, vol. 27, 01 2010.

[58] H. Kabakchiev, V. Behar, P. Buist, I. Garvanov, D. Kabakchieva, and M. Bentum, "Time of arrival estimation in pulsar based navigation systems," pp. 171–175, 06 2015.

[59] R. Odolinski and P. Teunissen, "Gps+bds rtk: A low-cost single-frequency positioning approach," *GPS World*, pp. 50–56, 09 2017.

Appendix A

Additional results

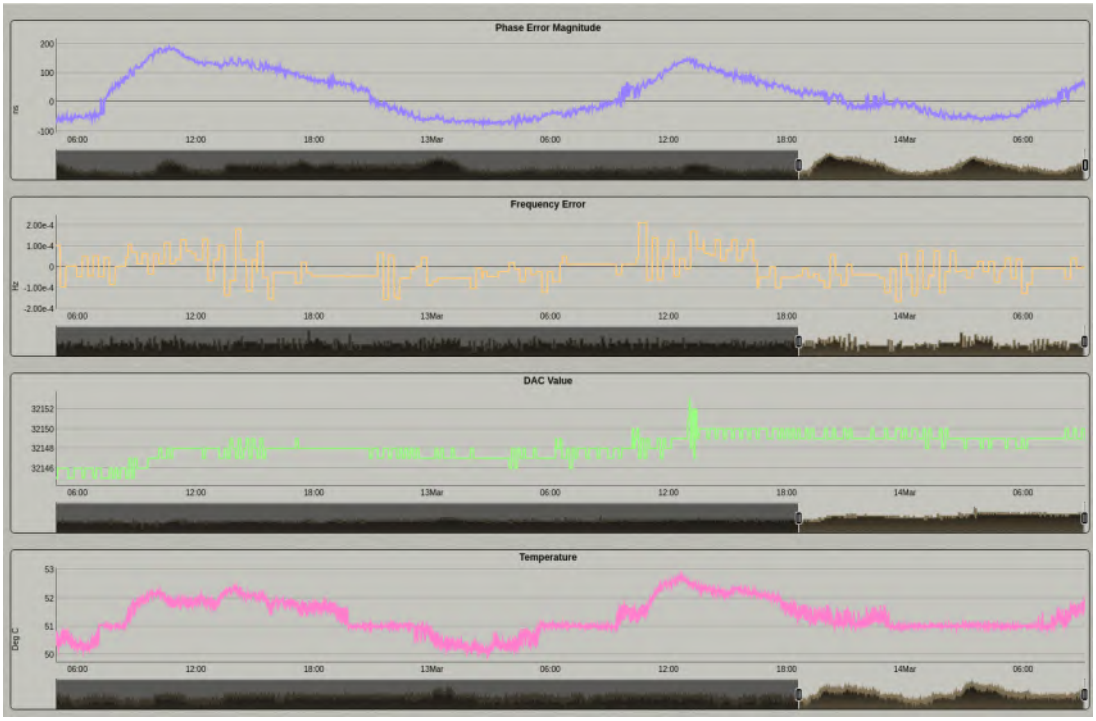

Figure A.1: Self-survey web interface of the Spectracom Time and Frequency Synchronization System (NetClock 9400 Series).

The blue curve in Figure A.19 represents the GTR's RF timing signal, the orange curve represents the pulsar template used by the radio telescope, and the result obtained from correlating the two is shown by the green curve. The center of the GTR's RF timing pulse can be determined as the signal's center of gravity using Equation 3.10. The RF timing pulse's center of gravity was determined relative to the GTR's on-board 1PPS thereby establishing traceability to UTC(ZA) and UTC through calibration.

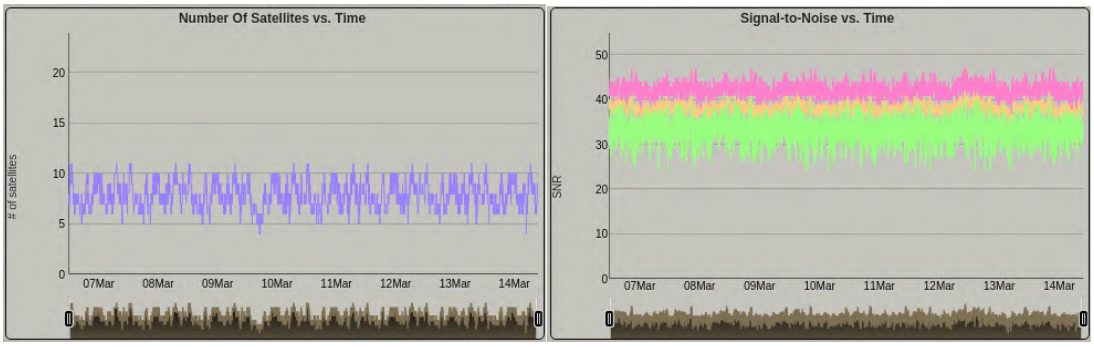

Figure A.2: Spectracom self-survey web interface showing the number of satellites tracked and respective signal strength.

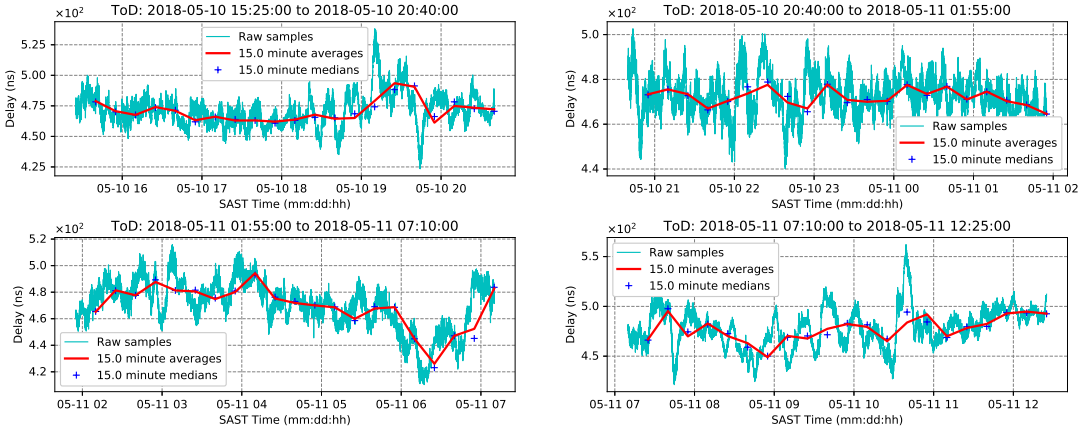

Figure A.3: 6 hour sets of delay measurements between UTC(ZA) and u-blox 1PPS.

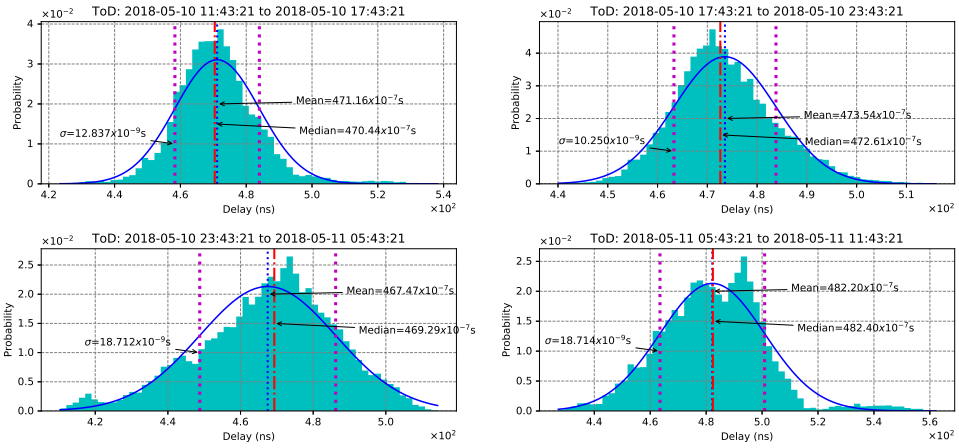

Figure A.4: 6 hour histograms sets of delay measurements between UTC(ZA) and u-blox 1PPS.

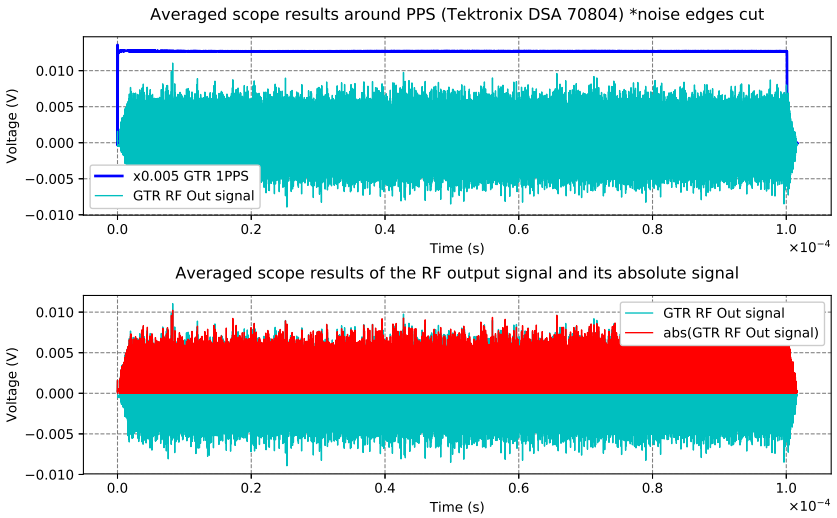

Figure A.5: Averaged scope results around PPS (Tektronix DSA 70804).

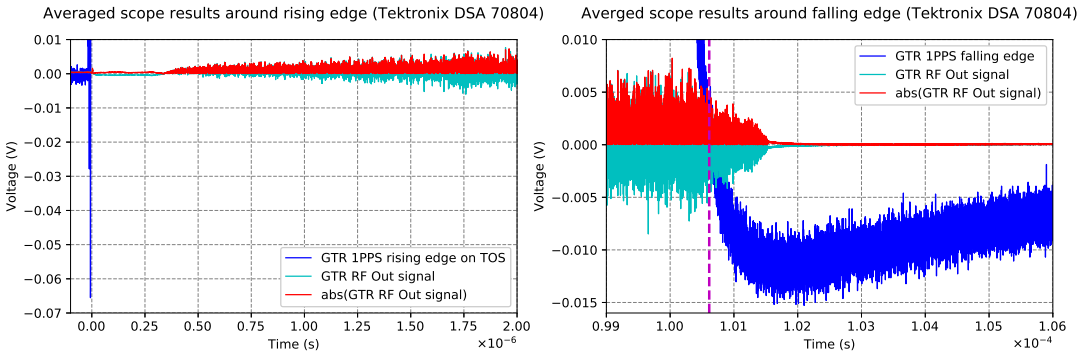

Figure A.6: Averaged scope results around rising and falling edge (Tektronix DSA 70804).

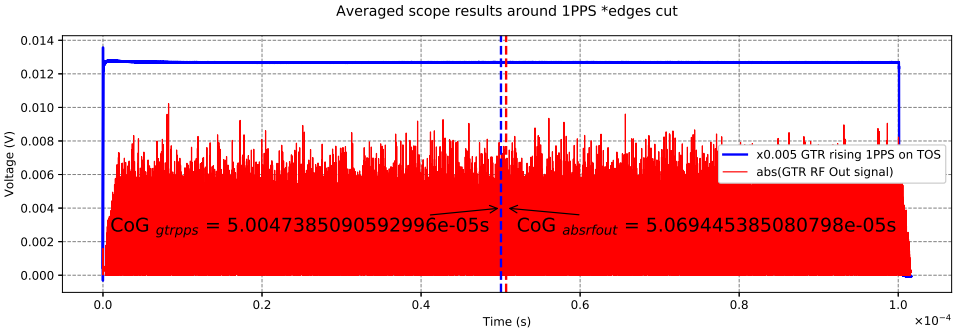

Figure A.7: Center of gravity comparison of GTR's 1PPS and RF timing signal.

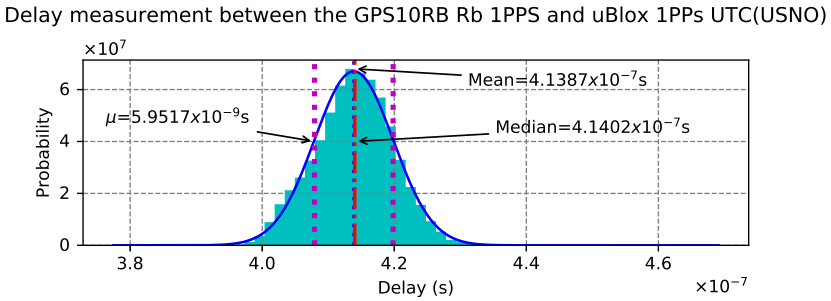

Figure A.8: 24 hour delay measurements between GPS10Rb and u-blox M8F with ANN-SM antenna.

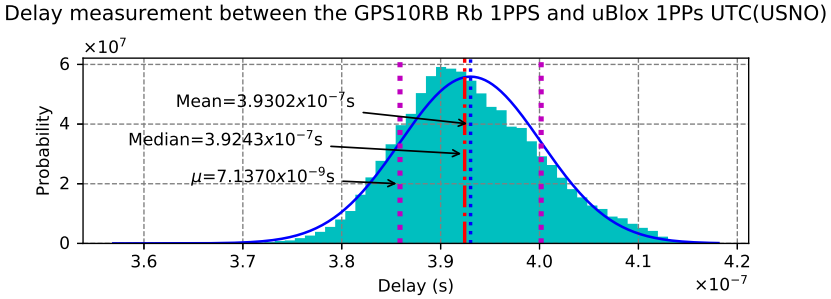

Figure A.9: 24 hour delay measurements between GPS10Rb and u-blox M8F with Taoglas antenna.

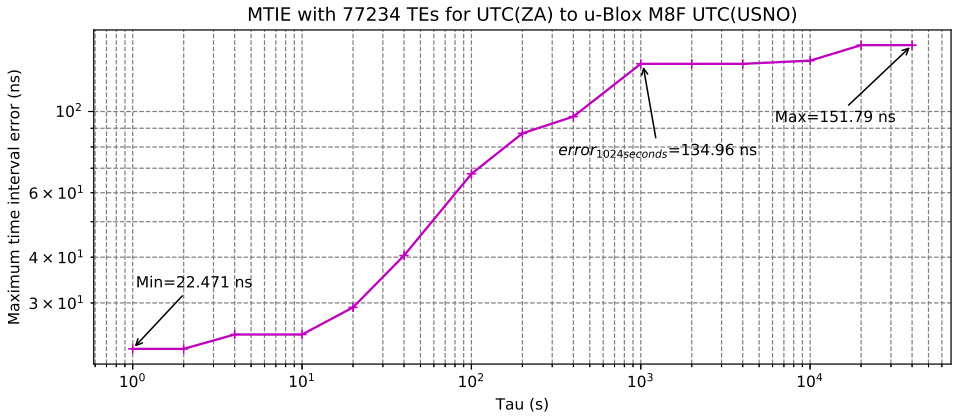

Figure A.10: Calibration MTIE of the u-blox GPS timing receiver with respect to UTC(ZA).

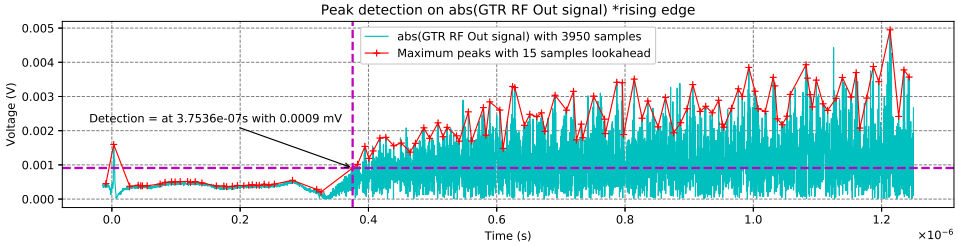

Figure A.11: Envelope detection and rising edge detection.

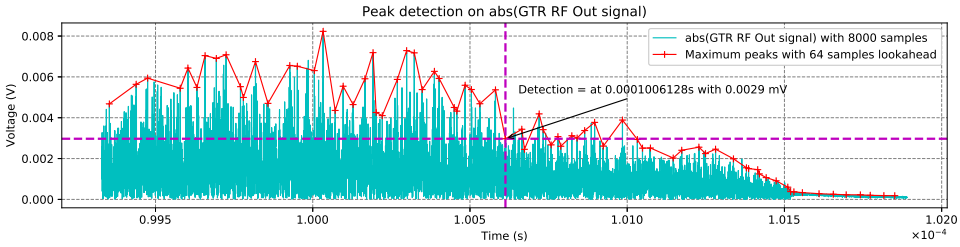

Figure A.12: Envelope detection and falling edge detection.

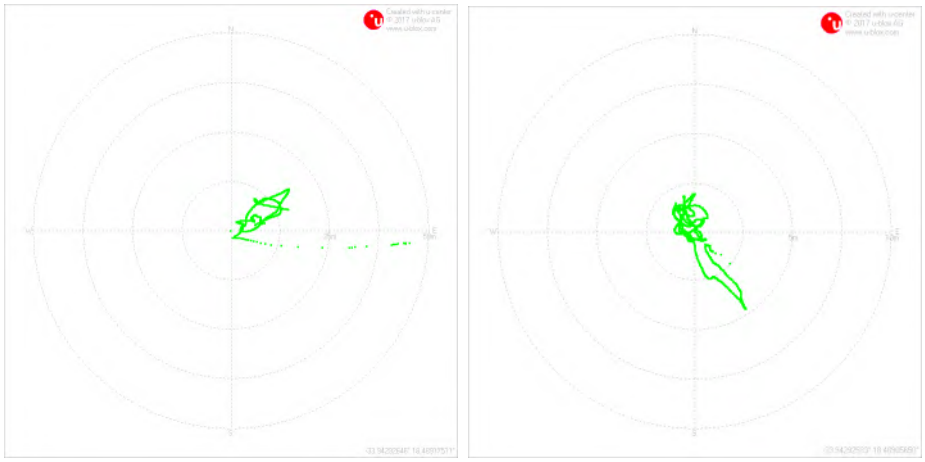

(a) Window (b) Roof top

Figure A.13: 30 minute window and roof top antenna placement experiment results.

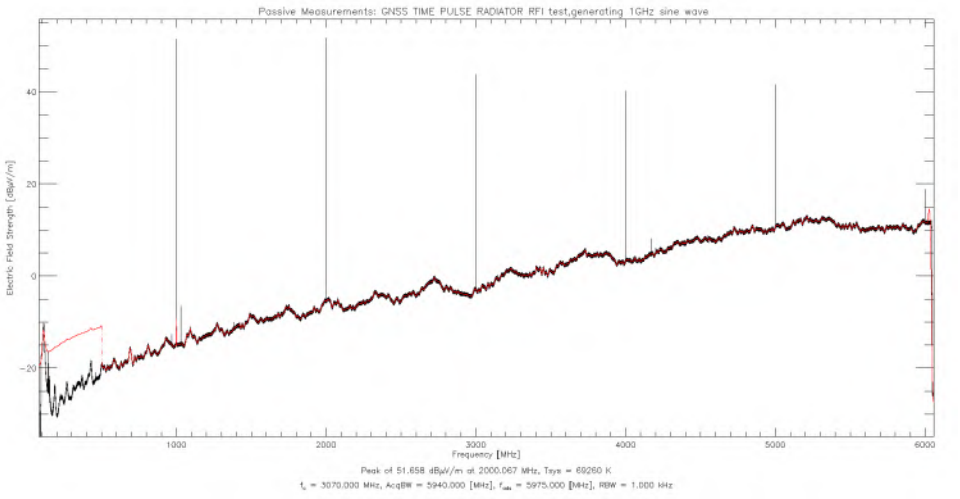

Figure A.14: RFI measurement of the GTR radiating a modulated timing signal with the 1 GHz tone (notice harmonics).

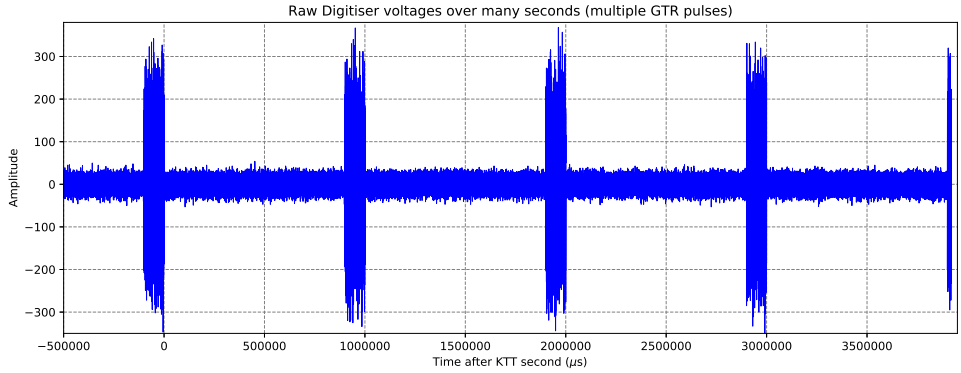

Figure A.15: MeerKAT raw Digitiser voltages over many seconds (multiple 1 Hz GTR pulses).

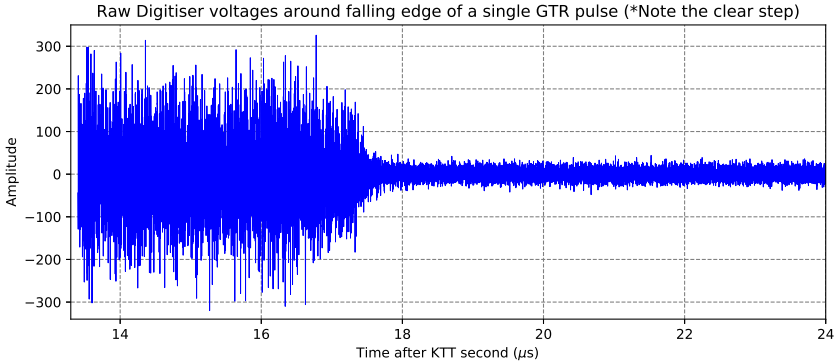

Figure A.16: MeerKAT raw Digitiser voltage around falling edge of a single 1 Hz GTR pulse.

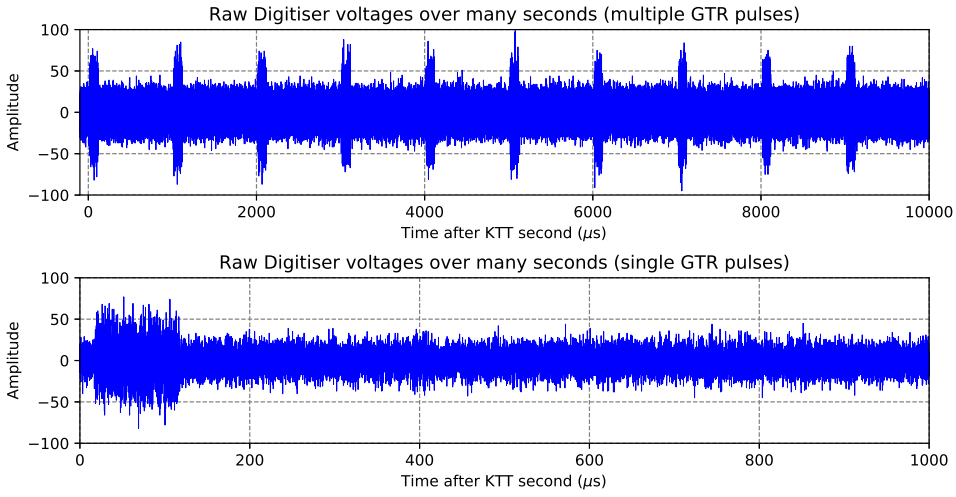

Figure A.17: MeerKAT raw Digitiser voltages over many seconds (multiple 1kHz GTR pulses).

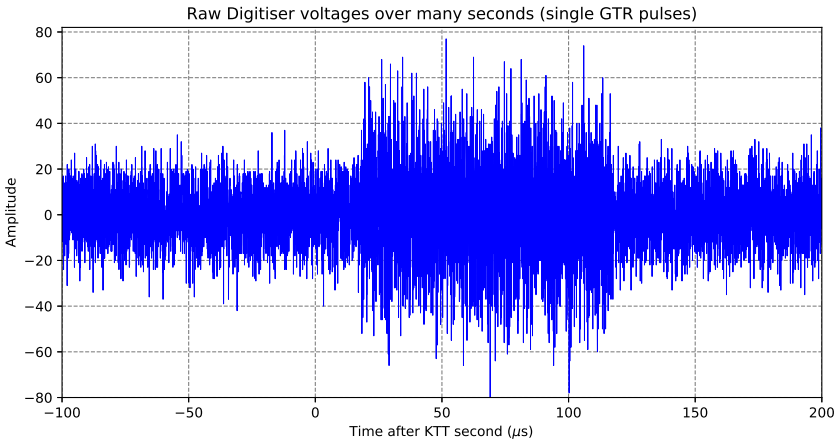

Figure A.18: MeerKAT raw Digitiser voltages over many seconds (multiple 1 kHz GTR pulses).

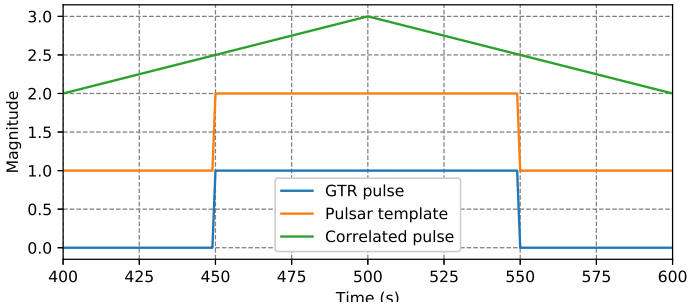

Figure A.19: TOA estimation of pulsar signals.

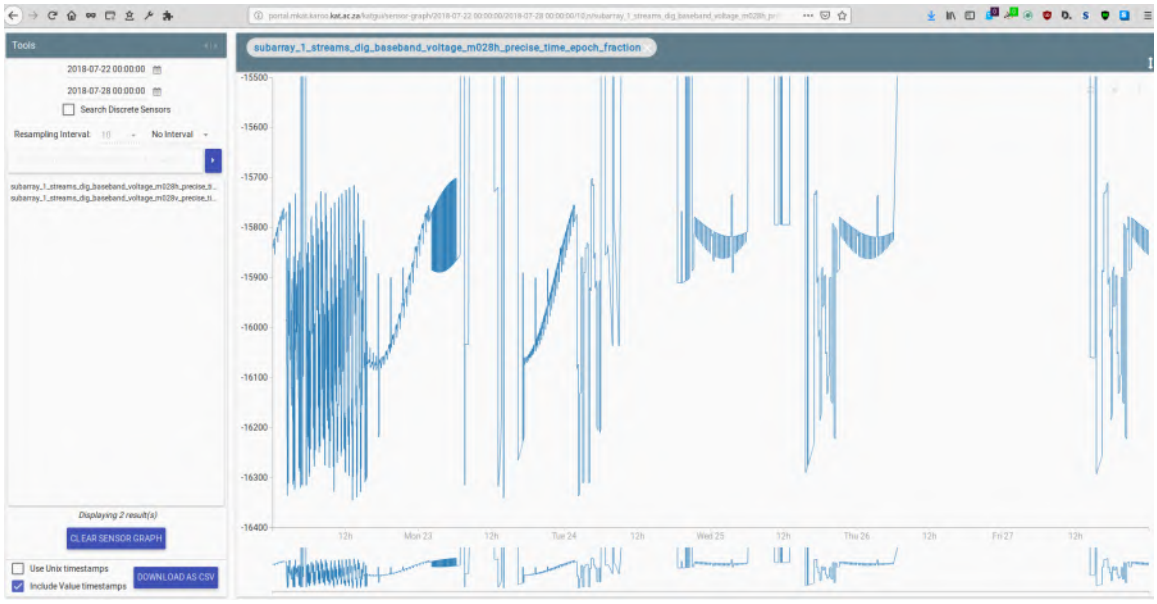

Figure A.20: KATGUI display of KATS round trip measurements of antenna M028 in nanoseconds.

Appendix B

Other resources

User manual

The GTR instrument's operator instructions are as follows:

1. Attach the antenna SMA connector to the GPS marked jack.
2. Connect the stub antenna to the Antenna marked jack on top of the instrument.
3. Plug in the 12V DC source from the battery.
4. Switch on the device by toggling the on switch.
5. Observe the green power led illuminating.
6. The blue PPS led will toggle rapidly before it locks on successfully to GPS satellites.
7. Once it successfully connects, the led toggles periodically at a single pulse per second.
8. Finally select the type of signal you desire to transmit, either noise or a 1GHz tone.
9. Consider charging the battery when the red low battery led illuminates.

Below are additional images of the GTR electronics and enclosure as discussed in Section 3.3.2.

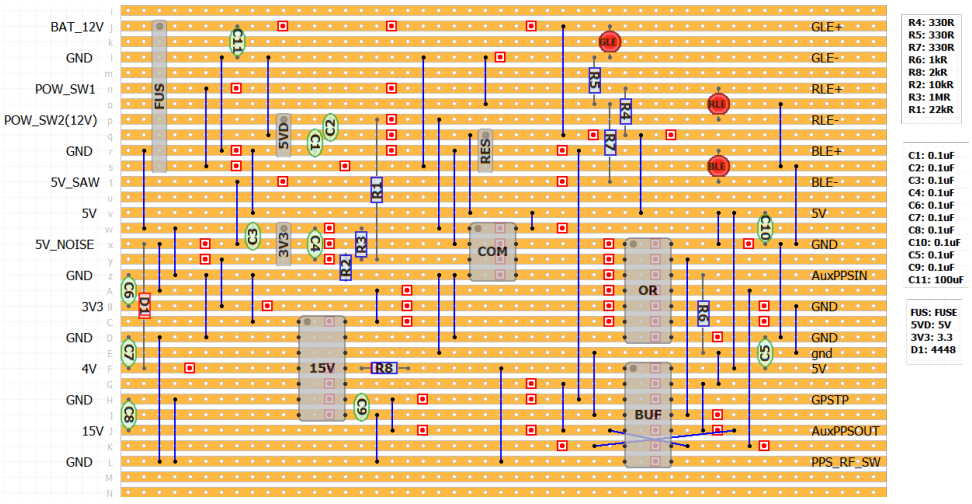

Figure B.1: GTR veroboard design layout.

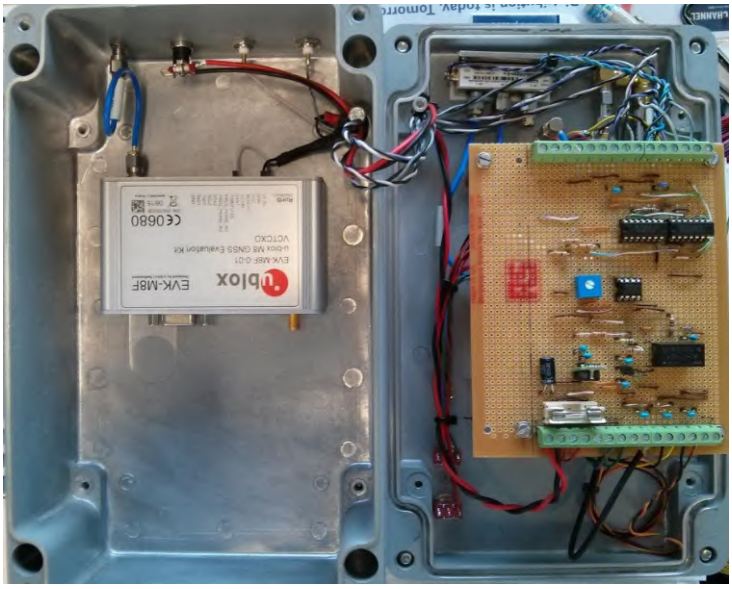

Figure B.2: Integrated GTR electronics and enclosure.

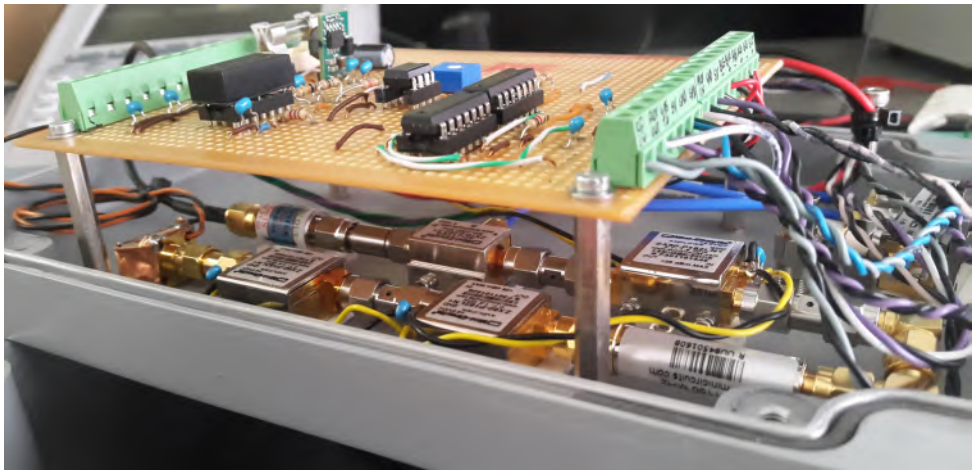

Figure B.3: Integrated GTR electronics.

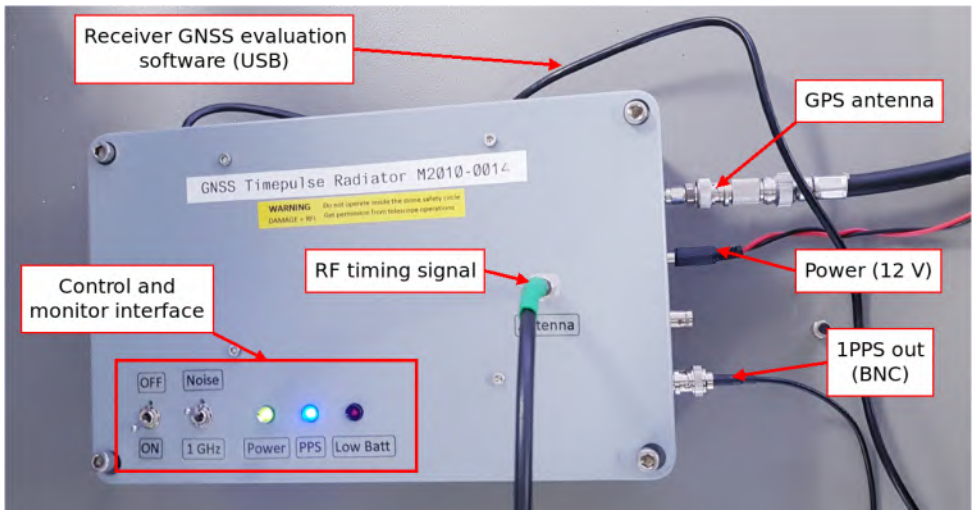

Figure B.4: RF switch characterisation set-up.

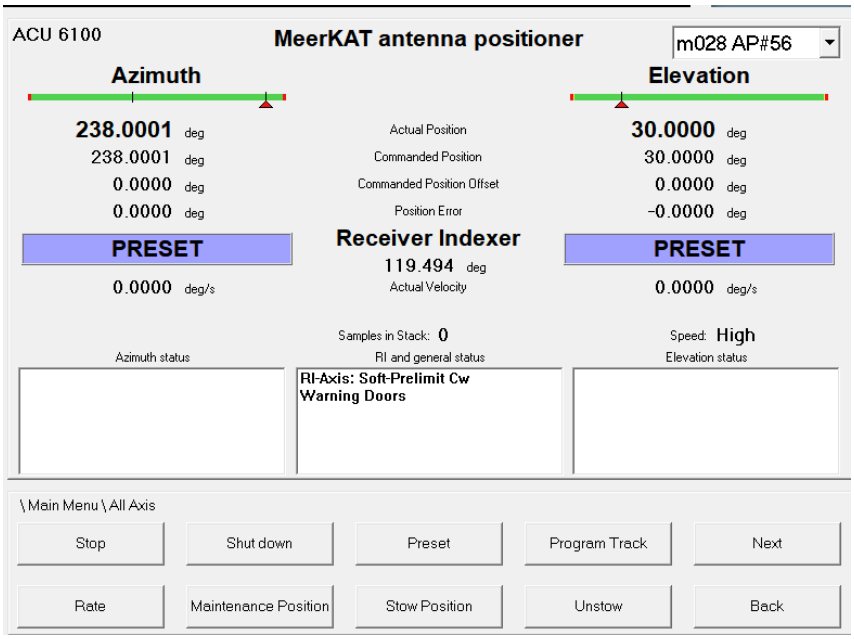

Figure B.5: MeerKAT antenna positioner set-up for receptor M028 experiment.